Wave Action on Offshore Monopile Foundations

A study on run-up, slamming & influence of secondary structure

BAKK10 Master Thesis

Authors:

Resmi Anna Abraham
Mari Kalmo
Ana Bermejo Jiménez

Supervisors:

Thomas Lykke Andersen
Morten Mejlhede Kramer

Aalborg University

June 8, 2016

AALBORG UNIVERSITY
STUDENT REPORT

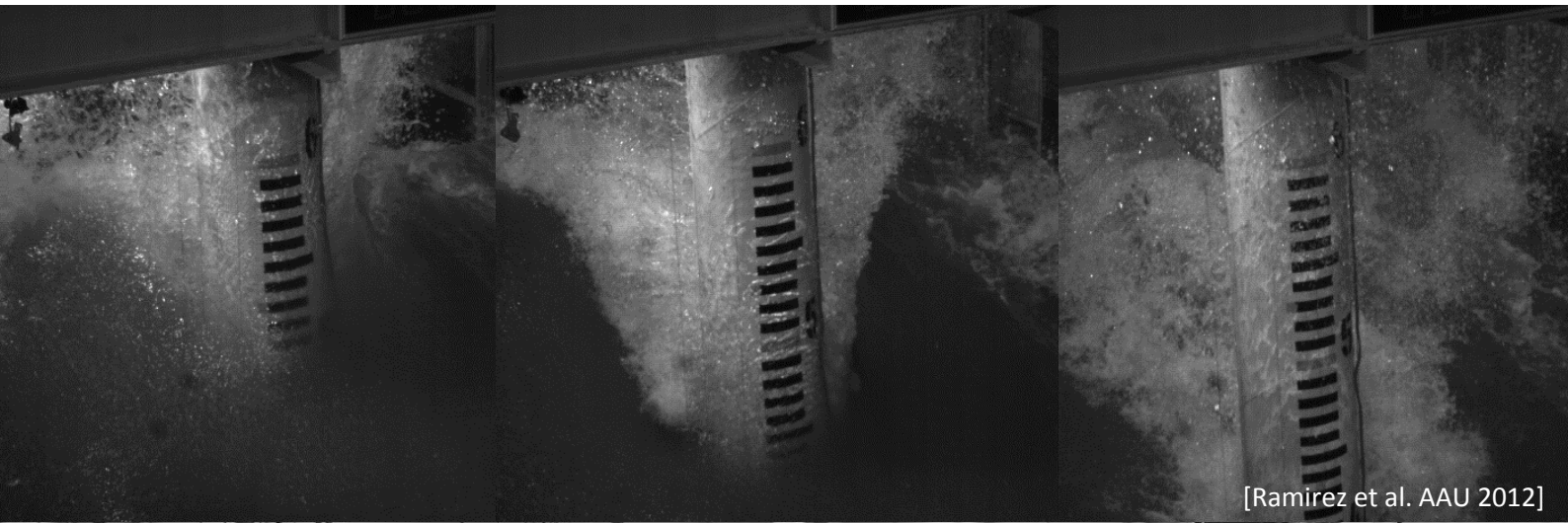

[Ramirez et al. AAU 2012]

Title: Wave Action on Offshore Monopile Foundations
Theme: Master Thesis
Project period: MSc. 9th - 10th semester. Sept. 2015 - June. 2016
Project group: Abraham, Kalmo & Bermejo

Participants:

Resmi Anna Abraham

Mari Kalmo

Ana Bermejo Jiménez

Supervisor:
Thomas Lykke Andersen
Morten Mejlhede Kramer

Issues: 8
Pages: 109
Appendix: 4
Annex-CD: 1
Turn-in: 08-06-2016

Synopsis:

This thesis report documents the analysis of several aspects of wave action on offshore monopile foundations. The first part deals with the run-up phenomenon on monopiles and strives to arrive at a modified run-up factor using previously conducted laboratory tests. The second part focuses on slamming forces and pressures on platforms on monopiles. Both solid and grated platforms with different solidity are analysed. Results from run-up and laboratory results for forces and pressures are used to obtain slamming coefficient and grate multiplication factor for platforms. In the final part of the report, results for wave forces from the recent experiments conducted in AAU for monopile foundation models are analysed. The objective is to study the effect of secondary structures on monopiles by attaching a simple cylindrical element to the model. The experimental results are also compared with the existing theories. Finally the conclusions from the entire study are presented.

PREFACE

This is the master thesis by students Resmi Anna Abraham, Mari Kalmo and Ana Bermejo Jimenez in the program, Master of Science in Structural and Civil Engineering at Aalborg University. The thesis has the title *Wave Action on Offshore Monopile Foundations* and analyses the effect of secondary structures on offshore wind turbines, with focus on platforms and structures similar to boat landings and J-tubes. The thesis is done with supervision and guidance by Thomas Lykke Andersen and Morten Mejlhede Kramer and is handed in on the 8^{th} June 2016.

Reading guide

Source Citation

Source references are developed by Harvard referencing system and refer to the full source list at the back of the report with author, title, publisher and year when available. A source will be indicated by name of the author(s) and year published, e.g. [Kriebel, 1992] or Kriebel [1992].

Figures, tables and formulas

Figures, tables and formulae in the report will be numbered under the chapter which they belong and the number in the sequence of tables, figures and formulae as they appear in the chapter. As an example, "Figure 5.2" can be found in Chapter 5 as the second figure. Equations' numbers appear in parentheses and are shifted to the right side of the document.

Appendix

Appendix is divided in accordance to letters of the alphabet and can be found in the back of the report.

Annex

The annexes will be available on a CD that will be available on the report's rear side. This CD will be referred as "Annex-CD" and will contain all the calculations underlying the report's contents.

List of Tables

List of Figures

Contents

Introduction 1

During the last decades, renewable energy sources like wind, solar and wave energy have gained prominence. Out of these, an increase in demand for wind energy has led to the installation of several onshore and offshore wind turbines. Lately, the focus has been shifted to offshore wind turbines due to factors such as more frequent winds in seas and lesser availability of land area and noise and aesthetic issues in the case of large onshore turbines. The present thesis is a study on certain challenging aspects in the design of foundation for offshore wind turbines.

1.1 Motivation

Compared to onshore turbines, for the optimum design of foundation of offshore wind turbines, additional environmental forces from currents, waves and ice need to be considered. In this report the forces on monopiles, which are the most commonly used foundations, are studied.

Out of the forces expected to act on these monopiles, the most critical contribution is supposed to be from waves in the form of slamming forces. Slamming forces can be caused either by breaking waves hitting a structure, or due to the run-up phenomenon on the pile.

Run-up of waves is the result of interaction between a wave and a structure. It is described as "the maximum vertical extent of wave uprush on a beach or structure above the still water level" [Sorensen, 1997].

The significance of run-up cannot be underestimated considering there had been considerable damages in the past due to run-up generated forces, the most famous example being the damaged platforms in Horns Reef offshore wind farm, Denmark.

It is observed that the wave forces on monopiles can be influenced by the presence of secondary structures such as boat landing and J-tubes. Also the position of secondary structure with respect to the incoming wave, distance from the monopile and the element length are supposed to determine the drag and inertia forces.

Another factor that seems to influence the forces is the surface roughness of the pile. The roughness is usually caused over time by marine growth which in turn, is not easy to predict accurately.

The standard codes such as DNV and API stipulate calculation precedure for these forces but there is still uncertainty in this field and the results from different codes do not entirely converge.

The scope of this project is therefore to investigate the run-up generated forces on platforms and the influence of secondary structures and surface roughness in order to optimize the equations and hence the design of offshore monopile foundations.

1.2 Structure of the report

The report is divided into further chapters as follows:

Chapter 2 introduces the background theories and empirical studies which are used as references for the present thesis.

Chapter 3 presents the re-analysis of previously conducted small scale and large scale laboratory tests to obtain modified run-up equation.

Chapter 4 shows the results from the analysis of large scale slamming tests on wind turbine platforms. The results from chapter 3 are used here to arrive at an equation for slamming forces.

Chapter 5 deals with experimental studies carried out in Aalborg University to analyse the influence of secondary structures and surface roughness of monopiles.

Chapter 6 summarizes the conclusions from the thesis studies and list the limitations and further recommendations from the same.

Problem analysis 2

A number of researchers have studied the wave run-up on piles, slamming forces and the influence of surface roughness and presence of secondary structures obtaining approximate formulae. This chapter outlines the theories and relevant studies related to this field.

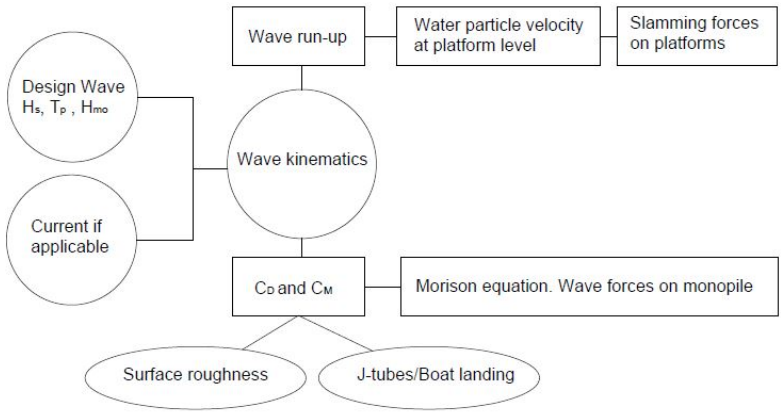

Figure 2.1. Process flow to calculate wave forces on monopile and slamming forces on platforms.

The first step while calculating wave forces or wave run-up as shown in Figure 2.1 is to select a design wave defined by a wave height and period. The design value should be optimum taking into account both cost and safety. The wave kinematics are then obtained by using the most appropriate wave theory for the selected sea state. The wave run-up on the monopile can be calculated from wave kinematics. This run-up is used to obtain the water particle velocity at the platform height from which the slamming forces are calculated.

For assessing the influence of surface roughness due to marine growth and secondary structures such as boat landings and J-tubes, different design codes propose values for drag and inertia coefficients. These are used to calculate the wave forces on monopiles.

The steps are described in detail in the following sections.

2.1 Determination of the design wave

Generally, a wave height with a probability of exceedance 0.02 in a year, also called a 50 year return period wave, and its corresponding period is chosen as design wave for ULS design. In addition, the design codes apply safety factors to the loads in order to take into account uncertainties. An alternative to using safety factors might be to start with a design wave with a lower exceedance probability for example 1000 years return period.

The design wave is obtained by analysing site measurements or using wind or wave hindcasting methods. When the measurements are taken in a different location in the

same fetch area, hindcast models can be calibrated to provide more reliable estimate for the site. Therefore the numerical model is beneficial when site investigation is challenging.

The devices for surface elevation measurements such as buoys, wave poles, pressure transducers, radars or echo sounders might use a band pass filter which would analyse the data in a certain frequency range excluding the rest. Among the devices, buoys are the most common.

The measurement data hence obtained is analysed in time domain to obtain characteristic values for wave heights and time periods. In many cases these instruments only obtain reliable estimates of H_s. Based on such dataset a 50 year H_s is found by extreme analysis. However, when accounting for shallow waters, Rayleigh distribution differs from the real distribution providing conservative results. Some empirical corrections were proposed by Stive [1986], Klopmann and Stive [1989], Battjes and Groenedijk [2000].

The characteristic values are used in extreme analysis using long term distributions such as Weibull or Gumbel to find the design sea state with a suitable return period. The choice of distribution is very important since higher wave heights give higher run-up values which lead to significantly larger impact forces.

As mentioned in the previous section, breaking waves has to be taken into account since they will create important slamming forces. The design wave can further be categorised as breaking or non-breaking. A breaking wave has reached a critical level for the amplitude. $\frac{H}{h}$,$\frac{H}{L}$ and the bottom slope define the breaking limits. For deep water the wave height limit for breaking is usually taken as in Lykke Andersen and Frigaard [2011]:

$$\frac{H}{L} = 0.142 \tag{2.1}$$

The upper limit for wave height in shallow water is usually taken as:

$$H <\sim 0.78h \tag{2.2}$$

For irregular waves in shallow waters, the above criteria applies for H_{max}. The next limit is typically used for significant wave height [Lykke Andersen and Frigaard, 2011].

$$H_s \approx 0.5h - 0.6h \tag{2.3}$$

Goda [2010] defines another method for determining wave height limit, taking into account the bottom slope, water depth and wave height at the location where the measurements are taken and the location of interest.

If a wave is found to be breaking, the type of breaking might also be an important factor influencing the impact force. Battjes [1974] defines the type of wave breaking regarding bottom slope and wave steepness combined in the so-called Iribarren number or breaker index:

spilling : $\xi < 0.4$
plunging : $0.4 < \xi < 2.0$
surging : $\xi > 2.0$

$$\xi = \frac{\tan(\alpha)}{\sqrt{s_o}} = \frac{\tan(\alpha)}{\sqrt{\frac{H_b}{L_o}}} \tag{2.4}$$

where

ξ Iribarren number
s_o H_b/L_o wave steepness at breaking point using deep water wave height
L_o Deep water wave length
α Bottom slope

The wave breaking types are classified in Figure 2.2.

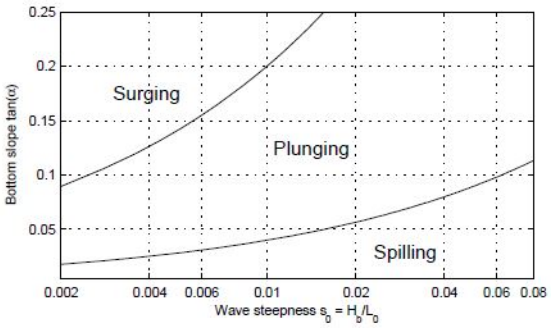

Figure 2.2. Types of wave breaking [Lykke Andersen and Frigaard, 2011].

Once the design wave is selected, wave kinematics are calculated by using different wave theories.

2.2 Selection of wave theory to calculate wave kinematics

The prediction of 2D-wave kinematics is done by different wave theories. The way of satisfying the boundary conditions at surface is different for each of them and the most appropriate for the selected sea state should be chosen.

In shallow waters stream function theory is generally used since it gives more realistic and accurate values. Figure A.1 in Appendix A shows the recommended wave theories as a function of normalised water depth and wave height. Figures A.2 and A.3 compare Stokes 2nd order and stream function theories with respect to η_{max}/H.

Wave velocities, accelerations and surface elevation time series are needed to calculate wave run-up and wave forces on the monopile.

2.3 Determination of wave run-up

The standard design code DNV RP-C205 (2014) specifies that the local run-up forces would be derived from model tests. Wave run-up has been investigated in many laboratory tests

and compared with analytical or empirical formulae based on wave parameters and water depth.

There are different theories which predict wave run-up. A brief review of the three most used in the last years is done in the sections below.

Linear diffraction theory

Linear diffraction theory allows to calculate the wave field around an arbitrary body [MacCamy and Fuchs, 1954]. It is possible to find only an approximation for run-up on a circular cylinder with a diameter D. The theory is valid for $D/L > 0.2$ for linear waves, underestimating the run-up for non-linear waves. An approximation is used in De Vos et al. [2006] in Equation 2.5.

$$\frac{R_u}{\eta_{max}} = \left[1 + \left(\frac{2\pi D}{L}\right)^2\right]^{0.5} = \left[1 + \Big(kD\Big)^2\right]^{0.5} = \left[1 + 4\Big(ka\Big)^2\right]^{0.5} \tag{2.5}$$

where

R_u	run-up
η_{max}	maximum surface elevation of the incident wave
D	diameter of cylinder
L	wave length
a	radius of cylinder
k	wave number

Superposition

Superposition method was proposed by Kriebel [1992] and Kriebel [1993] who divided an incoming regular wave into its Fourier components. For each of them, using linear diffraction theory, run-up was calculated as in Equation 2.5 [MacCamy and Fuchs, 1954]. Then superposition was applied to find the wave run-up as in Equation 2.6.

$$R_u = 2A\frac{r1}{H} + kA^2\left[\frac{r2}{H} + \left(\frac{r1}{H}\right)^2\right] \tag{2.6}$$

where

A	amplitude of the first fourier component ($H/2$) for the second order approximation)
H	wave height
$r1$ & $r2$	first and second order run-up terms obtained from equation 2.5 by using ka for $r1$ and $2ka$ for $r2$
ka	scattering parameter

The method can be used for higher orders and applies for small scattering parameters or slender cylinders with respect to wave length.

Velocity stagnation head theory

When a wave approaches a pile, as ilustrated in Figure 2.3, the kinetic energy transforms into gravitational potential energy and the relation in Equation 2.7 is obtained.

$$\frac{1}{2}\rho v^2 = \rho g \triangle z \tag{2.7}$$

$$\triangle z = \frac{v^2}{2g} \tag{2.8}$$

where

$\triangle z$	is the height reached by the water particle
v	initial vertical water particle velocity
g	acceleration due to gravity
ρ	water density

Hallermeier [1976] described the run-up above MSWL as a function of maximum surface elevation and $\triangle z$ from the equation above assuming that $v = u_{max}$ i.e. the maximum horizontal particle velocity in the wave crest :

$$R_u = \eta_{max} + \frac{u_{max}^2}{2g} \tag{2.9}$$

where

u_{max}	maximum horizontal water particle velocity at the wave crest
η_{max}	maximum surface elevation of the particle

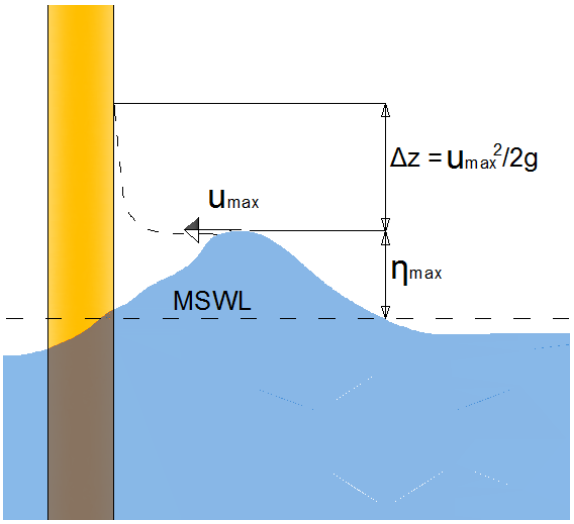

Figure 2.3. Wave approaching to a monopile.

2.3.1 Initial semi empirical run-up studies

In order to check the validity of the existing formulae in real problems, model tests were carried out by several researchers prior to the present thesis. The set-up was usually a pile model exposed to different sea states in a 2D flume where irregular or regular waves were generated. The majority of tests performed were in small scale. Recently, large scale tests were carried out to assess model scale effects. The general aims of these studies were to study run-up levels on piles from regular and irregular waves, and the influence of wave steepness, water depth, wave height and pile diameter in the results.

The initial studies on run-up dealt with wave run-up in lighthouses and circular islands. The results were close to those obtained from linear diffraction theory. However, the inaccuracy of diffraction theory was proved by Isaacson [1978] and the use of cnoidal theory gave results in better agreement for run-up tests in cylinders placed in shallow waters. Nevertheless, wave run-up was still underestimated.

Other researchers focused their studies on the influence of the pile cross section, finding that for a circular cylinder, the run-up distribution is symmetric Galvin and Hallermeier [1972].

Hallermeier who considered velocity stagnation head theory, applying solitary wave theory to calculate wave crest kinematics. This method offered good results for long waves and also for short waves when using stream function Haney and Herbich [1982].

2.3.2 Inclusion and calibration of m-factor

Different wave theories were used in order to find the values for wave kinematics applied in Hallermeier´s run-up formula. This lead to different results as it can be seen below.

After certain wave run-up tests on cylinders with irregular and regular waves, Niedzwecki and Duggal [1992] concluded that the linear diffraction theory underpredicts wave run-up. It was found that velocity stagnation head theory also underestimated the run-up when

the wave kinematics were calculated using linear wave theory. Hence they suggested a coefficient m in the existing formula which would fit the data.

This coefficient gives the relation between the kinetic and potential energy, so that if the coefficient gets a value 1 it means both have the same value. Experiments showed that the potential component tended to be higher than the kinetic and hence the m-factor becomes higher than 1.

Niedzwecki and Huston [1992] included another coefficient for cylinders in the formula from Niedzwecki and Duggal [1992] in pursuance of solving the problem of expressing wave crest as $H/2$.

Martin et al. [2001] experiments of run-up on monopiles due to regular waves showed that the previous semi-empirical formulae proposed by Niedzwecki and Huston overestimated the run-up, meanwhile most of the previous theories mentioned before underestimated it.

Mase et al. [2001] proposed a formula for $R_{u,2\%}$ or 2% excess run-up heights of random waves on small circular monopile in a uniform bottom slope 1:40 to 1:10. See Equation 2.10.

$$\frac{R_{u,2\%}}{h} = \left(0.24 - \frac{0.004}{\tan\theta}\right) + \left(11.43 - \frac{0.20}{\tan\theta}\right) exp\left[- \left(1.55 - 0.77exp\left\{ - 69.46\left(\frac{H_0}{L_0}\right)\right\}\right)\left(1.02 - \frac{0.015}{\tan\theta}\right)\left(\frac{h}{H_0}\right)\right] \quad (2.10)$$

A relationship between this $R_{u,2\%}$ and maximum run-up was established as Equation 2.11.

$$R_{u,max} = 1.22R_{u,2\%} \quad (2.11)$$

The theory is valid within the limits:

$$\frac{1}{40} \leq \tan(\theta) \leq \frac{1}{10} \quad (2.12)$$

$$0.004 < \frac{H_0}{L_0} < 0.05 \quad (2.13)$$

$$\frac{h}{H_0} < 6 \quad (2.14)$$

where

$\tan(\theta)$	bottom slope
H_0	deep water wave height
L_0	deep water wave length
h	water depth

As it was outlined before, an m-factor was included in the formula for velocity stagnation head theory as in Equation 2.15.

$$R_u = \eta_{max} + m\frac{u_{max}^2}{2g} \tag{2.15}$$

The inclusion is motivated by potential theory and the idea of an amplification in vertical particle velocities due to a back pressure generated by the monopile when the wave encounters it, as descibed in Lykke Andersen et al. [2011]. A pile in a uniform flow can be represented as the superposition of a dipole flow and a uniform flow [Brorsen, 2007]. Establishing the boundary conditions and fulfilling them, it is possible to find the velocity and pressure field around the pile. The velocity would be double in the horizontal side of the cylinder and equal to 0 at the stagnation point S. Therefore values between 1 and 4 for m are expected if there is no energy loss. See Figure 2.4

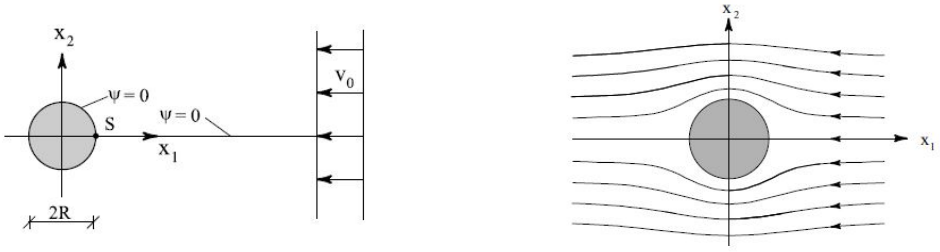

Figure 2.4. Two-dimensional potential flow around a circular cylinder Brorsen [2007].

The limitation of the previous run-up formulae and wave theories was revised by De Vos et al. [2006] who conducted experiments for irregular and regular waves on two different piles. One with a monopile foundation and the second one with a coned shaped gravity foundation. As a result from the tests, a new m factor was proposed for run-up due to irregular waves on a wind turbine placed in deeper water with a bottom slope of 1:100.

The run-up value used for irregular waves was the wave run-up $R_{u,2\%}$ reached or exceeded by two per cent of the waves tested/observed.

Stokes second order theory was used for wave kinematics with $H = H_{2\%}$ and $T = T_p$ The new m-factor was found by plotting $R_{u,2\%}$ measured against the theoretical value for $R_{u,2\%}$.

$H_{2\%}$ can be estimated by $H_{2\%} = 1.4H_s$ when waves are Rayleigh distributed. This is widely used knowing that the distribution is not adequate for shallow waters since large waves would break.

The highest run-up values corresponded to the lowest wave steepness. Nevertheless, it was not possible to obtain a clear relation between steepness and wave run-up.

Gravesen [2006] found a scatter in m-factors when re-analysed data from De Vos et al. [2006] and an influence in the results from water depth to diameter ratio h/D and H_{m0}/h.

Later on, Lykke Andersen and Frigaard [2006], performed additional tests and re-analysed the data obtained in De Vos et al. [2006] by using stream function theory, because the method is more accurate for wave kinematics and is widely used. The objective was to reduce the scatter in m-factors and to assess the influence of wave steepness, h/D and

H_{m0}/h in wave run-up since the data from De Vos et al 2006 follows $H_s/h < 0.42$. This means not depth limited waves.

Results for regular and irregular waves showed that the scatter for m-factors was reduced. Moreover, when using stream function for the data of De Vos et al. [2006], the results for m were in a range from 2.7 to 4.9 depending on the type of foundation.

The influence of h/D and H_{m0}/h on m-factor was very small meanwhile wave steepness clearly had a stronger influence. One of the main conclusions obtained was that m-factor is higher for small steepness.

Two m-factors were proposed in Lykke Andersen and Frigaard [2006] and in Lykke Andersen and Brorsen [2006a].

- $m = 4$ for $s_{op} = 0.020$
- $m = 3$ for $s_{op} = 0.035$

When performing a wave run-up test, splash is normally not taken into account as the wave gauges only measure the thick run-up layer. Therefore, in some occasions thin run-up layers will not be recorded since there is a gap of around 2 mm between the gauges and the pile.

For this reason Lykke Andersen et al. [2011] suggested the m-factor should be multiplied by 1.4 in order to take into account splash. This led to a good correlation between impact pressures and wave run-up.

Wave run-up from irregular waves on slender piles was studied at Grosser Wellenkanal (GWK), Forschungszentrum Küste (FZK) in Hannover, Germany Ramirez et al. [2013]. The test scale was 1:8 to 1:10 of typical wind turbines. High speed cameras were used to measure the wave run-up. The aim of the large scale tests was to reduce and clarify the importance of model and scale effects especially with respect to splash and spray, since measurement system in small scale tests were not able to register this and might also be subjected to scale effects.

Different sea states were tested with irregular waves generated from the JONSWAP Spectrum. The peak enhancement factor was $\gamma = 3.3$ and around 500 waves for each state were reproduced. It was only few waves which gave significant run-up at the pile, and therefore only these significant measurements were included in the analysis.

The run-up was categorized in following three levels:

- Level A for the thick layer, green water run-up ($R_{u,A}$)
- Level B for thin layer of water mixed with air ($R_{u,B}$)
- Level C for the maximum spray ($R_{u,C}$)

In addition to the experimental test, a value for m by use of the methodology of Lykke Andersen et al. [2011] was calculated as a function of deep water steepness which is calculated as in Equation 2.16. The results of fitted m-factors for each run-up level are shown in the Table 2.1.

$$s_{op} = \frac{2\pi H_{m0}}{gT_p^2} \tag{2.16}$$

where

H_{m0} is the significant wave height
T_p is the peak period

A good correlation between the experimental results and the values calculated with the new m-factors was observed. For the run-up level A and B there were no significant scale effects on the run-up heights, as fitted m values match with the small scale values from Lykke Andersen and Frigaard [2006]. Level C presented higher scatter which indicates that spray was not generated in some waves.

In order to investigate wave run-up on monopiles and to check the model effect due to measurement system, a 3D basin was used at Danish Hydraulic Institute (DHI) to carry out tests. Wave run-up was measured by a high speed camera helped by marks in the pile and wave gauges. It could register a higher run-up by using the videos than results from wave gauges which again gave the idea that run-up is underestimated when applying this measurement tool. In this case, the measuring error was referred to a disturbance in the gauges caused by the mixture of water and air.

The results obtained later on in Damsgaard et al. [2013] showed a relation between maximum wave run-up and water depth for depth limited waves expressed in Equation 2.17.

$$R_{u,max} = 1.75h \tag{2.17}$$

The most relevant existing formulae for run–up prediction based on velocity stagnation head theory is presented in Table 2.1

Researcher	**Theory**	**Formula & m value**
Hallermeier (1976)	-	$R_u = \eta_{max} + \frac{u^2}{2g}$ $m = 1$
Niedzwecki and Duggal (1992)	Linear	$R_u = \frac{H}{2} + m\frac{u^2}{2g}$ $m = 6.83$
Niedzwecki and Huston (1992)	Linear	$R_u = 0.56H + 6.5\frac{u^2}{2g}$ $m = 6.5$
De Vos et al (2006)	Stokes 2nd Order	$R_{u,2\%} = \eta_{max,2\%} + m\frac{u^2_{2\%}}{2g}$ $m = 2.71$ for monopile $m = 4.45$ for cone foundation
Lykke Andersen et al (2011)	Stream function	$R_{u,max} = \eta_{max} + m\frac{u^2_{max}}{2g}$ $R_{u,2\%} = \eta_{max,2\%} + m\frac{u^2_{max,2\%}}{2g}$ $m = 1.4 \cdot 3$ for $s_{op} = 0.035$ $m = 1.4 \cdot 4$ for $s_{op} = 0.02$
J.Ramirez (2013)	Stream function	$R_{u,max} = \eta_{max} + m\frac{u^2_{max}}{2g}$ Level A (green water): $m = -66.667s_{op} + 5.33$ for $s_{op} < 0.035$ $m = 3$ for $s_{op} > 0.035$ Level B(thin run-up): $m = -93.333s_{op} + 7.47$ for $s_{op} < 0.035$ $m = 4.2$ for $s_{op} > 0.035$ Level C(spray): $m = -200s_{op} + 16$ for $s_{op} < 0.035$ $m = 9$ for $s_{op} > 0.035$

Table 2.1. Existing formulae for run-up height.

During the initial analysis of the run-up tests in Lykke Andersen and Frigaard [2006], a bandpass filter removed frequencies below $0.33f_p$ and above $3f_p$. However, this procedure does not ensure taking into account necessary frequency range for the highly non-linear waves. Hence there is a need for re-analysing the data by removing the filter. Lower m-factor values are expected since initial analysis showed the maximum wave heights increase around 10% when bandpass filter is removed.

Also the reliability of using reflection analysis to obtain H_{max}, $H_{2\%}$ and T_p needs to be checked.

The run-up formula obtained from the above procedures is used to calculate the water particle velocity at platform levels and obtain the slamming forces on the secondary structures. The new m-factor values would give different results for the slamming coefficient, C_s used in Equation 2.19 and Equation 2.20. Further description about the theory and studies related to this problem is given in the next section.

2.4 Determination of loads on platforms

The procedure followed to obtain the slamming forces on platforms proposed by Lykke Andersen and Brorsen [2006b] consists of three steps:

1. Calculate the expected maximum wave run-up height with no platform, R_u
2. Use this run-up height to calculate the velocity at the level of the platform, $v(z)$
3. Use a slamming force model to get the maximum pressures and maximum total forces

In step 2, velocity is calculated from R_u using Equation 2.18, where the velocity, $v(z)$ at the platform height above MSWL (z) is obtained from velocity stagnation head theory as:

$$v(z) = \sqrt{2g(R_u - z)} \tag{2.18}$$

In step 3, the slamming pressure or maximum total force is calculated using Equation 2.19.

$$F_s = \frac{1}{2} C_s \rho v^2 A_{ref} \tag{2.19}$$

$$P_{max} = \frac{1}{2} C_s \rho v^2 \tag{2.20}$$

where

A_{ref}	reference area. Normally taken as half the platform area
C_s	slamming coefficient
ρ	density of water
$v(z)$	particle velocity at the platform height, z

The values for C_s have been investigated by many researchers and the recommended values for most of the design codes and late studies are shown in Table 2.2

Recent studies in small scale performed in the shallow flume at Aalborg University facilities, Lykke Andersen and Brorsen [2006b] and Lykke Andersen and Brorsen [2007] studied the slamming coefficients for horizontal and cone shaped platforms placed at different levels for regular and irregular waves.

In the case of regular waves Lykke Andersen and Brorsen [2006b], the pressure used to calculate the slamming coefficient was the maximum of 15 pressure cells. The values for m-factor proposed in Lykke Andersen and Frigaard [2006] were used.

Irregular wave analysis Lykke Andersen and Brorsen [2007] showed high slamming coefficients, which was expected due to the presence of breaking waves. Two different forces were used to find the slamming coefficient:

1. The maximum pressure registered in a test among all pressure cells. Used to design the prototype plate elements of generally 1 m^2
2. The pressure distribution at the time that maximum spatial averaged pressure from the transducers occurs, also called spatial averaged pressure

Regarding the platform shape and level, it was clear that the use of a cone shaped platform will reduce the forces significantly and the heights expected to give zero force were accurately predicted. Smaller slamming coefficients were obtained from spatial averaged pressures, since the peaks will not occur at the same time and have the same magnitude.

Method	**Regular waves [Lykke Andersen and Brorsen, 2006b]**	**Irregular waves [Lykke Andersen and Brorsen, 2007]**	**DNV (2004)-DS-449 (1983)**
Maximum pressure	Cone platform $C_s = 6$ Horizontal platform $C_s = 12$	Cone platform $C_s = 6$ Horizontal platform $C_s = 10$	$3 < C_s < 2\pi$ for horizontal cylinders
Spatial averaged pressure		Cone platform $C_s = 1.2$ Horizontal platform $C_s = 1.5$	

Table 2.2. C_s values for different platform configurations.

The results from the small scale studies by Damsgaard et al. [2007] were considered to be conservative because of the following reasons:

- The impact duration is around 0.05 s, which gives a very short time to the structure response
- The existence of a dynamic overshoot governed by the pressure cell dynamics which makes the load peak fall below zero

After assessing the slamming coefficients for different configurations and levels, the next question which arose was how to reduce these values for a horizontal solid platform. A possible answer was the use of platforms with gratings.

According to Lykke Andersen et al. [2010], it is possible to calculate the force on a solid plate hit by a steady jet as in Equation 2.21.

$$F_x = \rho Q[v_{x,in} - v_{x,out}] \tag{2.21}$$

where

ρ	water density
Q	flow rate
v_x	water velocity in x direction (jet direction)

If $v_{x,in}$ is equal to the jet velocity, v and $v_{x,out}$ is equal to 0 for a solid plate, then the force can be expressed as:

$$F = \rho v^2 A \tag{2.22}$$

where

v	jet velocity
A	jet area

By comparing Equation 2.22 with that for drag force in Equation 2.23, the value for drag coefficient, C_D would be equal to 2.

$$F_d = \frac{1}{2}\rho C_D v^2 A \tag{2.23}$$

where

F_d	drag force
ρ	total area
C_D	drag coefficient
A	reference area

Several authors tried to relate the drag coefficient for solid plates and plates with grates. This relationship depends on the porosity in Equation 2.24, grate solidity in Equation 2.25 and effective porosity β_e.

$$\beta = \frac{A_o}{A_1} \tag{2.24}$$

$$Solidity = 1 - \beta \tag{2.25}$$

where

A_o is the area open to flow
A_1 is the total area

The forces will decrease for non-perpendicular flows, therefore the value of C_D should be related to the angle of attack as in Table 2.4.

A couple of studies about drag coefficients on differet grates were carried out at Aalborg University, Lykke Andersen et al. [2007] and Lykke Andersen et al. [2006] and the following conclusions were made:

- The forces on the plates were reduced around 75% with the use of grates with porosity $\beta = 0.87$. Note that they were not galvanized and if so,the porosity would decrease
- The assumption of $C_D = 2$ for a solid plate was validated in Lykke Andersen et al. [2006]
- Furthermore, the angle of attack was investigated and found to be not influential for an interval between 50°to 90°. For higher angles, the in-plane forces increment depends on the grate rotation
- The influence of 10% air content in the drag coefficients was found to be small but still noticeable even for the solid plate
- The difference in size between the jet and the prototype conditions has to be taken into account, as well as the static condition of the tests. Being recommended the use of CFD models in order to perform further investigations and drop tests to reproduce slamming conditions

The next step to determine the grate multiplication factors was taken in 2010, when large scale tests on access platforms with gratings were performed by Lykke Andersen et al. [2010].

The grate multiplication factor is defined here as the relation between the peak load on the grate and the peak load on the solid plate for the same impact.

It was observed that the maximum force for a solid plate obtained using the C_s proposed in the small scale tests Lykke Andersen and Brorsen [2006b] and Lykke Andersen and Brorsen [2007] was close to the total load measured in large scale, but that further analysis was needed.

Grate solidity and grate multiplication factor acquire approximately the same values while ranking loads after peak but for extreme events the grate multiplication factor increases. See Table 2.3.

Porosity	Measured peak load	Grate multiplication factor
0%	2.3 kN	1.00
70%	1.05 kN	0.46
84%	0.51 kN	0.22

Table 2.3. Summary of peak loads and corresponding grate multiplication factor for the max load in the considered sea state [Lykke Andersen et al., 2010].

This fact leads to the idea that large scale tests represent more realistic conditions compared to the previous tests Lykke Andersen et al. [2007] and Lykke Andersen et al. [2006].

Table 2.4 shows the most relevant formulae to relate drag coefficient and porosity from Richards and Robinson [1999], Annand [1953],Lykke Andersen et al. [2007] and Morgan [1962].

Researcher	Formula
Richards and Robinson (1999)	$C_D = C_{D,normal} sin(\theta)$ θ = angle of attack $C_D = C_{D,solid}(1-\beta_e)$ $C_D = 1.2(1-\beta^2)$ free standing porous wall
Annand (1953)	$C_D = \frac{a(1-\beta^2)}{\beta^2}$ a = 0.55 for high Re
T.Lykke Andersen, M.Rasmusen, P.Frigaard (2007)	$C_D = C_{D,solid}(1-\beta)$

Table 2.4. Formulae for grate multiplication factor.

Researcher	β_e values
Richards and Robinson (1999)	$\beta_e = 0.75\beta$ slats with depth = width $\beta_e = \beta$ round wire mesh screen
Morgan(1962)	$\beta_e = \frac{2}{3}\beta$ flat webs

Table 2.5. Values for effective porosity depending on grate type.

Most of the data from the large scale tests performed at Grosser Wellenkanal (GWK), Forschungszentrum Küste (FZK) in Hannover, Germany, needs to be analysed in order to obtain more realistic slamming coefficients and grate multiplication factors.

Appart from slamming forces on platforms, wave forces on the monopile and another secondary structures should be calculated accurately. The formulae used for this purpose is presented in the next sections.

2.5 Forces on monopiles

Morison formula given in Equation 2.27 is generally used in the current offshore design codes to predict the wave forces. They present different values for drag and inertia coefficients, C_D and C_M, dependent on Reynolds number, R_e, surface roughness and Keulegan-Carpenter number, KC.

The empirical charts proposed by Sarpakaya [2010], can also be used to obtain the values within the range of KC, R_e and β (viscous frequency parameter) calculated by Equation 2.30, Equation 2.31 and Equation 2.32 (See Figure A.4).

It is important to consider the pile surface roughness when selecting drag and inertia coefficients and calculating wave forces. Surface roughness changes are due to the colonization of marine organisms, often referred as marine growth. It leads to an increment in the diameter of the structure, as is generally expressed as in Equation 2.26. It may also alter the natural frequency and increase vortex shedding. The presence and thickness of marine growth varies in time and from one location to another, for example, 200 mm thickness being reported in the North Sea. It depends on many conditions such as currents, temperature, salinity, sun light penetration, or dominant species. A site study is hence preferable to arrive at a realistic value. Its density is normally taken as 1325 kg/m^3.

$$D = D_c + 2t \tag{2.26}$$

where

D_c clean outer diameter
t average marine growth thickness

Table 2.6 and Table 2.7 from DNV and NORSOK N-003 can be used to find the average roughness height, k for different materials. Roughness effects are considered negligible for a surface coverage less than 3% [API, 2003].

Material	**k (meters)**
Steel, new uncoated	$5 \cdot 10^{-5}$
Steel, painted	$5 \cdot 10^{-6}$
Steel, highly corroded	$3 \cdot 10^{-3}$
Concrete	$3 \cdot 10^{-3}$
Marine growth	$5 \cdot 10^{-3}$ to $5 \cdot 10^{-2}$

Table 2.6. Surface roughness DNV [2014].

Water depth (m)	**56 to 59ºN t(mm)**	**59 to 72ºN t(mm)**
+2 to -40	100	60
below -40	50	30

Table 2.7. Marine growth thickness NORSOK [2007].

The values for drag and inertia coefficients are expressed in some design codes as a function of the rate between average roughness height k and the pile diameter D or relative roughness, refered as Δ or e.

The next tables show the procedure to obtain drag and inertia coefficients for circular cylinders in the design codes cited below:

- American Petroleum Institute - Recommended practice 2A-WSD(RP 2A-WSD) (API)
- Germanischer Lloyd - Guideline for the Certification of Offshore Wind Turbines (GL)
- NORSOK STANDARD N-003 Edition 2, September 2007
- Det Norske Veritas (DNV-OS-J101) - Design of Offshore Wind Turbine Structures (DNV)

The figures and formulae cited from Tables 2.8 to 2.12 refer to each standard code.

KC Range	Values for C_M	KC Range	Values for C_D
$KC \leq 3$	$C_M = 2$	$KC \leq 12$	Figure C2.3.1-6 C_D/C_{ds} Figure C2.3.1-4 C_{ds}
$KC > 3$	Figures C2.3.1-8 and C2.3.1-7	KC>12	Figure C2.3.1-5 C_D/C_{ds} Figure C2.3.1-4 C_{ds}

Table 2.8. C_M and C_D values as function of KC in API [2003].

Monopile	KC Range	Values for C_M	Values for C_D
Smooth	$KC > 30$	$C_M = 1.6$	$C_D = 0.65$
Rough		$C_M = 1.2$	$C_D = 1.05$
Smooth	$1 < KC < 6$	$C_M = 2$	$C_D = 0.65$
Rough		$C_M = 2$	$C_D = 0.8$
	$6 \leq KC \leq 30$	special analysis	special analysis

Table 2.9. C_M and C_D values as function of KC in NORSOK [2007].

Monopile	Values for C_M	Values for C_D	R_e Range
Smooth	$C_M = 2$	$C_D = 1.2$	$R_e \leq 2 * 10^5$
Rough	$C_M = 2$	$C_D = 1.2$	
Smooth	$C_M = 1.6$	$C_D = 0.7$	$R_e > 2 * 10^5$
Rough	$C_M = 2$	$C_D = 1.1$	

Table 2.10. C_M and C_D values as function of R_e in design code GL [2005].

The drag coefficient C_D may be multiplied with a factor up to 1.5 for rough cylinders with KC numbers between 8 and 30 according to GL [2005].

R_e	$> 10^6$	$\leq 10^6$
C_D	$C_{ds}\Psi$	Figure 6-6

Table 2.11. Drag Coefficient as Function of R_e in DNV [2014].

$\boldsymbol{KC}$	≤ 3	> 3	≤ 12
$\boldsymbol{C_M}$	2	Figure 6-8 Formula 6.9.1.2	
$\boldsymbol{\Psi}$			Formula 6.7.2.2 Figure 6-5

Table 2.12. Inertia coefficient and wake amplification factor as function of KC in DNV [2014].

The value of C_{ds} is calculated from 6.7.1.5 in DNV. This is independent of surface roughness if not a circular cylinder.

When performing laboratory tests, minimization of C_{ds} dependence on R_e is recommended. Further information is found in Sarpakaya and Isaacson [1982].

$$F = \rho C_M V \frac{du}{dt} + \frac{1}{2}\rho C_D A u \mid u \mid = F_m + F_d \tag{2.27}$$

where

ρ	density of water
V	volume of body per meter/displaced volume of water
u	fluid particle velocity
C_M	inertia coefficient
C_D	drag coefficient
A	shadow area of body per meter which is equal to the diameter, D
η	surface elevation of the wave
h	water depth
F_m	inertia force component
F_d	drag force component

Equation 2.27 has two components which are out of phase since the maximum acceleration and velocity take place at different times:

- Inertia force F_m, representing the force on a body in a uniformly accelerated flow of an ideal fluid
- Drag force F_d, representing the force on a body in a steady flow of a real fluid

In this case, the forces are integrated from the bed $z = -h$ to incoming wave surface $z = \eta$. Appropriate wave theories are used to find the wave surface elevation, velocities and accelerations.

Morison equation predicts accurately the peaks but not the force time variation. Slamming forces can also be included by adding a third contribution F_i as shown in Equation 2.28 and Equation 2.29 in Hallowel et al. [2015]. The impact area is taken as the crest elevation times the curling factor λ equal to $0.4 - 0.5$ for vertical cylinders.

$$F = F_m + F_d + F_i \tag{2.28}$$

$$F_i = \rho C_s R c^2 \tag{2.29}$$

$$KC = \frac{v_{max} T}{D} \tag{2.30}$$

$$R_e = \frac{Dv}{\nu} \tag{2.31}$$

$$\beta = \frac{R_e}{KC} \tag{2.32}$$

$$C_M = 1 + C_a \tag{2.33}$$

$$C_a = \frac{\text{added mass}}{\text{mass of fluid displaced}} \tag{2.34}$$

where

v_{max}	is the maximum particle velocity
T	wave period
D	diameter of the structure
C_a	added mass coefficient
v	fluid velocity
ν	kinematic viscosity of the fluid
F_i	slamming force per meter
R	radio of the structure
C_s	slamming coefficient equal to π for no pile effect.
c	wave celerity

The inertia coefficient C_M can be defined in terms of added mass coefficient C_a as in Equation 2.33. The added mass is defined as the inertia added to a system when a body moves in a fluid with certain acceleration. It is modelled as a fluid volume moving with the body.

Dominating wave forces in small structures where $D/L < 0.2$ can be identified from KC values as follows:

- $KC < 5$: Inertia dominated wave forces ($C_M = 2$ for circular cylinder)
- $KC > 40$: Drag dominated wave forces (separation occurs)
- $5 < KC < 40$: Both important(Morison equation). C_M and C_D dependent on KC, Re and roughness.

The presence of boat landing and J-tubes in the structure can alter the flow around the pile and consequently also drag and inertia coefficients. The next section describes the state-of-the-art related to this subject.

2.6 Effect of boat landing on wave forces on monopiles

The flow around cylinders involves many different phenomena. The most important would be vortex shedding, separation and turbulence. Using potential theory, the flow can be represented as a uniform steady flow in combination with a doublet. Even though potential theory is used for ideal flow and not real, it might be used to estimate velocities at secondary structure position.

It is possible to obtain the velocity of the steady disturbed flow at the positions where the boat landing will be placed as seen in Equation 2.37 (See Figure 2.5). The velocity value will depend on the distance between the monopile and the secondary item and the angle.

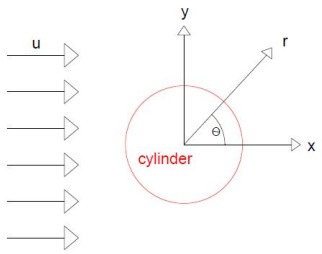

Figure 2.5. Cartesian and cylindrical coordinates for potential flow.

$$v_r = U\left(1 - \frac{R^2}{r^2}\right) cos\theta \tag{2.35}$$

$$v_\theta = -U\left(1 + \frac{R^2}{r^2}\right) sin\theta \tag{2.36}$$

$$v = \sqrt{v_r^2 + v_\theta^2} = U f_{flow} \tag{2.37}$$

$$f_{flow} = \sqrt{1 + \left(\frac{0.5D}{r}\right)^4 - 2\left(\frac{0.5D}{r}\right)^2 cos\left(\frac{2(\alpha - \theta)\pi}{180}\right)} \tag{2.38}$$

where

- r distance between cylinder centers
- D cylinder diameter
- α wave direction
- θ angle of boat landing with respect to monopile center
- U undisturbed flow velocity
- R cylinder radius

It is important to remember that no viscosity is considered in potential flow theory. In real fluids, separation occurs at approximately $\theta = \frac{\pi}{2}$ and thus, velocities at the rear side of the cylinder are different from above.

The previous formulae accounts for steady flow. If oscillatory flow is considered, the velocities in cylindrical coordinates are defined as in Equation 2.39 and Equation 2.40 from Moe [2008]:

$$v_r = g_o sinwt \left(1 - \frac{R^2}{r^2}\right) cos\theta \tag{2.39}$$

$$v_\theta = g_o sinwt \left(1 + \frac{R^2}{r^2}\right) sin\theta \tag{2.40}$$

$$g_o = \frac{g\eta_a}{w} \frac{cosh(z+h)}{coshkh} \tag{2.41}$$

While accounting for two cylinders, boat landing or J-tubes and monopile, the interaction between them will change the conditions cited above and consequently, drag and inertia coefficients, vibrations and forces on monopile.

A way to approach the problem could be considering the flow around a cylinder close to plane wall, since the boat landing size compared to the monopile is very small $D_b/D = 0.065$ approximately where D_b is the boat landing diameter and D is the pile diameter. Here, Reynolds number and the distance between cylinders condition drag and lift coefficients. Some researchers as Taneda [1965], Roshko and Chattoorgoon [1975], Price and Paidoussis [2002] and Lin and Lin [2005] studied this problem for different range of R_e. Table A.6 in Appendix A shows values for drag coefficient accounting for flow around circular cylinder near a plane boundary from some experimental studies.

There are also many studies about interaction between two cylinders in tandem arrangement where normally both cylinders have the same diameter but quite less regarding cylinders placed in parallel.

Wall-effect is also considered in DNV, where the values of drag and inertia coefficients of a cylinder placed close to a wall are found from figures 6-7 and 6-9 in the code. These curves correspond to Equation 2.43 and Equation 2.42.

$$\frac{C_D}{C_{D\infty}} = 2 - arctan\left(10\frac{d_m}{D}\right)\frac{2}{\pi} \tag{2.42}$$

$$\frac{C_M}{C_{M\infty}} = 2.29 - 1.29arctan\left(10\frac{d_m}{D}\right)\frac{2}{\pi} \tag{2.43}$$

where

d_m	gap or space between the wall and the cylinder
D	cylinder diameter
$C_{D\infty}$	drag coefficient for the cylinder in undisturbed flow
$C_{M\infty}$	inertia coefficient for the cylinder in undisturbed flow

In Yokoi and Hirao [2013], the interaction vortex around two parallel cylinders is studied. Different gap ratios, cylinder sizes and shapes are tested. In the case of two cylinders of different size, which is the most relevant for our case, the aspect of vortex shedding seems to depend on the gap ratio, being a single vortex street for $d_m/D = 0.16$, based gap flow for $d_m/D = 0.3$ and 0.6 and coupled vortex streets for $d_m/D = 2.5$.

Once the drag and inertia coefficients are obtained for the secondary item, it is reasonable to think that the total force on the monopile will be the sum of the individual forces from the boat landing and the monopile. If the influence of position and disturbed flow wants to be taken into account, the velocity and acceleration at the boat landing position calculated from stream function for an incoming wave should be multiplied by the factor f_{flow} in equation 2.38. The drag coefficient for the secondary structure is obtained from equation 2.42. If dividing the drag force on secondary structure(Equation2.44) by the drag force on monopile, a contribution C_{Dc} can be added to the drag coefficient for monopile and therefore an equivalent drag coefficient for the system can be obtained from Equation 2.45. The same procedure is done for the inertia coefficient in Equation 2.47.

$$F_D b = \frac{1}{2}\rho C_D (U f_{flow})^2 D_b \tag{2.44}$$

$$C_{De} = C_{Dmonopile} + C_{Dc} \tag{2.45}$$

$$C_{Dc} = C_{D\infty} f_{flow}^2 \left(\frac{C_D}{C_{D\infty}}\right)\left(\frac{D_b}{D}\right) \tag{2.46}$$

$$C_{Me} = C_{Mmonopile} + C_{Mc} \tag{2.47}$$

$$C_{Mc} = \left(C_{M\infty} - 1 + \frac{C_M}{C_{M\infty}}\right) f_{flow} \left(\frac{D_b}{D}\right)^2 \tag{2.48}$$

where

D_b secondary structure diameter
D monopile diameter

Segeren [2011] includes also the influence of secondary structures into the hydrodynamic coefficients and the results for different codes are compared for smooth and rough piles (DNV-OS-J101,GL,API and ISO 19902).

The proposed equations for modified drag and inertia coefficients are as follows:

$$C_{D_{mod}} = C_D \frac{D + D_b}{D} \tag{2.49}$$

$$C_{M_{mod}} = C_M \frac{D^2 + D_b^2}{D^2} \tag{2.50}$$

The total drag force on the structure with secondary element is calculated using a circular cylinder with the diameter D but with the modified coefficient.

The standard codes for offshore structures propose different methods to calculate drag coefficients which lead to variation between 18% and 22% in its value. The difference in wave forces on monopile for marine growth is up to 30%.

The study highlights the noticeable influence of secondary structures such as J-tubes or boat landings as well as the presence of marine growth on wave forces. The increment in forces is given in the following Table 2.13.

Case 1	**1Boat landing and 2J-tubes**		**1Boat landing**		**1J-tube**	
Roughness	F_{max}	M_{max}	F_{max}	M_{max}	F_{max}	M_{max}
DNV - Low	112%	115%	103%	105%	104%	105%
DNV-High	114%	117%	104%	106%	105%	105%
API - Low	111%	114%	103%	106%	104%	105%
API - High	114%	117%	104%	106%	105%	106%
GL	109%	114%	109%	102%	109%	103%

Table 2.13. Increment of hydrodynamic loads due to different secondary steel options using the modified coefficient method [Segeren, 2011].

The previous studies can be used as references to understand the problem related to wave forces on monopiles in general. It is clear that size difference, gap value and position (parallel, tandem, oblique) plays an important role in flow interactions.

The uncertainty in general regarding this topic shows there is scope for further research and analysis in this field and this is the motivation behind the present thesis.

Re-analysis of wave run-up 3

In this chapter, the data from the small scale tests conducted at Aalborg University and the large scale tests at Grosser Wellenkanal, Hannover on slender piles is re-analysed to compare with the previous analysis results.

As mentioned in the previous chapter, wave frequency range below $0.33f_p$ and above $3f_p$ is considered in the re-analysis but not in earlier analysis. The results from both the small scale and large scale tests are used to arrive at the final m-factor values for design equation for run-up.

3.1 Test description

In November 2006, 2D physical model tests were performed in the shallow water flume at Aalborg University (AAU), Denmark. These small scale tests were carried out to analyse how the run-up on piles is affected by ratio of water depth and pile diameter, h/D and ratio of wave height and water depth, H_{m0}/h.

In order to study possible scale effects in the small scale model tests for run-up, some large scale tests from Grosser Wellenkanal (GWK), Germany in 2012 are also analysed, scal 1:50. The test set-ups for small scale and large scale tests are shown in Figures 3.1 and 3.2.

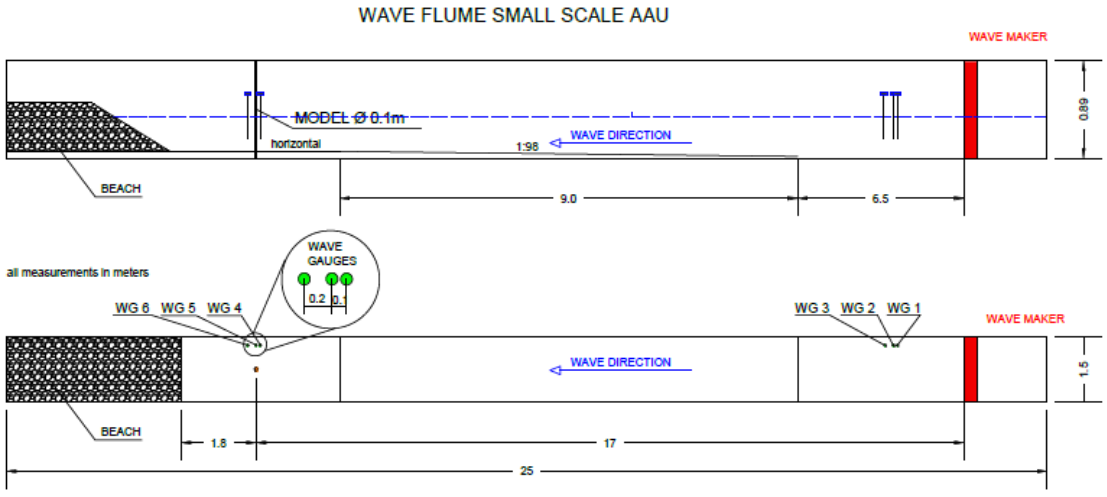

Figure 3.1. Test set up for small scale test at AAU, Denmark [Lykke Andersen and Frigaard, 2006].

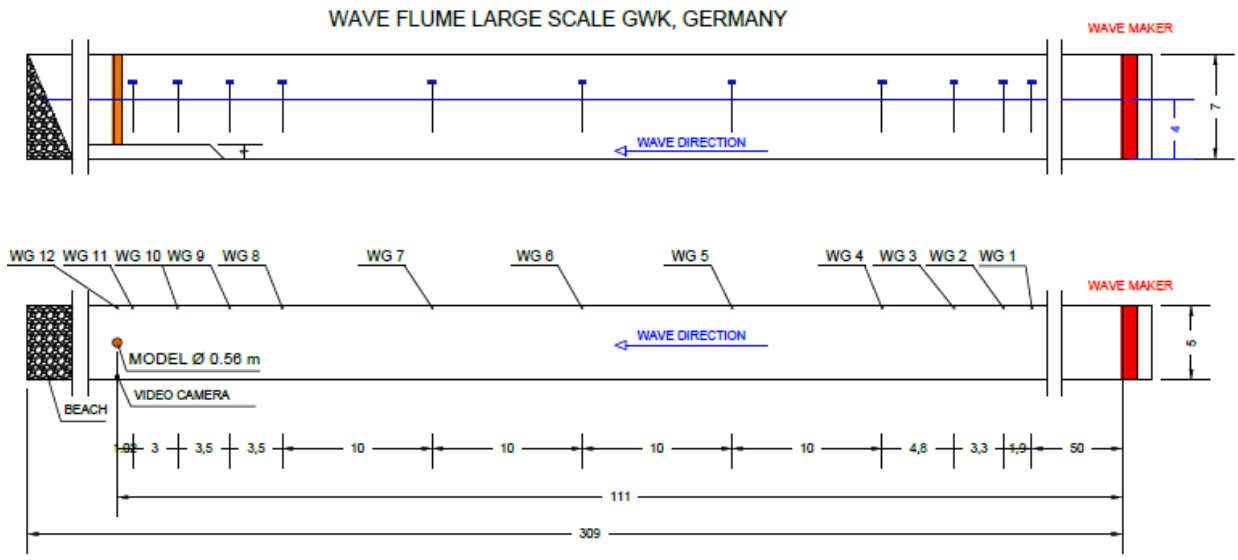

Figure 3.2. Test set up for large scale test at GWK, Germany [Ramirez et al., 2013].

3.2 Small scale tests

The wave spectrums obtained from the small scale lab tests are analysed using reflection and time series analyses in Wavelab. Incident H_{m0} from reflection analysis using the method presented in Skjelbreia and Hendrickson,and total H_{m0} from different channels are plotted in Figure 3.3.

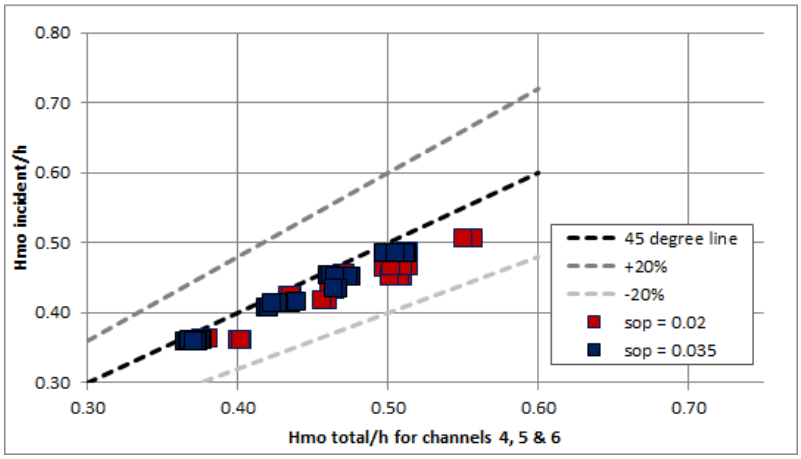

Figure 3.3. H_{m0} from reflection & time series analysis normalised with water depth, h.

It is clearly observed from the plot that H_{m0} from individual gauges is observed to be higher than that from the reflection analysis especially when the waves are high. In Figure 3.4, these waves seem to correspond to the longest waves which give most reflection from a beach.

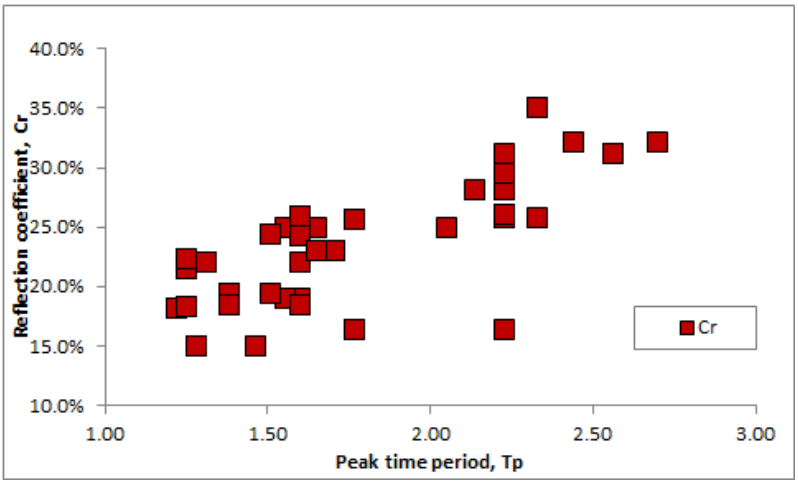

Figure 3.4. Reflection for short and long waves.

Further, it is observed from Figure 3.5 that as the reflection coefficient increases, the difference between total and incident H_{m0} increases. The influence of reflection is evident from all the above plots. Taking also into account the fact that reflection analysis would give more conservative results for m-factor, reflection analysis has been performed here to calculate the run-up.

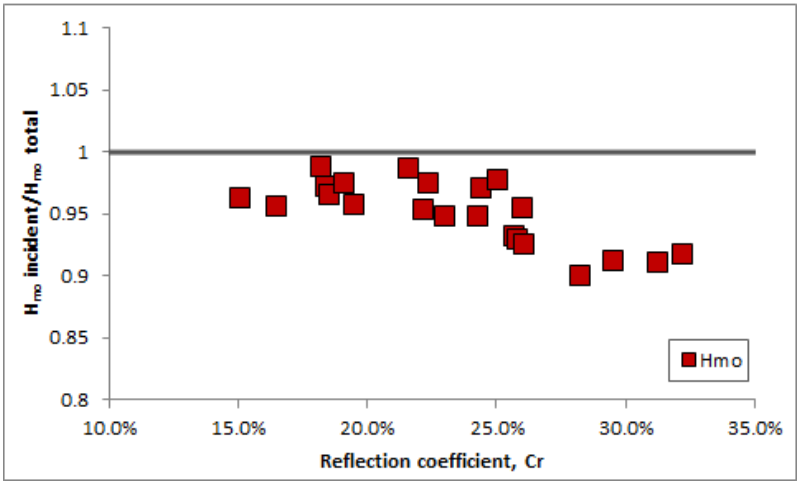

Figure 3.5. Comparison of wave heights from reflection & time series analysis for channel 5 at water depth, h= 0.2.

The software, Stream is used to calculate surface elevation, η_{max} and velocity of the wave particle in the crest, u_{max} by applying stream function. Using the run-up values measured in the small-scale tests, m-factor is calculated using Equation 3.1.

$$m = (R_u - \eta_{max})\frac{2g}{u_{max}^2} \tag{3.1}$$

where

R_u	2% or maximum run-up
η_{max}	2% or maximum surface elevation of the particle in wave crest
u_{max}	2% or maximum horizontal velocity of the particle in wave crest

The m-factor obtained for different wave steepnesses are plotted in Figure 3.6 which are used to calculate R_u using Equation 2.9. These run-up values are referred as R_u^{calc} throughout the report whereas the run-up measured during lab tests are called R_u^{meas}.

The R_u^{calc} values are plotted against R_u^{meas} for different m-factor values and the plots with the data points close to the 45 °line were found to have:

$$m = 1.4 \text{ for } s_{op} = 0.02 \qquad \& \qquad m = 1.8 \text{ for } s_{op} = 0.035 \tag{3.2}$$

This is shown in Figures 3.6, 3.7 and 3.8.

From the relations in Equation 3.2, a linear equation relating m and s_{op} can be calculated as given in Equation 3.3

$$m = 26.67 s_{op} + 0.87 \quad \text{for } 0.02 \leq s_{op} \leq 0.035 \tag{3.3}$$

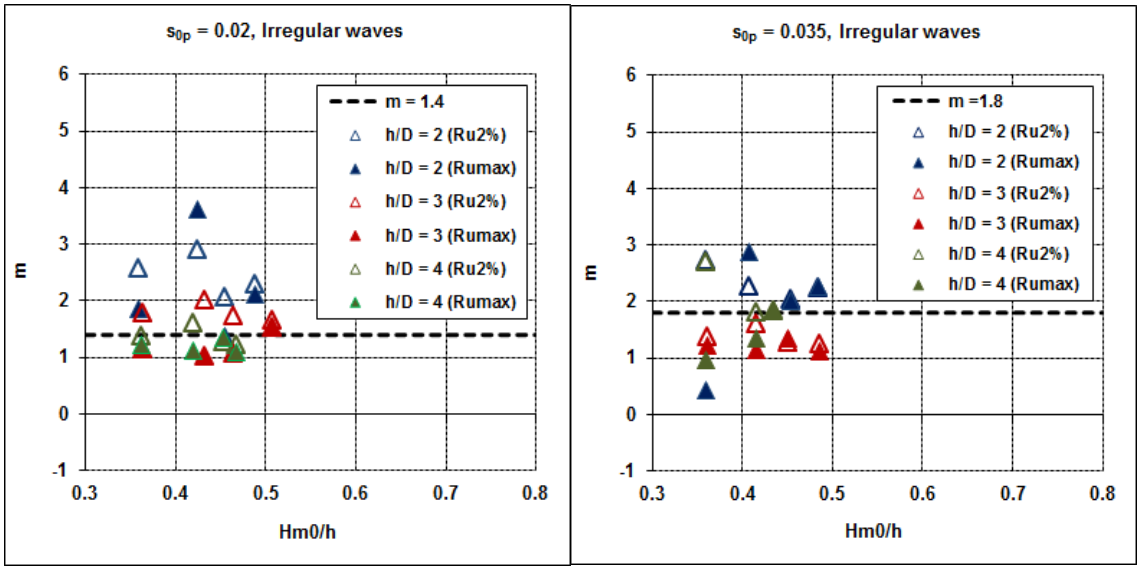

Figure 3.6. Irregular waves: m coefficients for wave steepness,s_{op} = 0.02 & 0.035 with maximum and 2% run up.

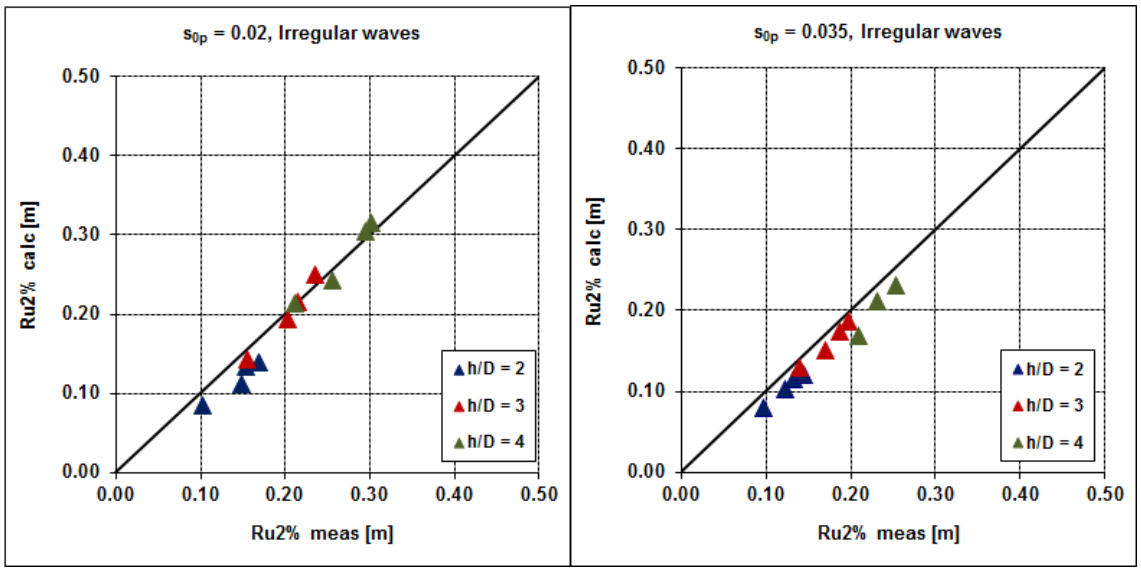

Figure 3.7. Calculated $Vs.$ measured run-up for $R_{u2\%}$ for s_{op} = 0.02 & m =1.4, s_{op} = 0.035 & m =1.8.

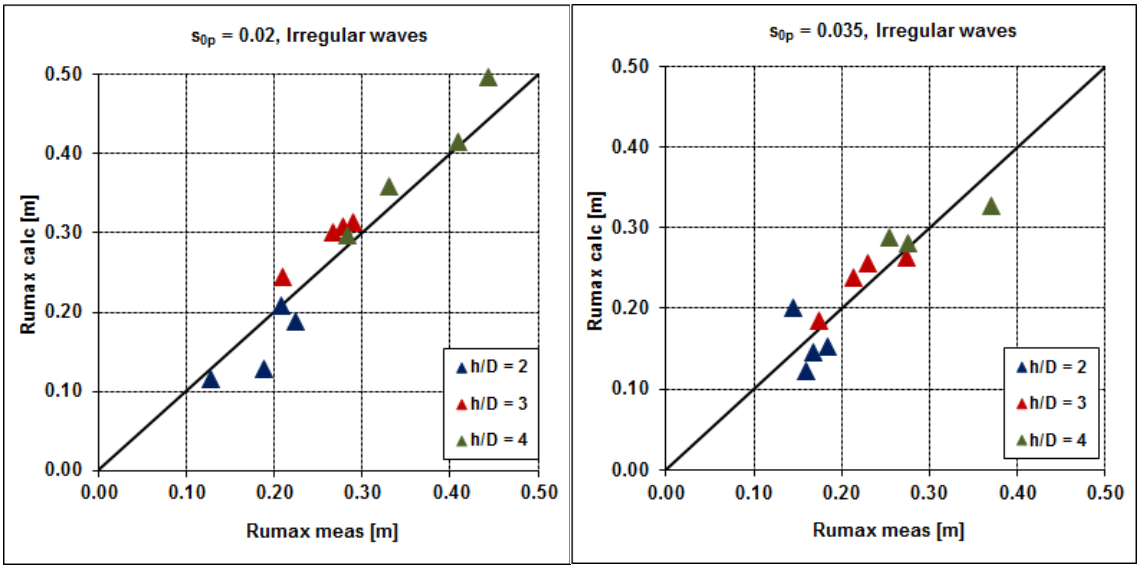

Figure 3.8. Calculated $Vs.$ measured run-up for R_{umax} for s_{op} = 0.02 & m =1.4, s_{op} = 0.035 & m =1.8.

It is therefore concluded that, for irregular waves with steepness between 0.02 and 0.035, m-factor is found to increase with increasing wave steepness. This is in contrary to the conclusions from the previous study conducted at AAU.

It is further observed that the m-factor has decreased to approximate half from the previous analysis (more for long waves and less for steep waves). This is in line with the expectations that when the bandpass filter includes wider frequency range, the wave characteristics of non-linear waves can be better calculated hence providing improved m-factor values.

Equation 3.3 obtained from small scale analysis results is validated in the next section using large scale experiment data.

3.3 Large scale tests

Out of numerous large scale tests conducted at GWK, Germany, three tests with run-up data for irregular waves are analysed here.

The test conditions at the pile for these tests are given in Table 3.1.

	h	Tp	H_{m0}	H_{max}	$H_{2\%}$	S_{op}
Test 1	3	4.7	0.91	1.41	1.16	0.026
Test 2	3	6.0	1.00	1.66	1.23	0.018
Test 3	2	6.0	0.81	1.08	0.96	0.014

Table 3.1. Experimental conditions at the pile for model scale.

Run-up measurements in large scale tests are taken using high speed cameras. These run-ups are divided into three different levels of monopile.

Level A: is the thick layer, level for the green water run-up

Level B: is the level of water and air mixture, where the water layer is no longer attached to the surface of the pile or high spray concentration

Level C: is the level for maximum spray when the spray goes higher than the maximum level marked on the pile. This is hard to measure accurately and is here estimated using the high speed cameras

The large scale data is analysed the same way as the small scale. By use of Equation 3.1 and the R_u^{meas}, m-factor values are calculated and plotted in Figure 3.9 for level A against s_{op}. In Figures 3.10 and 3.11 for levels B and C, Equation 3.3 is multiplied by a factor to fit the data for thin run-ups and spray. The final equations for m and s_{op} are given below:

$$\textbf{Level A} : m = 26.67 s_{op} + 0.87 \tag{3.4}$$

$$\textbf{Level B} : m = 2(26.67 s_{op} + 0.87) \tag{3.5}$$

$$\textbf{Level C} : m = 4(26.67 s_{op} + 0.87) \tag{3.6}$$

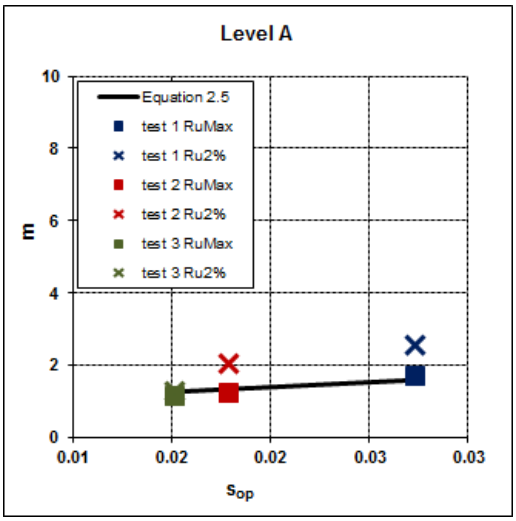

Figure 3.9. Calculated m values for Level A.

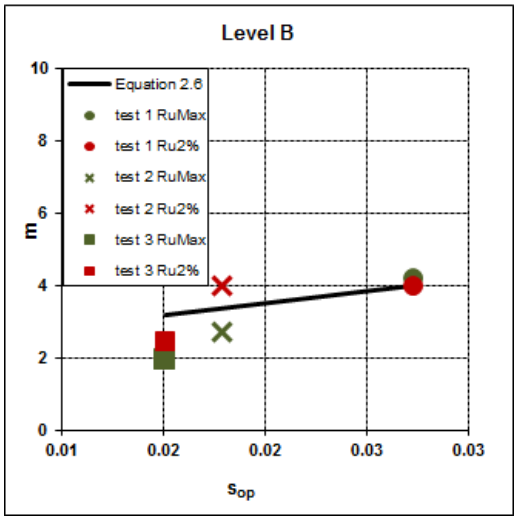

Figure 3.10. Calculated m values for Level B.

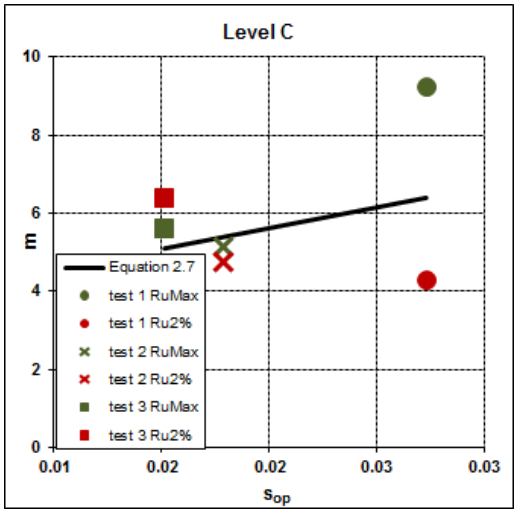

Figure 3.11. Calculated m values for Level C.

In order to validate the relations between m and s_{op}, calculated run-up is plotted against measured run-up and compared with a 45° line in Figures 3.12, 3.13 and 3.14.

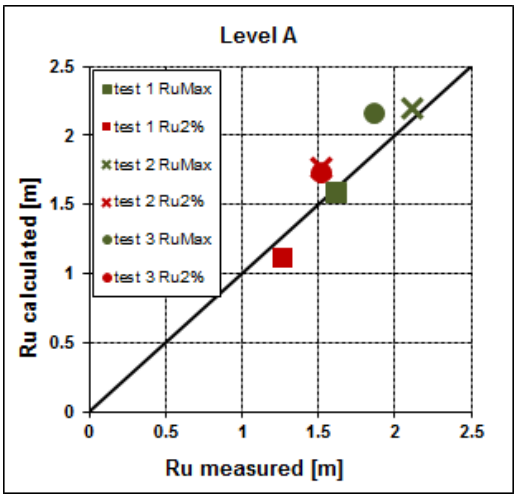

Figure 3.12. Calculated and measured Ru for Level A.

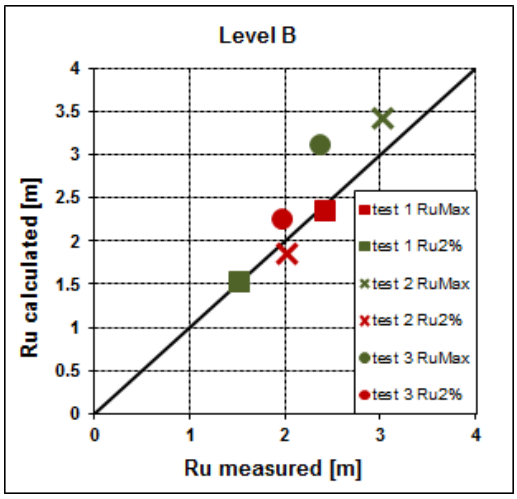

Figure 3.13. Calculated and measured Ru for Level B.

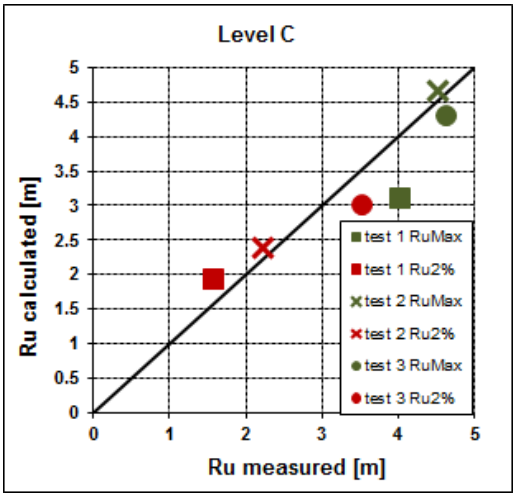

Figure 3.14. Calculated and measured Ru for Level C.

The plots shows that the results for the calculated run-up are mostly similar to the run-up measured are close to the 45°line. This is especially for level A and level B, while there is somehow more scattered results for level C, possibly due to spray formation being very sensitive to detailed wave kinematics.

In order to compare the run-up values from small scale and level A for large scale analyses, R_u normalised with respect to water depth, h and wave height, H_{m0} are plotted together in Figures 3.15 and 3.16.

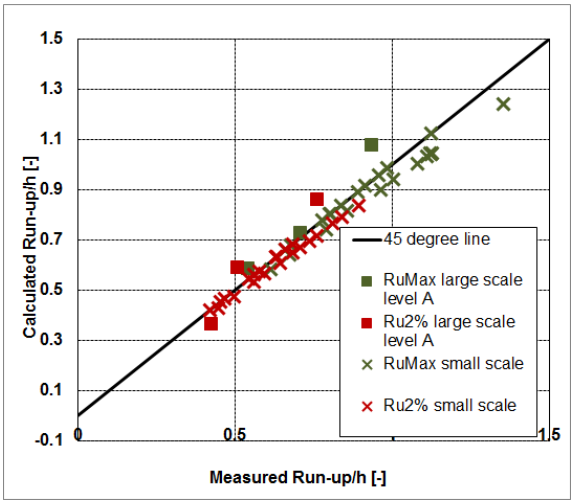

Figure 3.15. Calculated $Vs.$ measured run-up normalised with water depth.

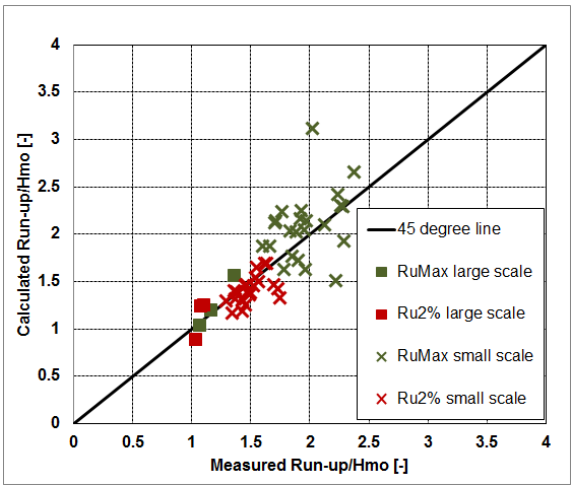

Figure 3.16. Calculated $Vs.$ measured run-up normalised with H_{m0}.

3.4 Relation between wave shape and run-up

The relation between run-up level and wave shape is studied for large scale tests in this section by analysing the slope for the individual waves in test 1 and test 2.

Since incident wave trains are available from the reflection analysis at a given coordinate, the spatial shape cnnot easily be analysed graphically. Instead, the following relation is taken as " frontal slope":

$$slope = \frac{\eta_{max}}{\Delta t} \tag{3.7}$$

where

η_{max} maximum surface elevation of the particle in wave crest
Δt time difference between η_0 and η_{max}

The results are shown in Figure 3.4.

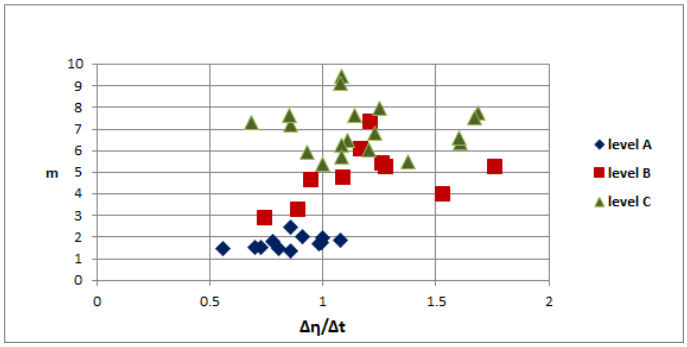

Figure 3.17. Relation between wave shape and m for tests 1 and 2.

For level A, the run-up values are very close and the slope seems to increase. It seems that there is a trend of highest run-up caused by the waves with high frontal slope values in level B, and therefore a higher slope would tend to cause spray or a thin run-up layer. For level C, the scatter is important and more tests should be analysed in order to reach a solid conclusion. Further analysis of focused waves and adopting a method which finds the wave slope in spatial units are recommended.

3.5 Conclusions

From the re-analysis of small scale and large scale data, the following conclusions can be drawn:

1. The small scale tests are found to be compatible with those from level A in large scale
2. For level A, the m-factor values obtained in the re-analysis are approximately half of that of the initial analysis
3. The m-factor values are found to be increasing with increasing levels of run-up

The modified equations for run-up obtained are used in the next chapter to determine the slamming forces on platforms.

Analysis of wave forces on platforms 4

This chapter investigates data from large scale slamming tests conducted in Grossen Wellenkanal (GWK), Hannover, Germany. The aim is to find a slamming coefficient, C_s, to use in the equation for determining the slammming force and pressure. A grate multiplication factor is also calculated to find the effect of porosity of the platforms.

4.1 Test description

A total of 21 irregular slamming tests with different sea states were conducted on different types of platforms placed at varying heights as shown in Table 4.1 and Table 4.2. The platforms used were located at a distance z from the MSWL as seen in Figure 4.1 and with were either solid og grated as illustrated in Figure 4.2. The sea states used were the same as the three run-up tests given in Table 3.1. This is to match the wave run-up with the corresponding slamming event even though they are recorded seperately.

Platform No.	**Solidity [%]**
1	100
2	40
3	20

Table 4.1. Solidity of platforms used in tests.

$$Solidity = \frac{A_{grate}}{A_{solid}} \tag{4.1}$$

where

A_{grate} area of platform with grates
A_{solid} area of solid platform

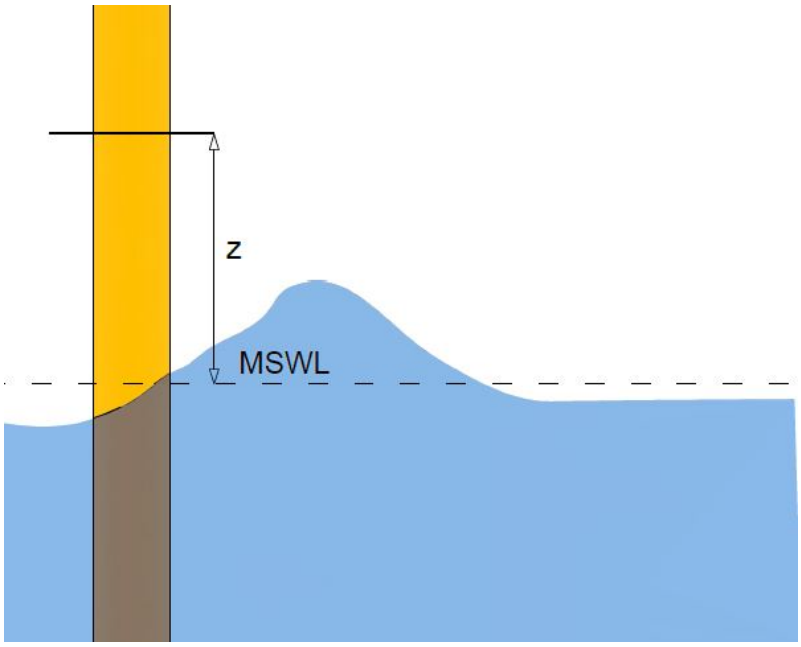

Figure 4.1. Illustration of the grated platforms used in the tests.

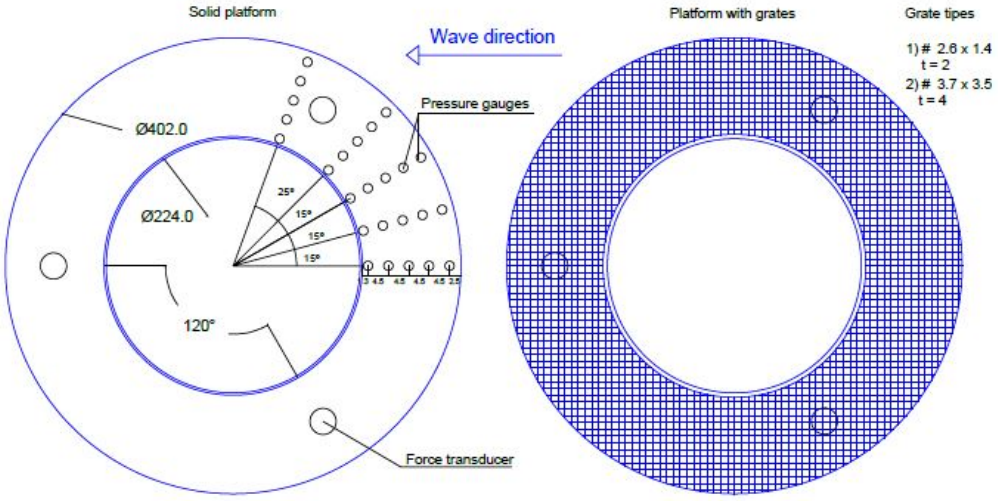

Figure 4.2. Illustration of the solid platforms used in the tests.

Date and test number	Corresponding run-up test	Platform No	z
031109 – 09	2	platform 3	1.75
041109 – 06	2	platform 3	1.50
041109 – 07	1	platform 3	1.50
041109 – 12	2	platform 3	1.25
051109 – 06	1	platform 2	1.25
051109 – 07	2	platform 2	1.25
051109 – 11	1	platform 2	1.00
061109 – 06	2	platform 2	1.53
061109 – 07	1	platform 2	1.53
091109 – 05	2	platform 2	1.75
091109 – 06	1	platform 2	1.75
101109 – 02	1	platform 1	1.75
101109 – 14	2	platform 1	1.75
111109 – 05	2	platform 1	2.25
111109 – 11	2	platform 1	2.00
111109 – 12	1	platform 1	2.00
111109 – 13	2	platform 1	2.00
121109 – 05	1	platform 1	1.50
121109 – 06	2	platform 1	1.50
121109 – 07	3	platform 1	2.00
121109 – 08	3	platform 1	1.50

Table 4.2. Slamming force test for irregular waves conducted.

The slamming is determined either by use of force transducers or pressure gauges placed as seen in the above figures. The pressure gauges could only be installed on the solid platform.

4.2 Analysis of slamming forces and pressures

In this section, the run-up results from Ramirez et al. [2013] and the calculated run-up using m-factor from the previous chapter is used to determine the slamming coefficient, C_s. Two different C_s are obtained from forces and pressure measurements.

4.2.1 Alignment of run-up and slamming tests

Since the run-up and slamming tests are conducted seperately, the first step in the analysis is to match the run-up with each slamming event. A test with same sea state should give similar waves and to verify this the waves are aligned in time as seen in Figure 4.3.

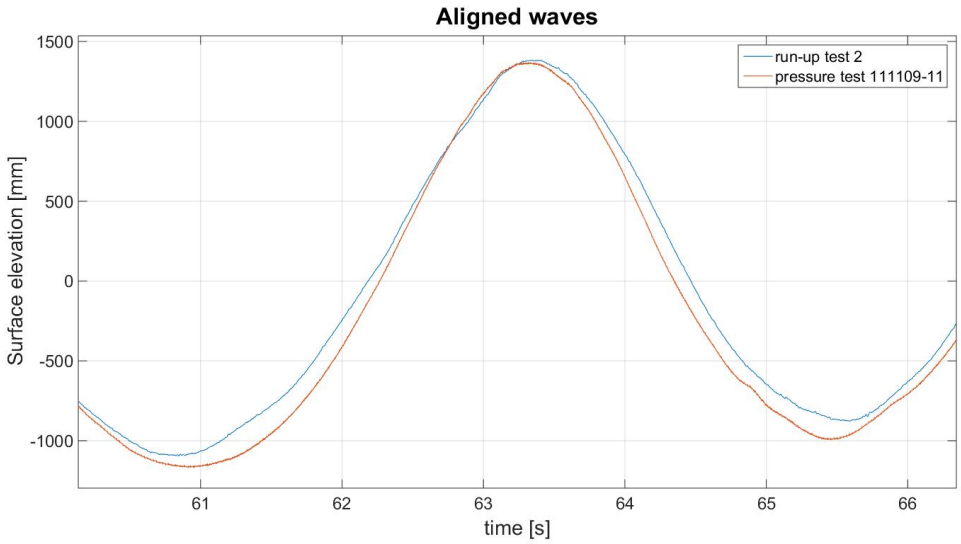

Figure 4.3. Aligning waves from run-up and slamming tests.

4.2.2 Slamming forces

In the analysis of slamming forces, the sum of three force transducer measurements are used. The peak slamming forces from each test are obtained from the peak over threshold method. Figure 4.4 shows the result from test 111109-11. The figure shows force measured and which POT values are used, a long with the run-up value for the three different levels. As seen, the wave run-up does not always result in slamming forces due to the platform being at a higher level.

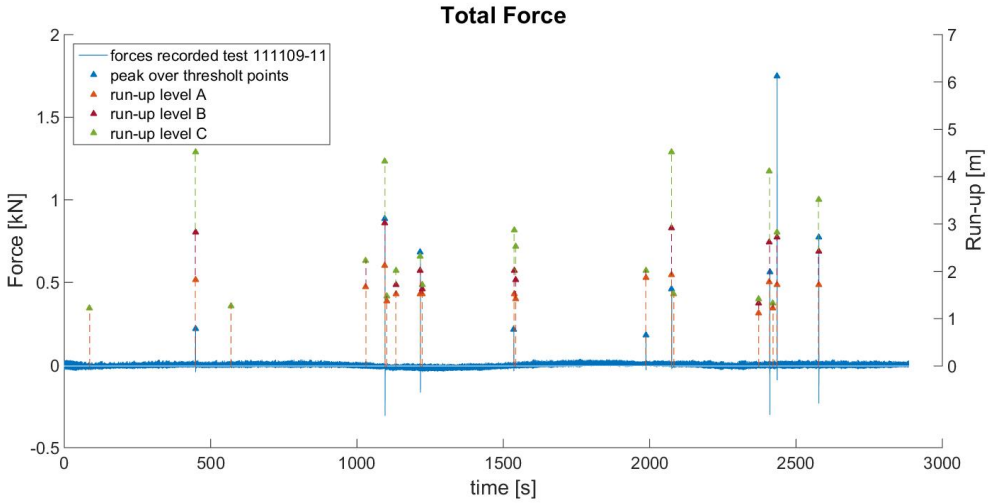

Figure 4.4. Peak over threshold for the force.

The run-up velocity, v, is calculated by use of the measured run-up values and the platform height as seen in Equation 4.2. This velocity is then used in Equation 4.3 to determine the force on the platform.

$$v(z) = \sqrt{2g(R_u - z)} \tag{4.2}$$

$$F_{max} = \frac{1}{2}\rho v^2 C_s A_{ref} \tag{4.3}$$

where

v	run-up velocity
R_u	run-up level
z	distance between the platform and MSWL
C_s	slamming coefficient
A_{ref}	reference area, taken as half the platform area

Table 4.3 shows the results from Test 111109-11. It is important to highlight that the there are 3 calculated force values for each value of measured force. This is because the run-up is divided into three different levels, A, B and C.

Measured force[kN]	$\frac{1}{2}\rho v^2 A_{ref}$ **for level A [kN]**	$\frac{1}{2}\rho v^2 A_{ref}$ **for level B [kN]**	$\frac{1}{2}\rho v^2 A_{ref}$ **for level C [kN]**
0.222	0	2.168	6.664
0.886	0.317	2.697	6.135
0.681	0	0.053	0.846
0.214	0	0.053	2.301
0.182	0	0.053	0.053
0.460	0	2.433	6.664
0.562	0	1.639	5.606
1.750	0	1.904	2.168
0.773	0	1.111	4.019

Table 4.3. Measured total forces and calculated forces without slamming coefficient from test 111109-11.

The table above shows some zero values for level A which is due to run-up measured with the high speed camera for level A is below platform level. The values in italics in Table 4.4 represent the highest run-up value and slamming force and it is seen that in this test they do not occur along at the same time, which might also be the case for other tests as well. Therefore run-up values calculated from Equations 3.4, 3.5 and 3.6 derived in Chapter 3 are also used along with the measured run-up in the following sections to compare the results.

time [s]	Run-up measured level A [m]	Slamming force registered [kN]
448	1.820	0.222
1096	*2.120*	0.886
1217	1.520	0.681
1537	1.520	0.214
1987	1.870	0.182
2075	1.970	0.460
2410	1.770	0.562
2435	1.720	*1.750*
2578	1.720	0.773

Table 4.4. Run up measured and corresponding slamming force from test 111109-11.

The above procedure is conducted for all slamming tests with solid platform. Figure 4.5, Figure 4.6 and Figure 4.7 below display the results with different levels and with measured run-up value and new calculated run-up value. The reference area, A_{ref}, is taken as half the platform area.

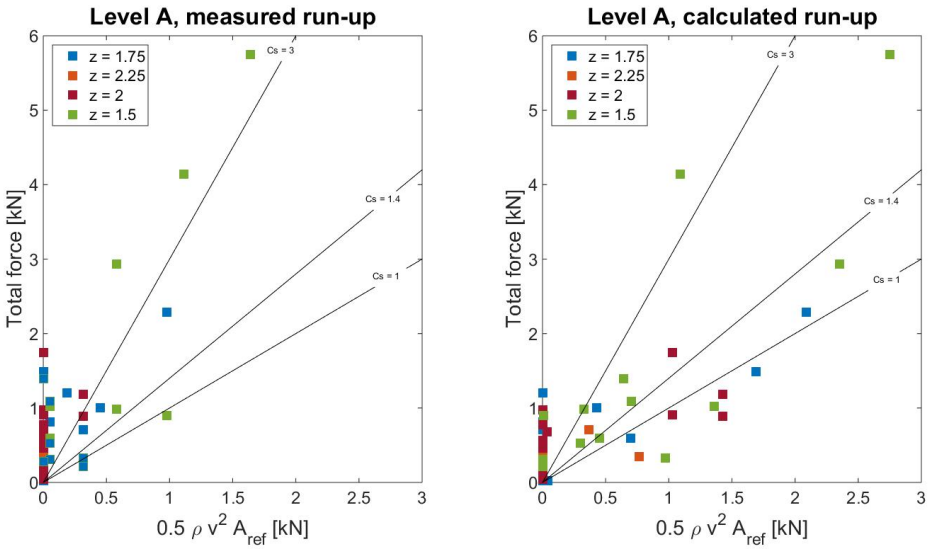

Figure 4.5. Calculated and measured forces for Level A.

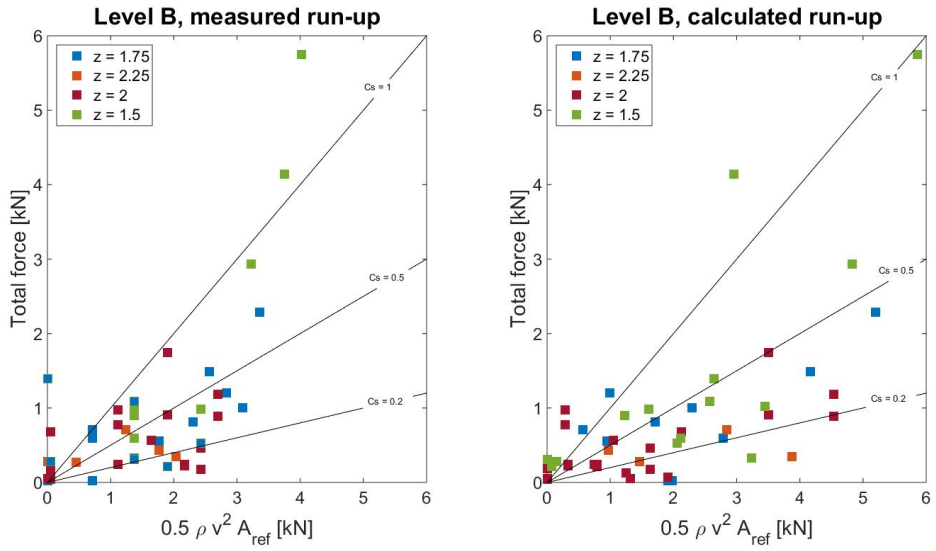

Figure 4.6. Calculated and measured forces for Level B.

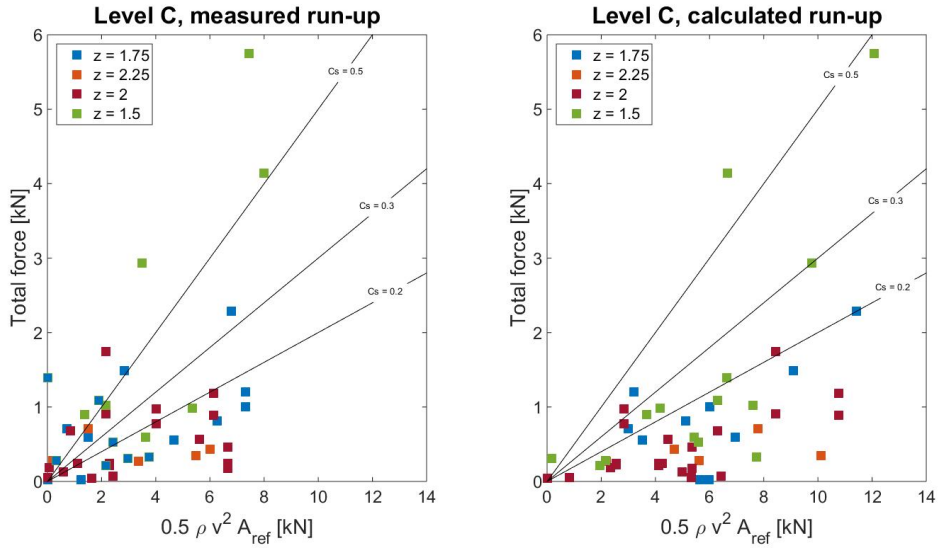

Figure 4.7. Calculated and measured forces for Level C.

It can be seen that for level A, some measurements are located on the y-axis. As discussed earlier, this is due to run-up being lower than the platform height resulting to a velocity, and therefore force becomes equal to zero. With the calculated run-up values, the amount of results lying on y-axis are reduced. Another analysis is performed where the maximum force and maximum run-up value is used regardless of time at which they occur and these results are found in Appendix B.

This problem reduces at level B, and especially in level C, where it is seen that the results are more spread due to higher run-up values. Table 4.5 shows the best fitted values for each level by use of both the run-up measured with high speed camera (R_u HSC) and the calculated run-up values(R_u calculated).

Run-up level	C_s (R_u HSC)	C_s (R_u calculated)
A	3.0	1.4
B	0.5	0.2-1
C	0.3	0-1

Table 4.5. Chosen C_s for different levels and run-up values.

4.2.3 Analysis of slamming pressure

When analysing the slamming pressure the same method as described above is performed. However, now the slamming is recorded by pressure transducers. These are installed only in the solid platform as illustrated in Figure 4.2 and therefore this analysis only include the tests with platform 1 given in Table 4.2.

The maximum pressure is taken from each pressure transducer. Figure 4.8 shows the peak over threshold results from test 101109-14. Again, it is observed that the wave run-up does not always result in slamming due to the height of the platform.

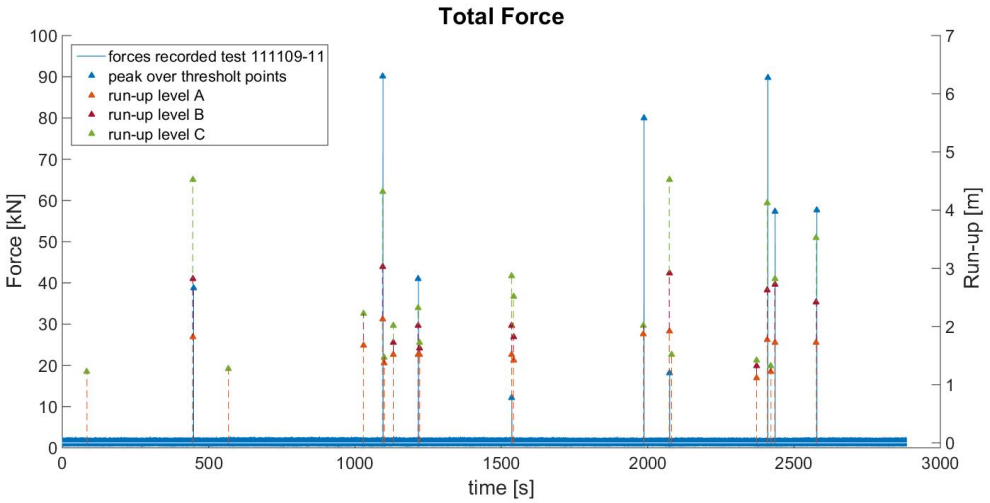

Figure 4.8. Peak over threshold for the pressure.

C_s is then calculated using Equation 4.4 following the same procedure as explained in the previous section.

$$p_{max} = \frac{1}{2}\rho v^2 C_s \tag{4.4}$$

where

p_{max}	maximum slamming pressure
v	run-up velocity
ρ	density of water
C_s	slamming coefficient

Table 4.6 shows the results of test 101109-14 with measured pressure and calculated pressure without slamming coeffcient.

Measured pressure $[kN/m^2]$	$\frac{1}{2}\rho v^2$ **for level A** $[kN/m^2]$	$\frac{1}{2}\rho v^2$ **for level B** $[kN/m^2]$	$\frac{1}{2}\rho v^2$ **for level C** $[kN/m^2]$
27.420	0.687	10.497	27.174
28.320	0	4.611	4.611
273.213	3.630	12.459	25.212
18.767	0	0	2.649
48.890	0	2.649	5.592
37.233	0	2.649	10.987
97.736	1.177	2.649	2.649
77.939	1.668	11.478	27.174
309.988	0.196	8.535	23.250
97.133	0	9.516	10.497
121.463	0	6.573	17.363

Table 4.6. Measured pressure and calculated pressures without slamming coefficient.

Figure 4.9, Figure 4.10 and Figure 4.11 below shows the results for all the tests and with different C_s values to find the best fitted factor.

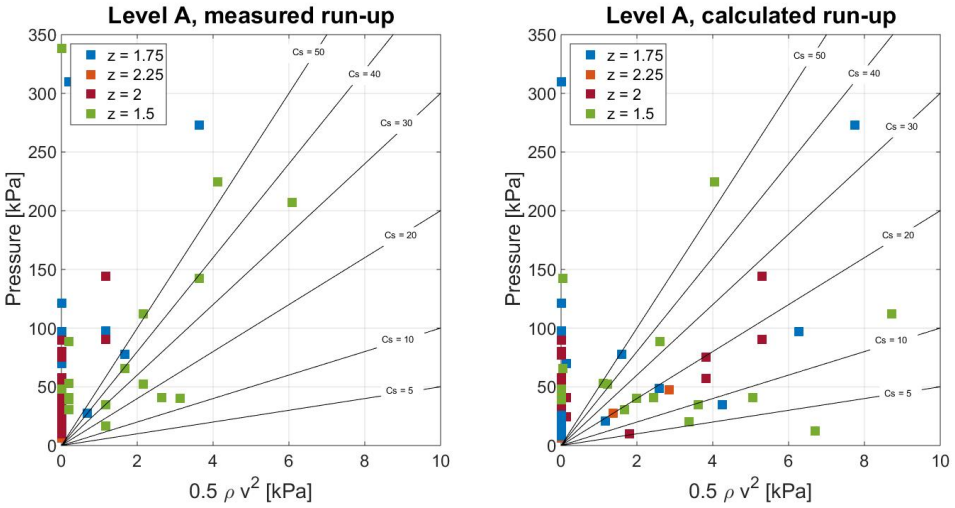

Figure 4.9. Calculated and measured pressure for Level A.

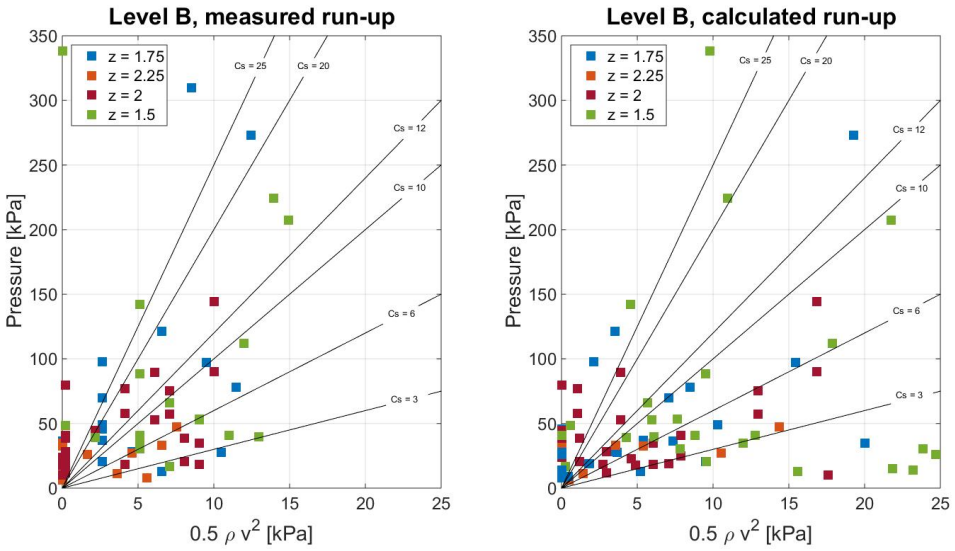

Figure 4.10. Calculated and measured pressure for Level B.

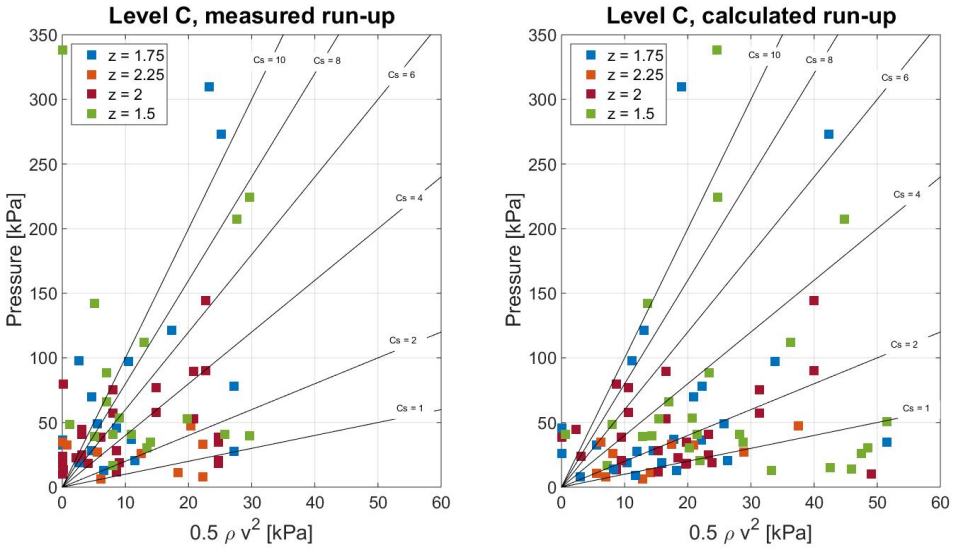

Figure 4.11. Calculated and measured pressure for Level C.

In Appendix D the results for the max slamming pressure can be found.

Table 4.8 shows the best fitted value for each level by use of both R_u HSC and R_u calculated.

Run-up level	C_s (R_u **HSC**)	C_s (R_u **calculated**)
A	50	20
B	12	12
C	8	1-10

Table 4.7. Chosen C_s for different levels and run-up values.

4.3 Analysis of solid platform versus platform with grates

To determine the effect of grates on slamming forces, platform of solidity 20% and 40% have been compared with a solid platform. To make the comparison accurate, only tests with identical sea state and platform height has been compared. The multiplication factor is chosen by use of LMS, the result and corresponding error is given in Table

test	z	solidity	multiplication factor	error [%]
2	1.75	20%	0.20	2.7
2	1.75	40%	0.35	13.0
2	1.5	20%	0.11	10.4
2	1.5	40%	0.14	11.1
1	1.5	20%	0.08	5.0
1	1.5	40%	0.10	0.2

Table 4.8. Multiplication factor found by LMS

Figure 4.12, Figure 4.13 and Figure 4.14 shows the results of test 1 and 2 with different platform heights.

The forces on solid and grated platforms are also sorted and these sorted values are compared with each other in Figure 4.12, Figure 4.13 and Figure 4.14.

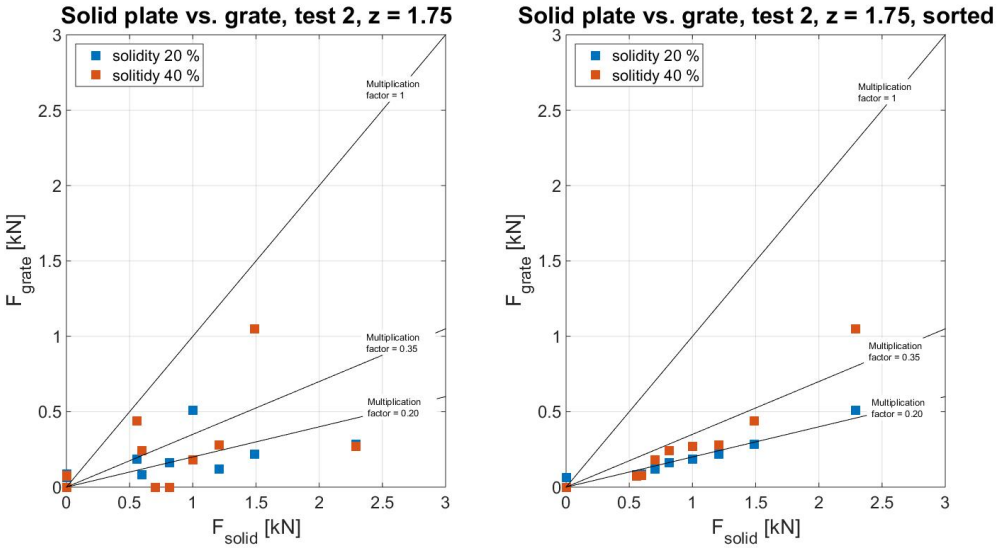

Figure 4.12. Results for test 2 with platform height equal to 1.75.

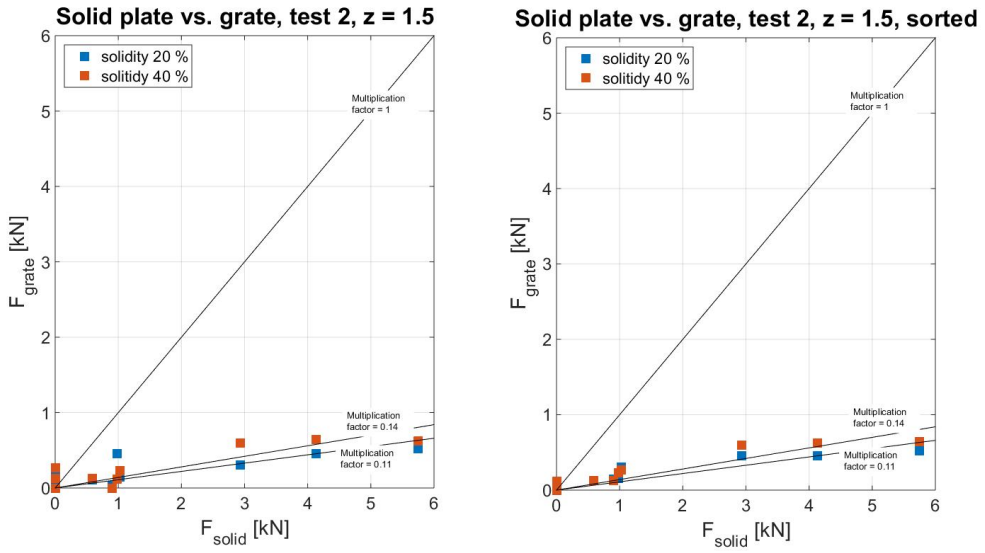

Figure 4.13. Results for test 2 with platform height equal to 1.5.

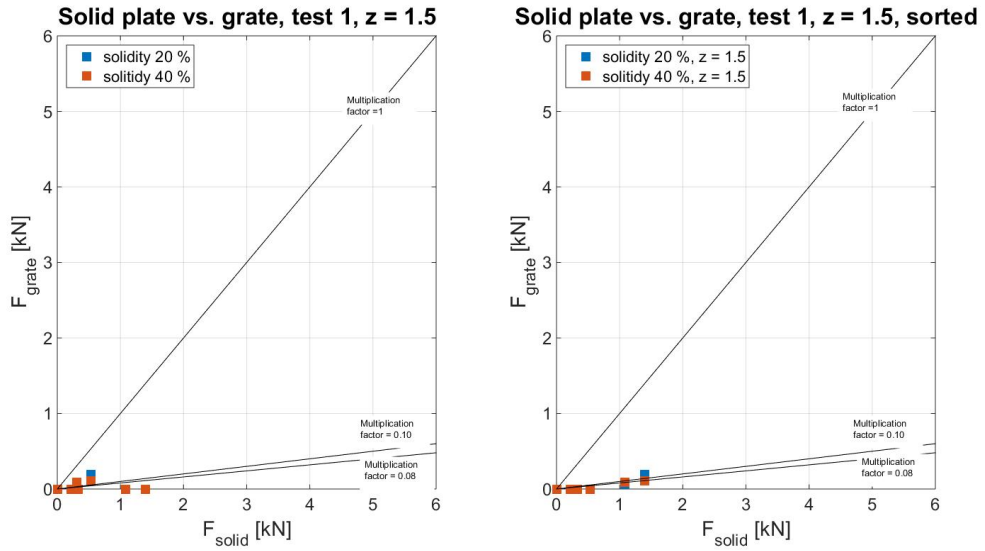

Figure 4.14. Results for test 1 with platform height equal to 1.5.

There are some results showing that the platform with highest solidity gives higher slamming force than the platform with lower solidity. Overall, the solid platform always gives the highest slamming forces as expected. Setting the multiplication factor equal to 0.18 for solidity of 20% and equal to 0.25 for solidity of 40% seems to be optimum.

4.4 Results and conclusion

Slamming coefficient

The recommended C_s values given in one of the previous sections is used for calculating the slamming force and pressure. The measured values and the calculated are compared to confirm the validity of the chosen C_s. The Figures below shows the results.

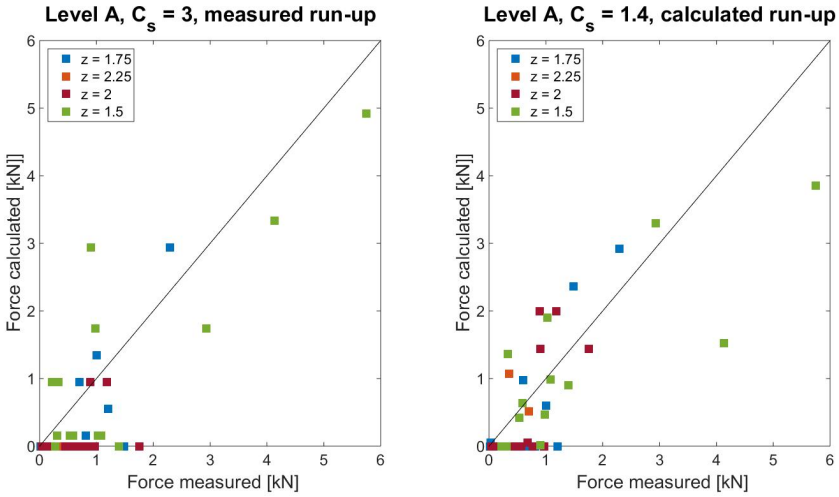

Figure 4.15. Calculated and measured force for level A.

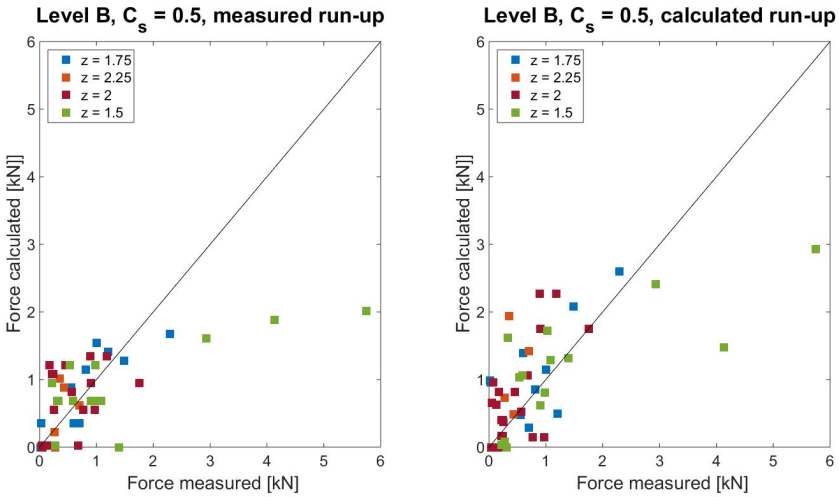

Figure 4.16. Calculated and measured force for Level B.

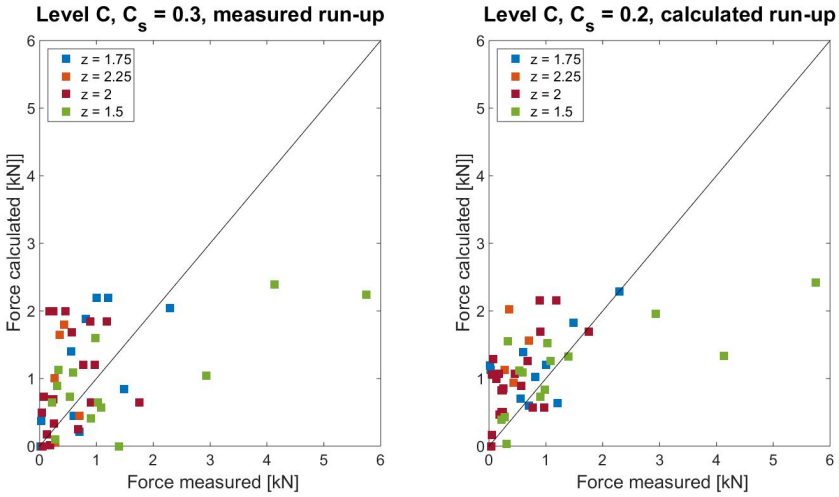

Figure 4.17. Calculated and measured force for Level C

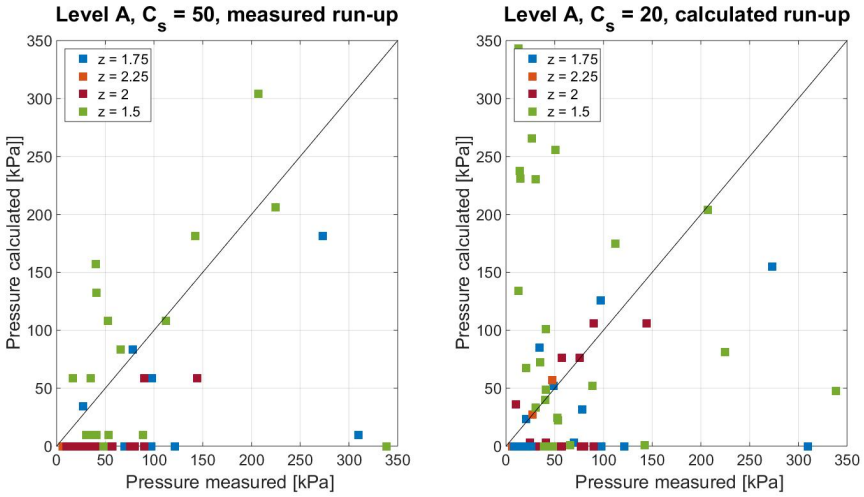

Figure 4.18. Calculated and measured pressure for level A.

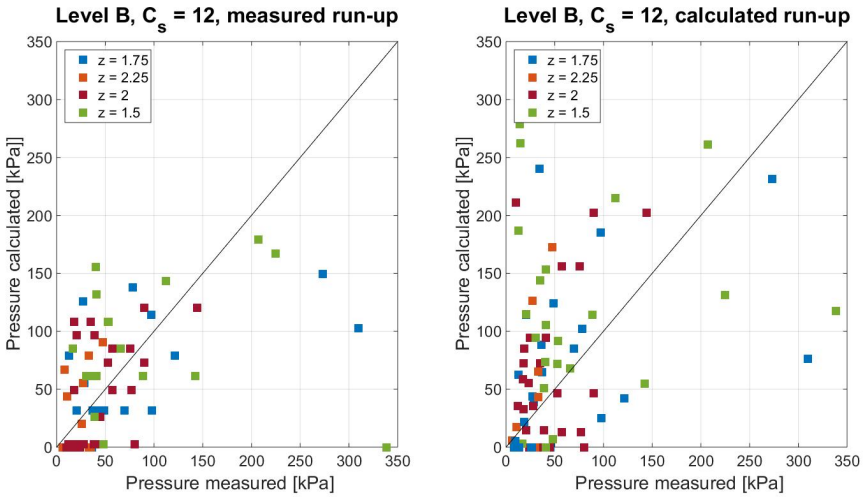

Figure 4.19. Calculated and measured pressure for Level B.

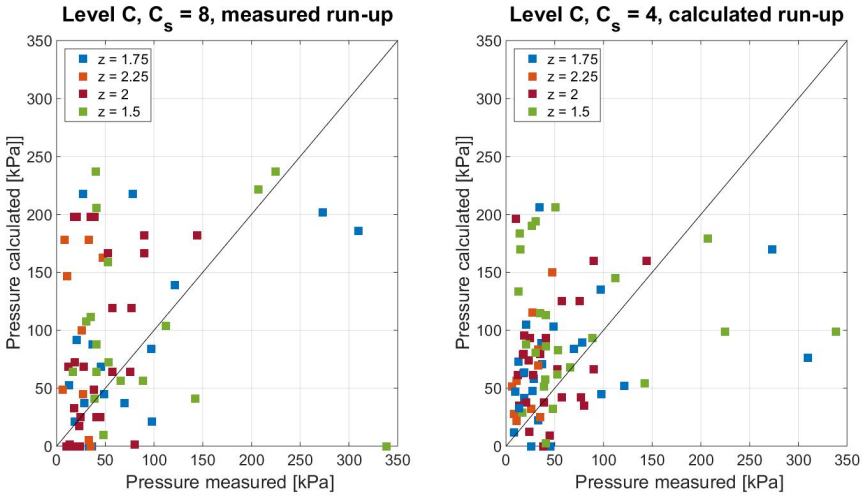

Figure 4.20. Calculated and measured pressure for Level C.

The figures indicates the recommended slamming coefficients are:

- $C_s = 0 - 1$ **for calculating the slamming force for level B**
- $C_s = 0 - 10$ **for calculating the slamming pressure for level C**

Grate multiplication factor

The recommended multiplication factor given in the previous section is used for calculating the slamming force for solid platform to compare with platform with grates. It is used two different multiplication factors depending on the solidity. Figure 4.21 and Figure 4.22 shows the results.

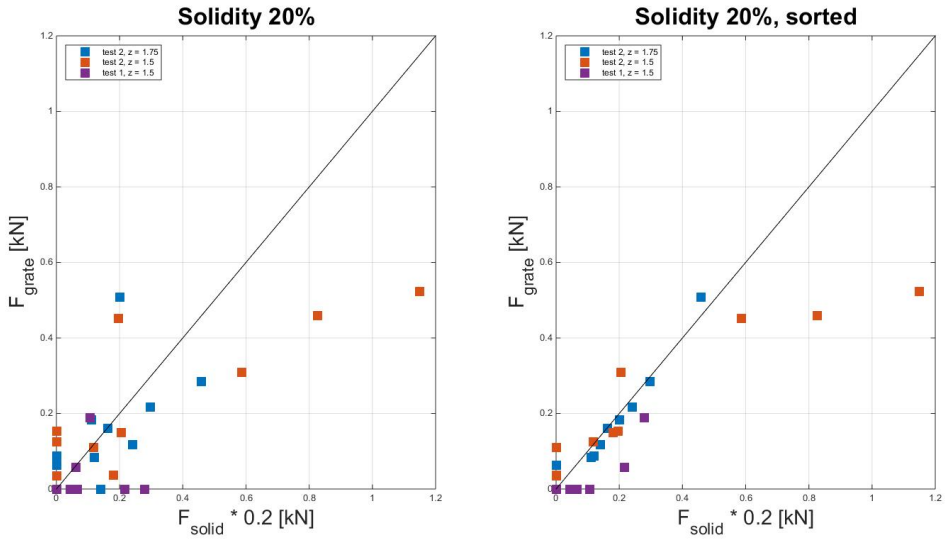

Figure 4.21. Comparison of solid platform and plaform 20% solidity.

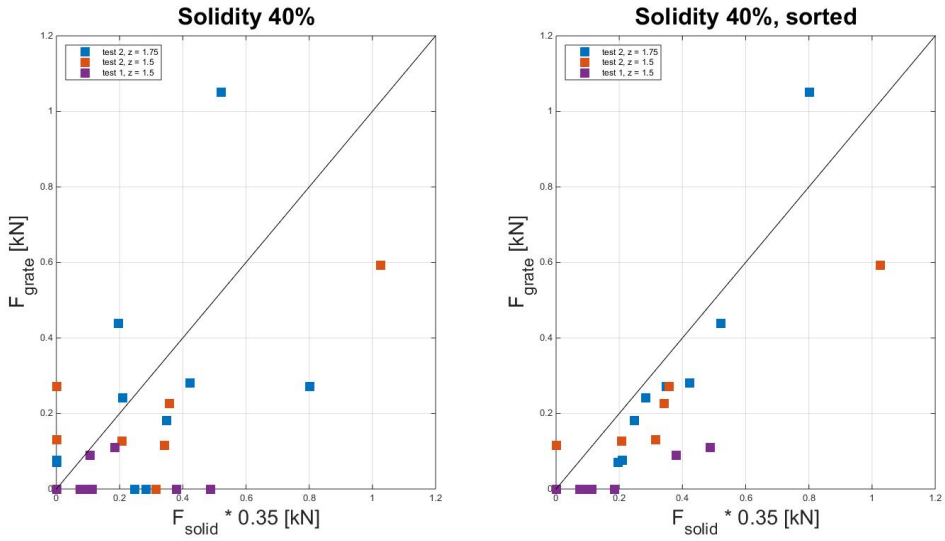

Figure 4.22. Comparison of solid platform and plaform 40% solidity.

The recommended multiplication factors are:

- **Grate factor = 0.20 for calculating platform with grates with solidity of 20 %**
- **Grate factor = 0.35 for calculating platform with grates with solidity of 40 %**

The results of this analysis are valid for cases with following conditions:

- ratio between the pile diameter and the diameter of the platform is 0.55
- ratio between run-up value and pile diameter are between 3.1 and 16.1

Wave forces on secondary structures 5

The last part of this thesis studies the influence of secondary structures on wave forces on monopile foundations. Small scale tests were conducted in the facilities of Aalborg University during February-March 2016 and the results are presented.

5.1 Objective

The objective of the model tests was:

- To analyse and compare the wave forces on the pile with and without simplified secondary structure similar to one element of a boat landing. Further, the effect of position of the secondary structure was also studied

The objective was achieved by attaching a small cylinder of diameter, 0.01 m to a monopile model of 0.16 m. The orientation of the cylinder with respect to the incoming wave was changed during tests.

This was studied for two surface roughnesses (smooth and rough), using two monopile models as shown in Figure 5.1. The rough model was made by gluing sand (Dansand A/S, D_{50} = 1.04 mm) on the surface, which is within the range for surface roughness k for marine growth given in Table 6-1 in Environmental Conditions and Environmental Loads by DNV.

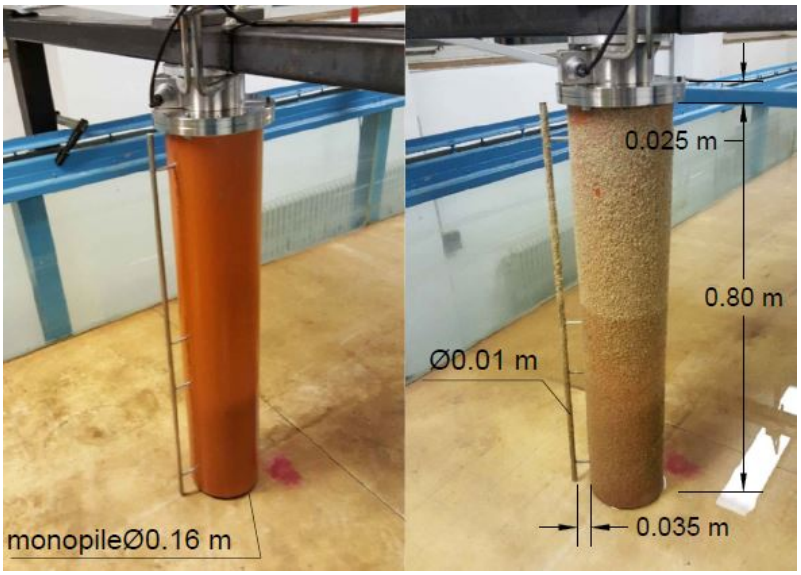

Figure 5.1. Smooth and rough monopile models.

5.2 Test set-up and layout

Figure 5.2 illustrates the layout of the experimental study.

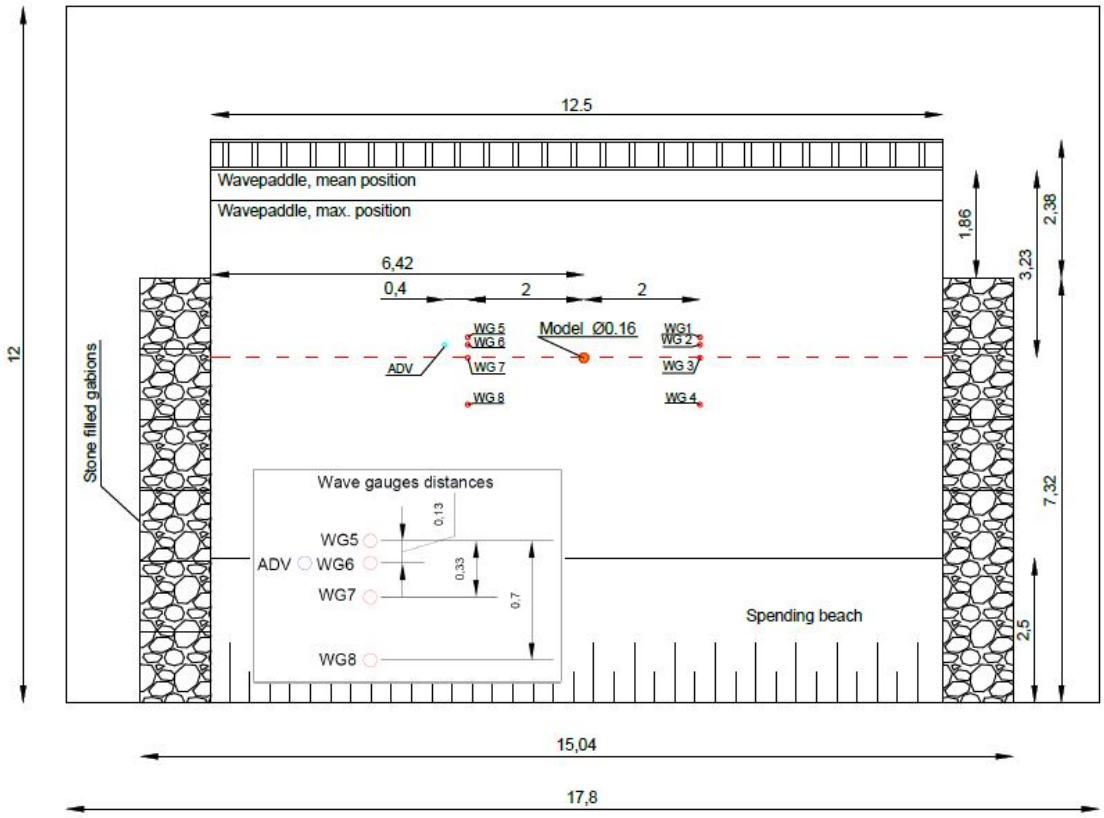

Figure 5.2. Laboratory set up at AAU facilities (annotations in meters).

- **Pile model**: The pile model of 0.16 m diameter was placed at a distance of 3.23 m from the wave paddle and 6.42 m from the left basin wall
- **Wave gauges**: 8 wave gauges (WG) were installed as shown in Figure 5.2. Placing 4 on each side of the model at a distance of $2m$.
- **Force transducer**: The wave forces and moments in x, y and z direction on the model were measured by a Multi-Axis force transducer as shown in Figure 5.3 and Figure 5.4.

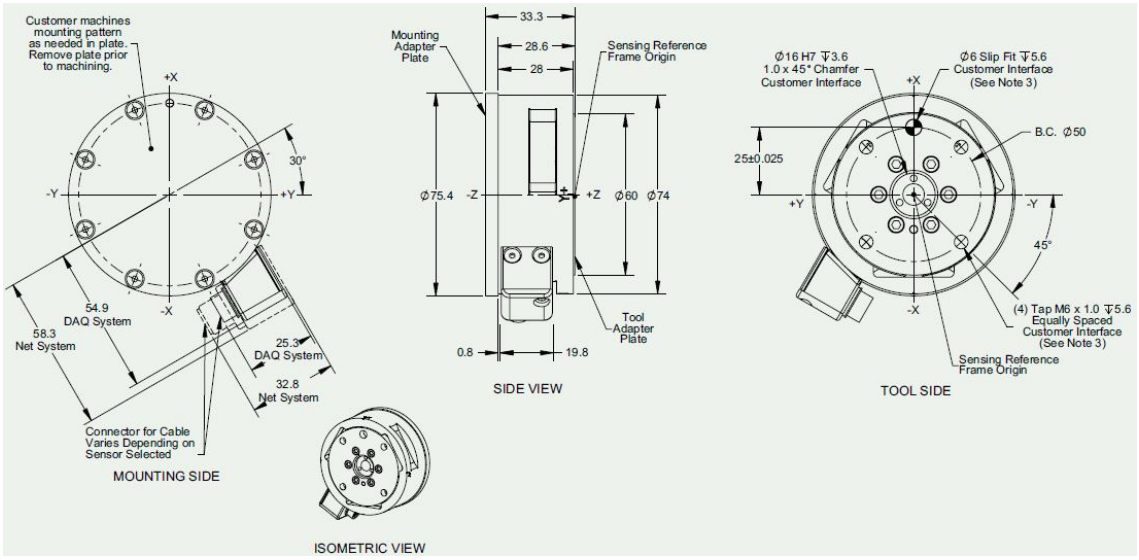

Figure 5.3. Multi-Axis transducer used in the tests [ATI, 2014]

The force transducer used for regular wave tests was replaced during irregular tests by a new transducer with higher range of measurements.

- **Velocity sensor**: A 3-D velocity sensor (ADV) was placed at 2.4 m from the model as shown in Figure 5.2 at a height of 0.23 m from the water bed.

  ADV uses one transmit transducer and four receiver transducers. A glass powder is added to the water for smooth velocity measurements. The recommended concentration is 0.01 g/L. The volume of water in the basin was calculated to be around 54600 L which makes the recommended powder amount to be 546g. Practically, it was observed that for clear measurements, the quantity in the test basin should be at least 250 g.

The sample frequency of all the measurement devices was set to 500 Hz. For the waves with long period waves, high reflection was observed and the beach slope was flattened from 1 : 2.3 to 1 : 3 in irregular tests.

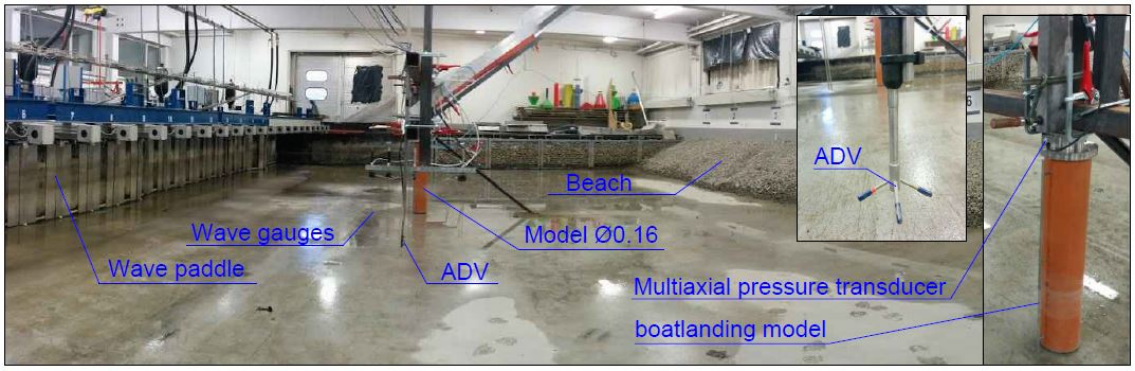

Figure 5.4. Test set up in the basin.

The secondary structure was attached at different angles to the incoming wave. 7 angular positions were tested for regular waves and 3 for irregular waves. These are shown in Figure

5.5.

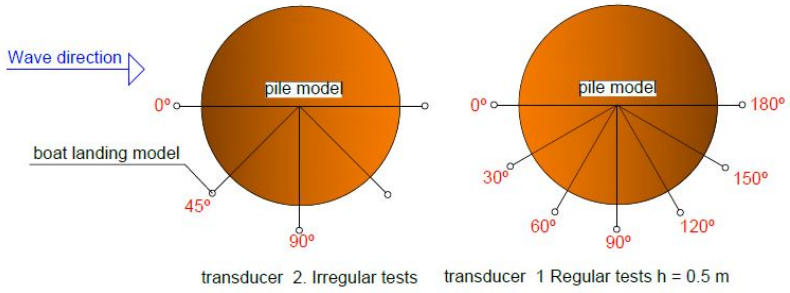

Figure 5.5. Positions for secondary structure.

5.3 Test description

The tests were conducted under regular and irregular wave conditions. The sea states for regular waves are given in Table 5.1 and Table 5.2 and for irregular waves in Table 5.3.

Regular waves	Wave A	Wave B	Wave C	Wave D	Wave E	Wave F
$h(m)$	0.5	0.5	0.5	0.5	0.5	0.5
$H(m)$	0.025	0.05	0.025	0.05	0.025	0.05
$T(s)$	1.26	1.26	1.90	1.90	2.53	2.53
$L(m)$	2.21	2.22	3.82	3.83	5.32	5.34

Table 5.1. Target conditions for tests for smooth and rough models with and without boat landing on smooth pile.

Regular waves	Wave G	Wave H	Wave I	Wave J
$h(m)$	0.45	0.45	0.45	0.45
$H(m)$	0.1	0.2	0.1	0.2
$T(s)$	1.90	1.90	2.53	2.53
$L(m)$	3.73	3.92	5.19	5.49

Table 5.2. Target conditions for tests for smooth model without boat landing on smooth pile.

Irregular waves	Wave K	Wave L	Wave M	Wave N	Wave O	Wave P
$h(m)$	0.45	0.45	0.45	0.45	0.45	0.45
$H_{m0}(m)$	0.125	0.18	0.125	0.2	0.125	0.2
$T_p(s)$	1.26	1.26	1.90	1.90	2.53	2.53
$L(m)$	2.22	2.33	3.73	3.82	5.19	5.49

Table 5.3. Target conditions for tests for smooth and rough model with and without boat landing.

For ease of distinguishing, the different tests conducted are named as shown in Table 5.4 below. The tests will be referred to by these names.

Name	Pile Model	Position of secondary structure
Test s	Smooth	without secondary
Test 0s	Smooth	0°
Test 30s	Smooth	30°
Test 45s	Smooth	45°
Test 60s	Smooth	60°
Test 90s	Smooth	90°
Test r	Rough	without secondary
Test 0r	Rough	0°
Test 30r	Rough	30°
Test 45r	Rough	45°
Test 60r	Rough	60°
Test 90r	Rough	90°

Table 5.4. Naming convention for conducted tests.

Dynamic amplification filter

The model eigen frequency was found and used to filter the data and remove the dynamic amplifcation from the measured forces. The eigen frequency was found to be 10.6 Hz when testing regular waves and 13.5 Hz for irregular tests due to the use of different force transducers. See Table C.1 with eigen frequencies. An unnatural behaviour for the eigen frequency for the model without water was found, probably due to experimental set up. These disturbances are shown in the left picture in Figure 5.6, while the right one illustrates the eigen frequecy test for the irregular tests model.

The dynamic amplification filter used for irregular tests is shown in Figure 5.7.

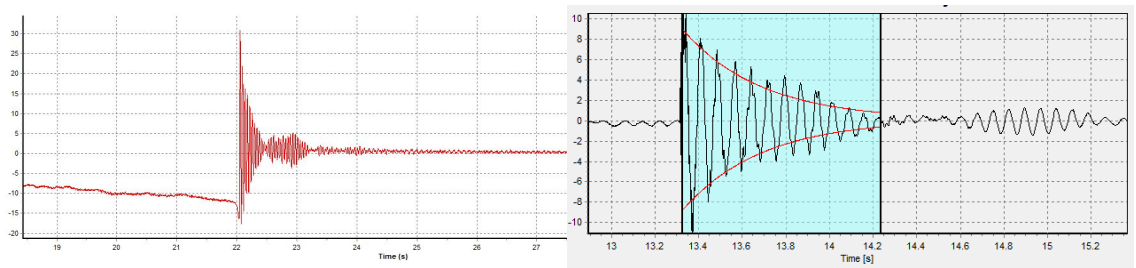

Figure 5.6. Disturbance in eigen frequency test for rough model with secondary structure at 90º.

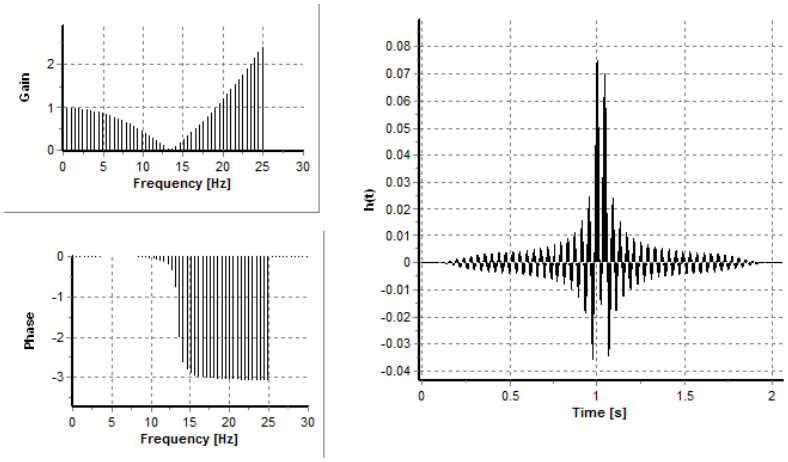

Figure 5.7. Dynamic amplification filter applied on data.

5.4 Results

In this section the results from the laboratory tests are discussed in detail.

5.4.1 Regular waves

Figure 5.8 compares the surface elevation, η and force, F_x for wave A which is inertia dominated. The surface elevation measurements shown are from wave gauge 3, referred as $WG3$.

No significant difference in F_x is observed with and without secondary structure or between secondary structure at different positions. See Appendix C for the time series of the rest of regular waves.

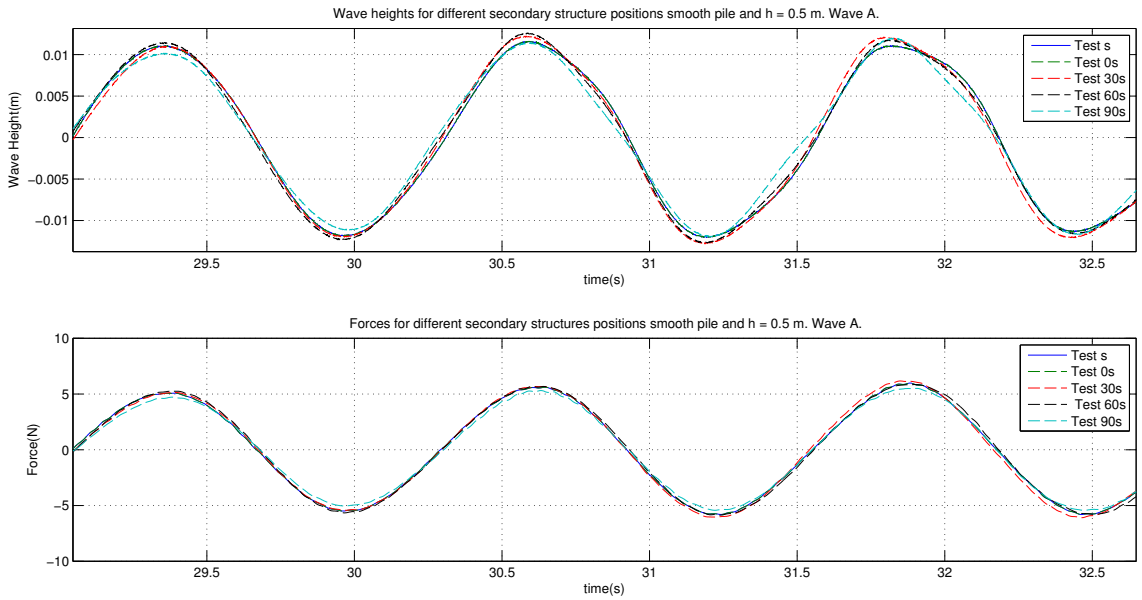

Figure 5.8. Wave forces for smooth pile with and without secondary structure at different positions for wave A.

5.4.2 Irregular waves

A total of six irregular sea states with at least thousand waves each, were tested for all the different configurations of monopile and secondary structure cited before. JONSWAP spectrum with a peak enhancement factor of 3.3 is used for the sea states.

The time series for surface elevation, η and F_x for wave K is shown in Figure 5.9. The results for the rest of the waves are shown in Appendix C.

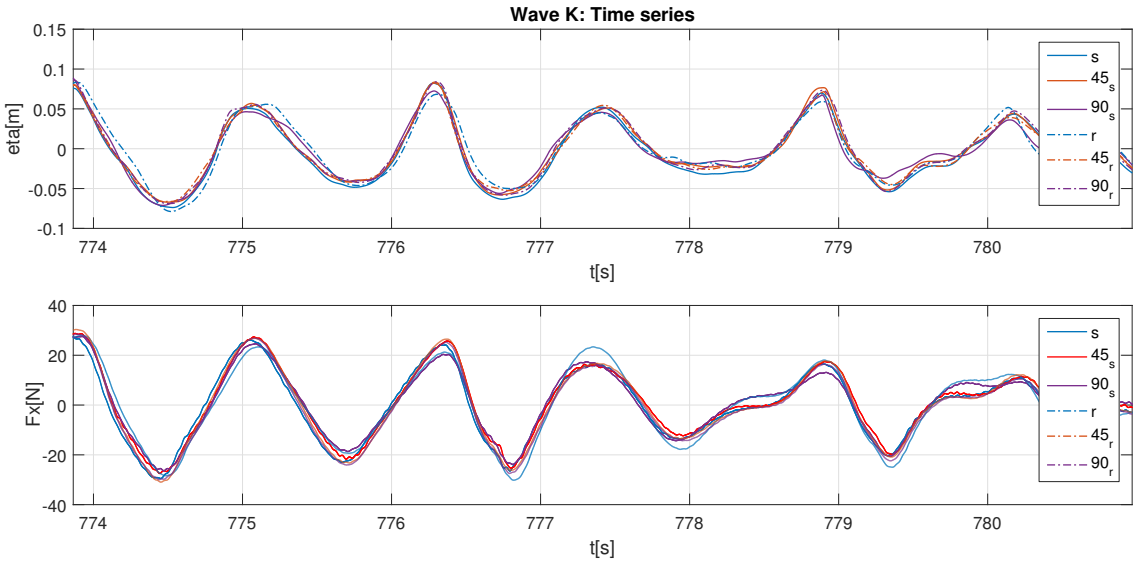

Figure 5.9. Time series for surface elevation for wave K tests.

It is clear that not all tests have similar wave shapes which is assumed to be due to minor water level fluctuations during tests. In some waves the reflection coefficient was found to be high, hence these tests are excluded from further analysis.

Weibull fitting of results

Since it is difficult to determine the difference between the forces directly from the time series of irregular waves, the peaks for wave height, H and force F_x are fitted with Weibull distribution and plotted together. These Weibull plots are shown in Figures 5.10-5.17.

A Weibull 2-parameter distribution with maximum likelihood method (MLM) is used to fit 100 highest peaks of both F_x and H. In Figures 5.10, 5.12, 5.14 and 5.16, the waves for the highest or extreme F_x peaks are highlighted in boxes and the waves for these peaks are shown as inset plots. This is to observe the wave shape and steepness of the extreme peaks. As it can be seen from the plots, these waves tend to be steep and almost on the verge of breaking.

The distribution plots for remaining waves L and N are shown in Appendix C.

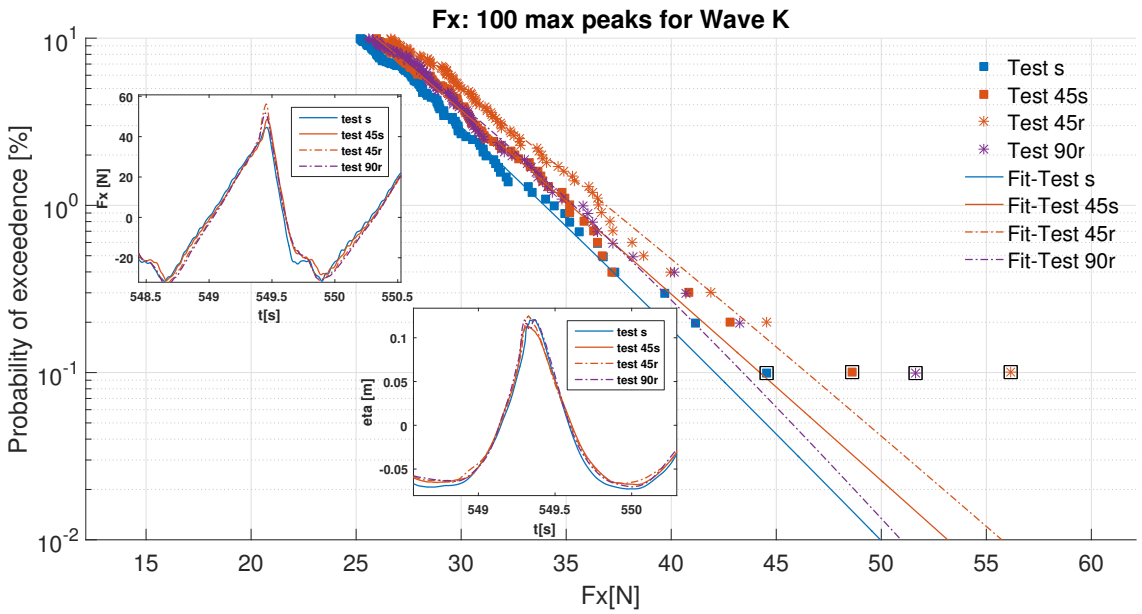

Figure 5.10. Weibull fit for 100 F_x peaks for wave K tests. Peaks in boxes shown in inset.

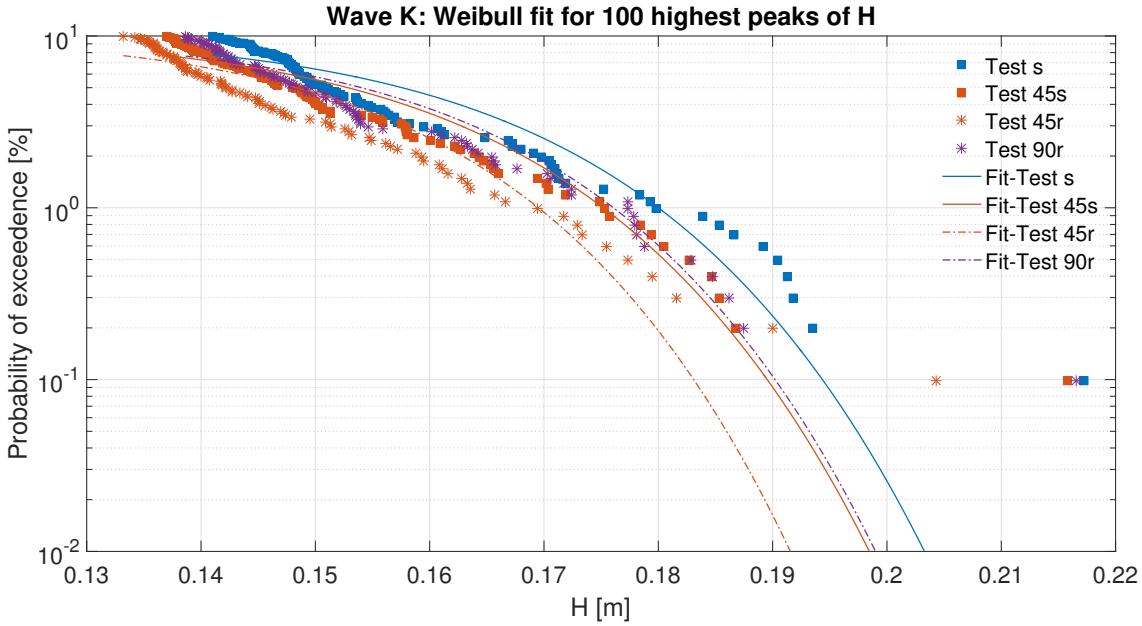

Figure 5.11. Weibull fit for 100 H peaks for wave K tests.

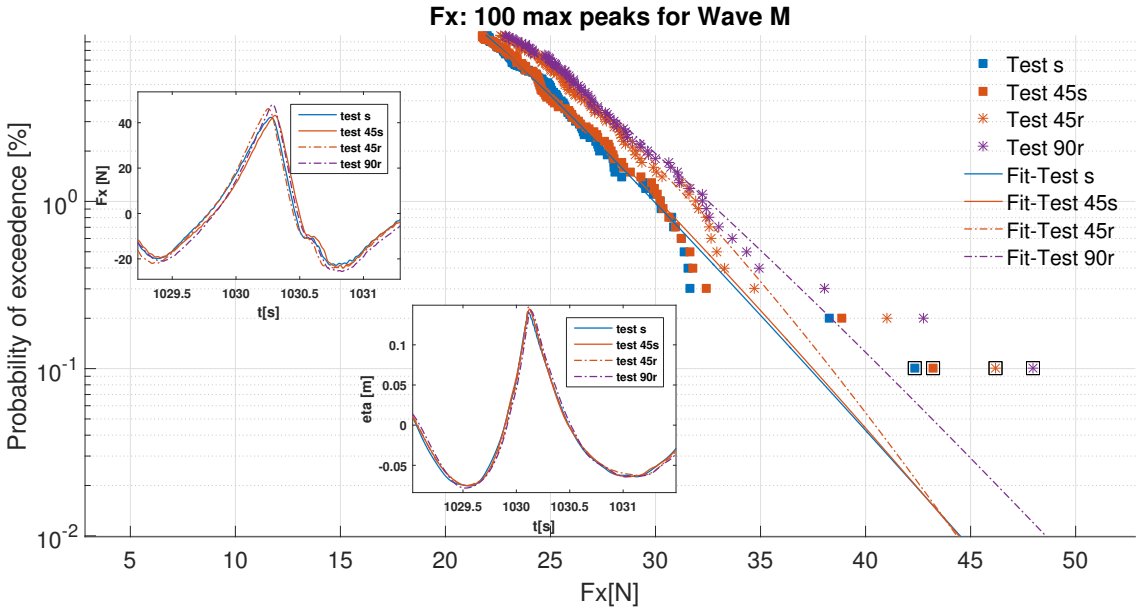

Figure 5.12. Weibull fit for 100 F_x peaks for wave M tests. Peaks in boxes shown in inset.

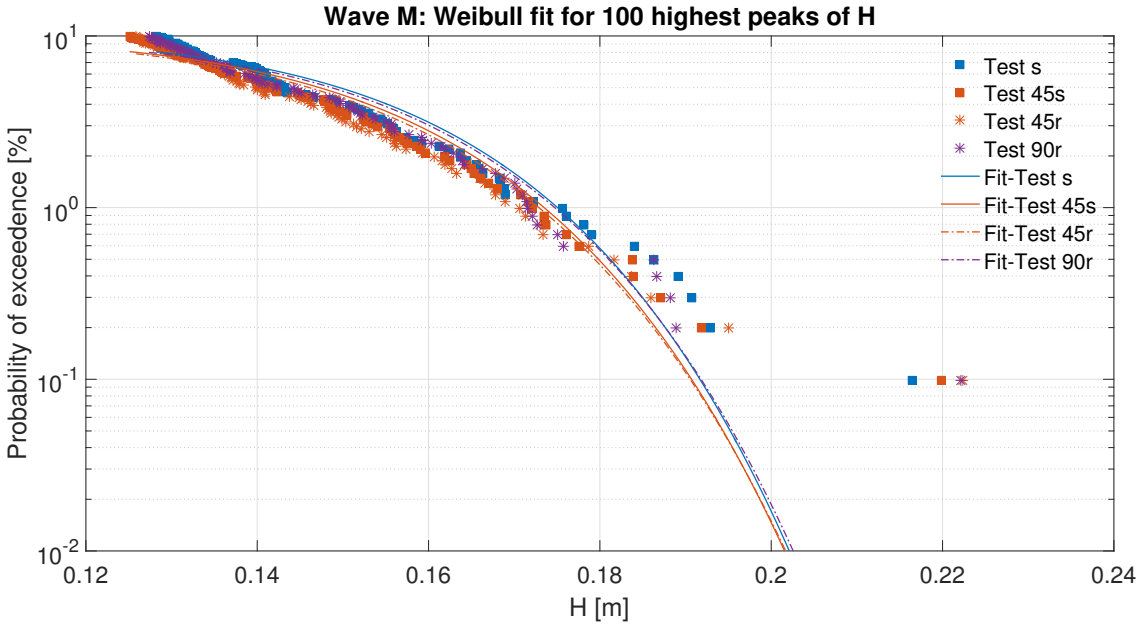

Figure 5.13. Weibull fit for 100 H peaks for wave M tests.

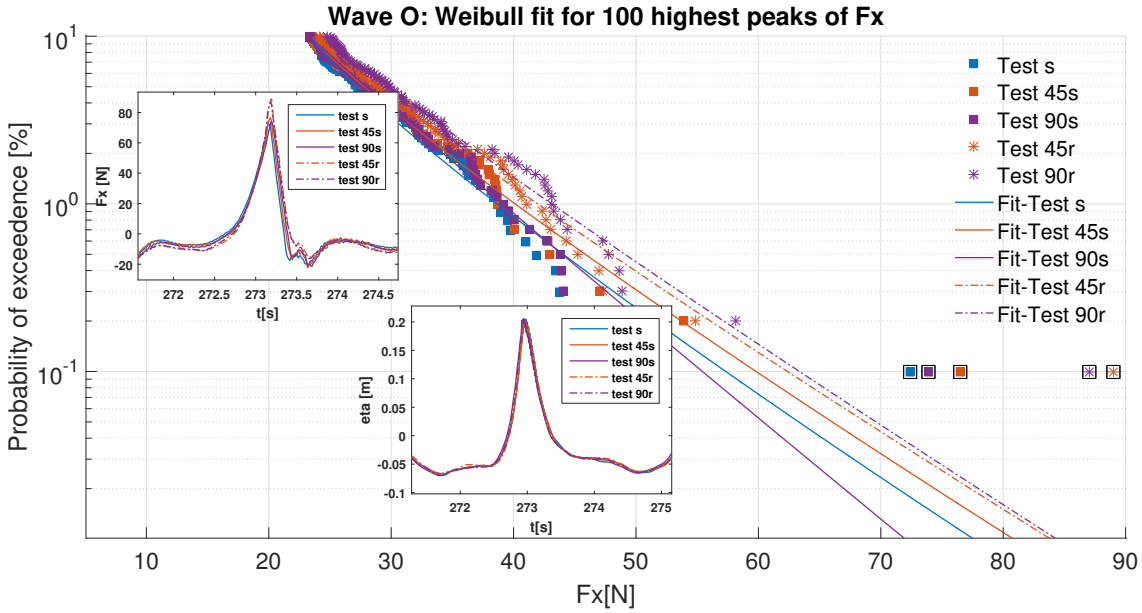

Figure 5.14. Weibull fit for 100 F_x peaks for wave O tests. Peaks in boxes shown in inset.

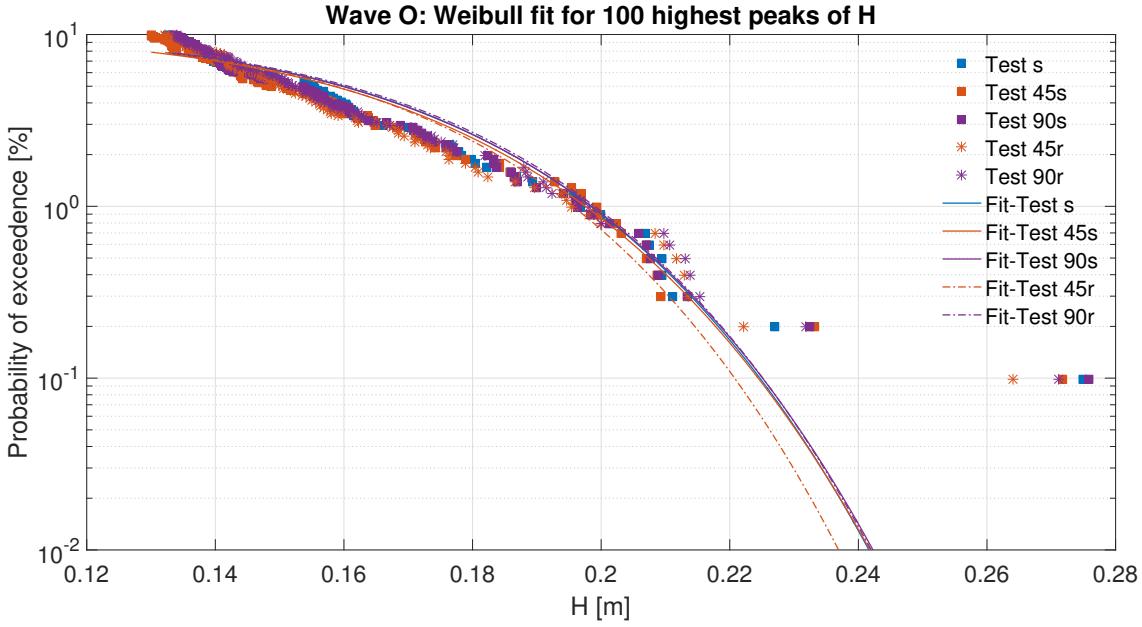

Figure 5.15. Weibull fit for 100 η peaks for wave O tests.

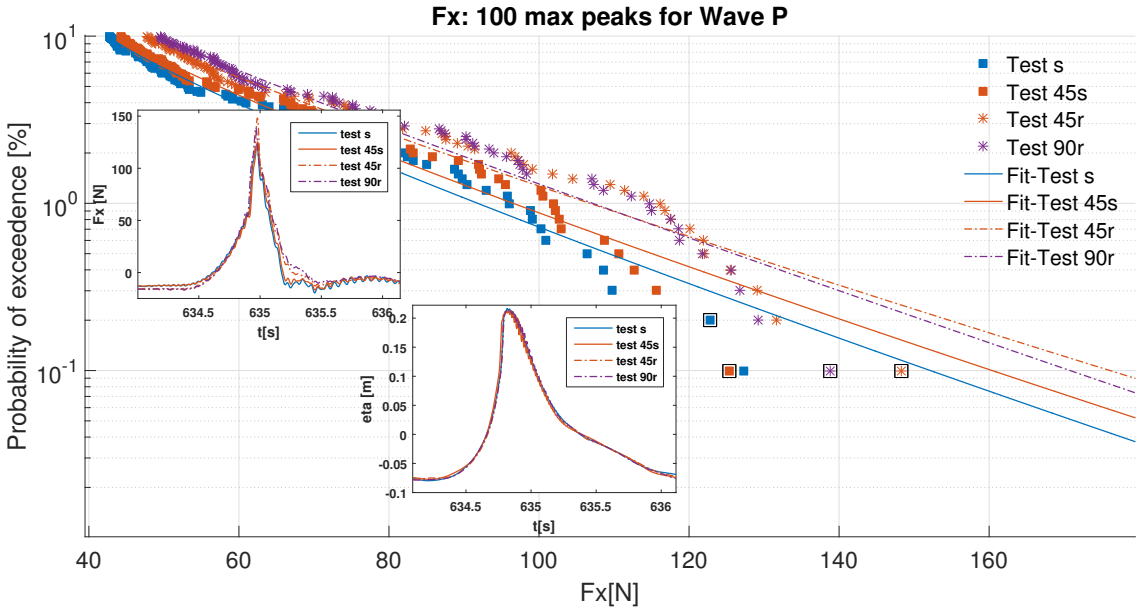

Figure 5.16. Weibull fit for 100 F_x peaks for wave P tests. Peaks in boxes shown in inset.

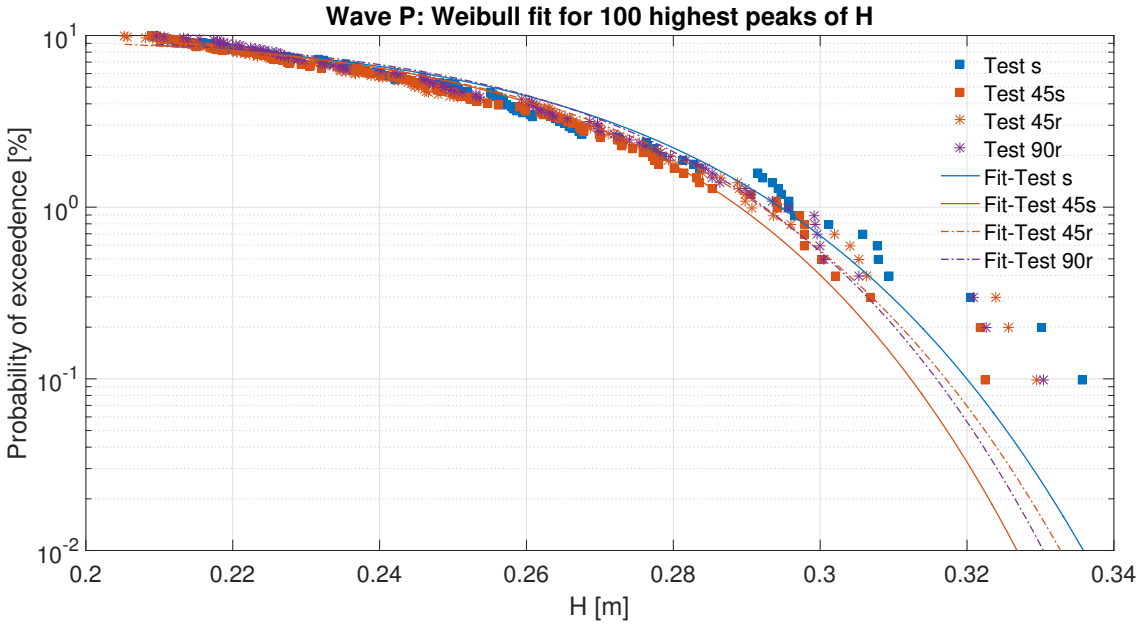

Figure 5.17. Weibull fit for 100 H peaks for wave P tests.

From each of the above plots, design values for F_x and H are calculated. This is done by finding the 0.1% probability of exceedance values, namely, $F_{x0.1\%}$ and $H_{0.1\%}$, from the distribution. Hence, the design F_x is found for each test and the design wave height is found as an averaged from the different tests within the same sea state. For eg:, for wave K, design $F_{x0.1\%}$ is read from the plot for test s, test 45s, test 45r and test 90r whereas for design $H_{0.1\%}$, the average of 0.1% values for all 4 tests is taken.

In order to study the effect of extreme values on the distribution fit, another set of distributions were plotted for H with only the 20 highest peaks to estimate the variation in design wave height from extreme analysis. These plots are shown in Figures C.15-C.20.

The comparison of design values from 100 peaks and 20 peak distributions is also shown in Table C.2.

The design values from 100 peaks are later used in the theoretical calculations for comparison with lab results. Table 5.5 and Table 5.6 show these 0.1% exceedance probability values of H for each wave and test in 100 peaks Weibull distributions and their corresponding KC, β, R_e, C_D and C_M values for both rough and smooth monopile.

The drag and inertia coefficients were calculated from Figure 5.19 and 5.18, since the values for β are out of range for the other Sarpkaya charts shown in Figure A.4 and Figure A.5.

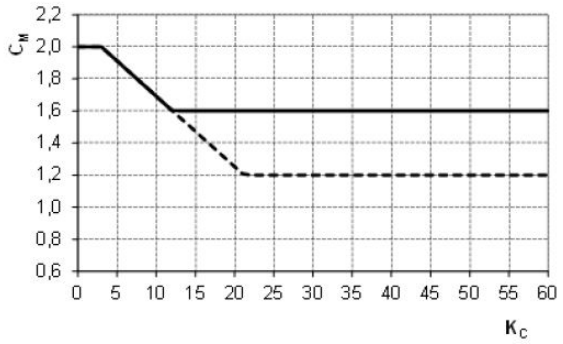

Figure 5.18. Inertia coefficient values as a function of KC and surface roughness. DNV [2014]

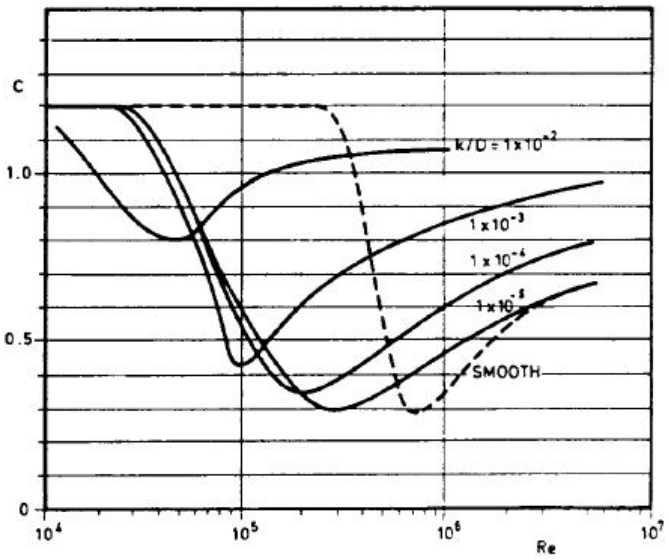

Figure 5.19. Drag coefficient values as a function of R_e and surface roughness. DNV [2014]

Smooth monopile							
Wave	$H_{avg}[m]$	$T_p[s]$	KC	R_e 10^{-4}	β	C_D	C_M
K	0.189	1.26	5.55	11.2	20236	1.2	1.89
L	0.215	1.26	6.59	13.3	20236	1.2	1.84
M	0.191	1.90	7.72	10.3	13420	1.2	1.79
N	0.275	1.90	12.24	16.4	13420	1.2	1.6
O	0.224	2.53	12.72	12.82	10078	1.2	1.6
P	0.316	2.53	19.4	19.29	10078	1.2	1.6

Table 5.5. Design waves from Weibull fit for 100 peaks. Smooth monopile

Rough monopile							
Wave	$H_{avg}[m]$	$T_p[s]$	KC	R_e 10^{-4}	β	C_D	C_M
K	0.189	1.26	5.48	11.3	20766	0.76	1.89
L	0.215	1.26	6.51	13.5	20766	0.78	1.84
M	0.191	1.90	7.62	10.5	13771	0.75	1.79
N	0.275	1.90	12.08	16.6	13771	0.82	1.6
O	0.224	2.53	12.55	12.98	10342	0.76	1.57
P	0.316	2.53	18.89	19.54	10342	0.85	1.3

Table 5.6. Design waves from Weibull fit for 100 peaks. Rough monopile

Morison forces were calculated for the above design waves in the case of monopile with no secondary structure for rough and smooth model. As Table 5.7 indicates, the analytical values were lower than those obtained from lab tests, therefore a new calculation of forces is done using $C_M = 2$, giving closer results. The slamming contribution was also taken into account since breaking waves were expected in most of the wave series. It has to be mentioned that in this case, when using wave celerity in the formula for slamming contribution, the values were very high. By using u_{max} instead, and adding this contribution to the drag and inertia forces, the results matched better with the lab measurements. As stated earlier, due to high reflection, some tests were excluded from analysis as shown in Table 5.7.

Wave	**Avg $F_{x0.1\%}$ [N]**	**Avg $H_{0.1\%}$ [m]**	T_p **[s]**	**Morison [N]**	**Morison [N] $C_M = 2$**
K s	41.83	0.189	1.26	41.54	43.94
K 45s	44.01				
K 90s	excluded				
K r	excluded			42.56	45.04
K 45r	46.55				
K 90r	43.19				
L s	60.27	0.215	1.26	47.35	51.42
L 45s	58.74			slamming	slamming
L 90s	excluded			9.35	9.35
L r	excluded			48.42	52.62
L 45r	63.02			slamming	slamming
L 90r	66.00			10.08	10.08
M s	37.20	0.191	1.90	33.22	36.88
M 45s	37.49				
M 90s	excluded				
M r	excluded			33.38	37.19
M 45r	38.49				
M 90r	40.99				
N s	96.55	0.275	1.90	52.22	63.19
N 45s	97.33			slamming	slamming
N 90s	98.99			22.05	22.05
N r	excluded			50.98	62.70
N 45r	100.10			slamming	slamming
N 90r	106.40			22.34	22.34
O s	57.36	0.224	2.53	38.46	46.15
O 45s	59.80			slamming	slamming
O 90s	55.35			11.09	11.09
O r	excluded			36.11	45.03
O 45r	62.28			slamming	slamming
O 90r	63.31			11.24	11.24
P s	152.1	0.316	2.53	65.99	77.38
P 45s	160.1			slamming	slamming
P 90s	excluded			38.50	38.50
P r	excluded			52.58	74.29
P 45r	175.9			slamming	slamming
P 90r	170.4			39.00	39.00

Table 5.7. Forces obtained from Weibull fit of 100 peaks from laboratory tests and Morison forces on monopiles for the obtained design waves

The maximum force on secondary structure and values for drag and inertia coefficients

were calculated following the same procedure as for the monopile. In the laboratory tests only a smooth item was used with calculated $C_D = 1.2$ and $C_M = 1.6$.

When calculating forces for monopile with secondary structure, two approaches can be used. The first one consist of adding the boat landing force to the monopile force and finding the maximum value. The second one takes into account wall effects and flow disturbance, using the formulae presented in Chapter 2 to obtain the equivalent drag and inertia coefficients for each secondary structure position.

Table 5.8 and Table 5.9 present the increments in forces for the monopile with secondary structure from experimental results, force of the system by using potential flow and wall effect and by adding forces from the monopile and the secondary structure together. For the last approach the force will be the same at all secondary structure positions.

Smooth monopile						
Wave	$F_{x0.1\%}[N]$	%increment in force	Morison + pot flow [N]	%increment in force	Morison pile+sec [N]	%increment in force
K s	41.83	-	41.54	-	41.54	-
K 45s	44.01	5.2	41.70	0.4	41.68	0.3
L s	60.27	-	47.35	-	47.35	-
L 45s	58.74	-2.5	47.57	0.5	47.54	0.4
M s	37.20	-	32.22	-	32.22	-
M 45s	37.49	0.8	33.51	0.9	33.46	0.7
N s	96.55	-	52.22	-	52.22	-
N 45s	97.33	0.8	52.15	1.8	52.99	1.5
N 90s	98.99	2.5	53.79	3.0	52.99	1.5
O s	57.36	-	38.46	-	38.46	-
O 45s	59.80	4.3	39.26	2.1	39.12	1.7
O 90s	55.35	-3.5	39.82	3.5	39.12	1.7
P s	152.10	-	65.99	-	65.99	-
P 45s	160.10	5.3	67.90	2.9	67.56	2.4

Table 5.8. Increment in forces for laboratory tests, Morison with potential flow and Morison monopile + secondary structure for smooth pile

For smooth pile, the prediction seems accurate for waves M, O and N. Meanwhile, for waves K, L and P the analytical approach seems to underestimate the increment in forces. Negative values mean that the force did not increased when adding the secondary structure or when moving it to another position. Results showed that in some cases, when the secondary structure was placed at 45^o, higher forces were registered than when placing it at 90^o. A possible explanation is that the item was almost positioned at the same place as the monopile front and breaking waves might create a slamming contribution.

Rough monopile					
Wave	$0.1\%F_x[N]$	%increment in force	Morison + pot flow [N]	%increment in force	Morison pile+sec [N]
K 45r	46.55	-	42.73	-	42.71
K 90r	43.19	-7.2	42.79	0.1	42.71
L 45r	63.02	-	48.63	-	48.60
L 90r	66.00	4.7	48.71	0.2	48.60
M 45r	38.49	-	33.63	-	33.59
M 90r	40.99	6.5	33.76	0.4	33.59
N 45r	100.10	-	51.69	-	51.57
N 90r	106.40	6.3	52.16	0.9	51.57
O 45r	62.28	-	36.72	-	36.62
0 90r	63.31	1.7	37.14	1.1	36.62
P 45r	175.9	-	54.35	-	54.03
P 90r	170.4	-3.1	55.65	2.4	54.03

Table 5.9. Increment in forces for laboratory tests, Morison with potential flow and Morison monopile + secondary structure for rough pile

The increment in forces is higher for rough monopile and underestimated by the analytical approach.

The gap between monopile and secondary structure d_m and the secondary item diameter D_b influence the forces as depicted in Figure 5.20. For the experimental analysis, d_m value was 0.035 m and D_b was 0.01 m.

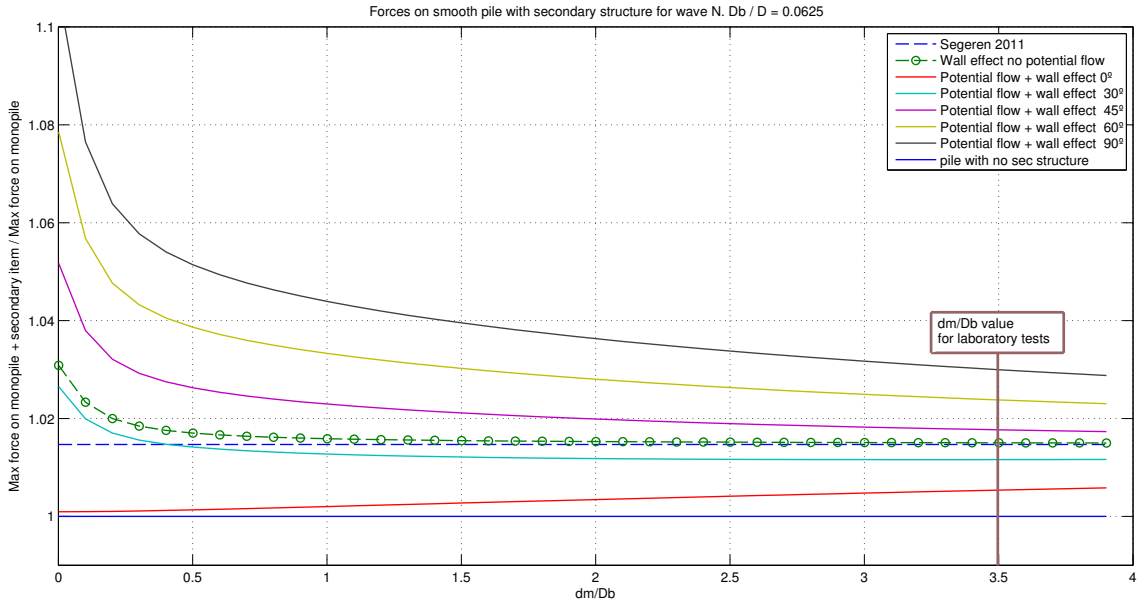

Figure 5.20. Forces on smooth monopile with secondary structure for wave N as a function of d_m/D_b.

As seen in Figure 5.20 and the previous results in the tables above, small values of d_m/D_b and higher waves give a more significant increment in forces.

Different values of d_m/D_b should have been used in the experimental analysis in order to obtain a conclusion about the influence of distance and diameter difference between monopile and secondary structure.

The use of more than one secondary structure would also be recommendable since boat landings consist of more than a single item and the interference between them will disturb the flow in a different way than just a single unit.

When analysing the results, the use of drag dominated regular waves would help to understand the forces obtained for irregular series and to see how drag and inertia coefficients vary for each secondary sturcture position. The presence of breaking waves plays an important role since a position expected to have less forces might end up reaching the highest due to slamming contribution.

Further research needs to be performed in order to assess this subject and large scale tests are expected to give more realistic results.

5.4.3 Validation of results

In order to validate the results obtained, the following were checked:

- The wave gauges aligned with the pile measured the same wave height. These are shown in Figure C.21 and Figure C.22.
- The measured forces, wave surface elevations and velocities were compared with Morison equation and stream function. The results were in agreement. The plots are shown in Figure C.23, Figure C.24 and Figure C.25
- The scatter in the force peaks was checked by uncertainty analysis. 5 consecutive tests were conducted in the lab for wave M and N and the peaks of F_x are fitted using Weibull distribution. The amount of scatter is found to be acceptable. For waves M and N Weibull fit is shown in Figure 5.21 and Figure 5.22.

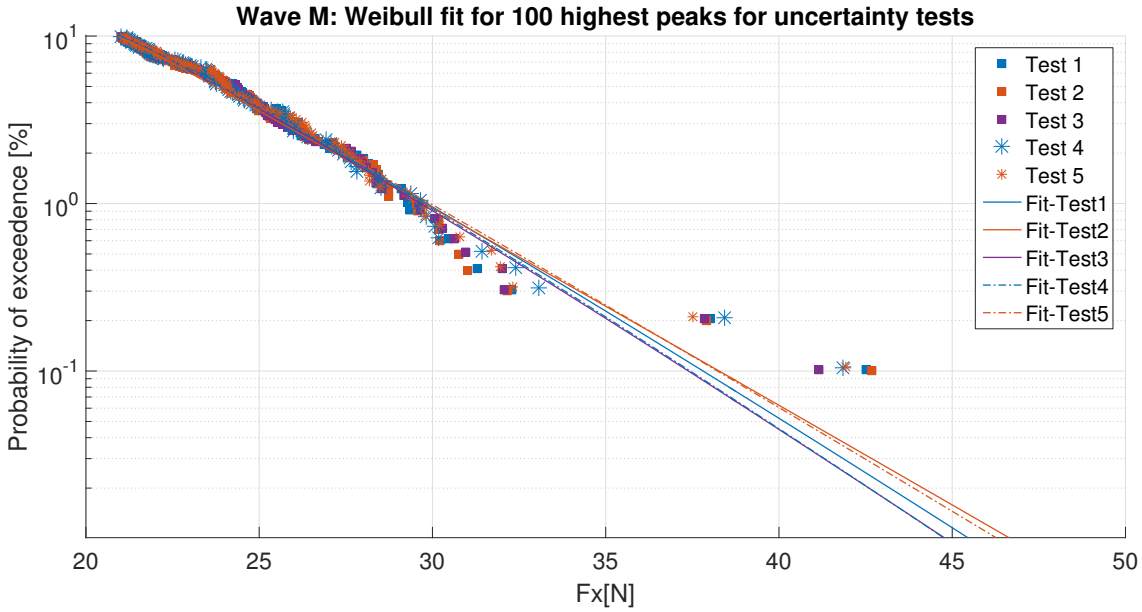

Figure 5.21. Weibull fit for uncertainty tests for wave M.

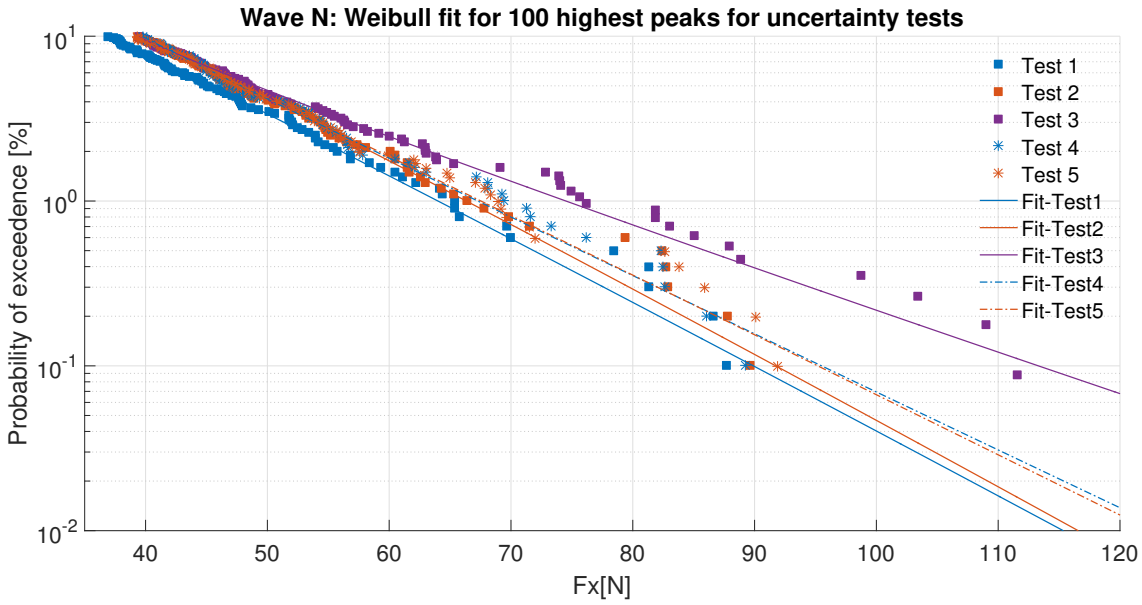

Figure 5.22. Weibull fit for uncertainty tests for wave N.

The uncertainty in the tests was quantified by calculating the deviation of $F_{x0.1\%}$ from each test from that of their mean $F_{x0.1\%}$. As shown in Table 5.10, there is an average deviation of 0.89% in the wave M results whereas wave N varies on an average 6.66%.

Wave	100 Peaks	$F_{x0.1\%}$ [N]	Mean $F_{x0.1\%}$ [N]	Deviation from mean	Mean of % Deviation
M	Test 1	37.86	37.84	0.05%	0.89%
	Test 2	38.29		1.18%	
	Test 3	37.35		1.3%	
	Test 4	37.49		0.93%	
	Test 5	38.22		1.00%	
N	Test 1	89.33	96.78	7.70%	6.66%
	Test 2	91.47		5.49%	
	Test 3	112.9		16.65%	
	Test 4	95.12		1.72%	
	Test 5	95.11		1.73%	

Table 5.10. Deviation of $F_{x0.1\%}$ of each uncertainty test from the mean $F_{x0.1\%}$.

5.5 Conclusions

- Experimental results show higher forces on monopile with secondary structure than predicted by theories. However, the uncertainty associated especially in waves with frequent slamming should be considered while reading these results
- Secondary structure at 45° are found sometimes to register higher forces than at 90°. This may be due to the fact that at 45°, the secondary structure is aligned with the front face of the monopile which in turn receives more slamming than at 90°
- In general, roughness of the monopile is found to increase the forces

Conclusion 6

This chapter summarizes the three main studies carried out in the thesis, dealing with wave run-up on monopiles, slamming forces on platforms and wave forces on monopiles with secondary structures. The conclusions obtained from each study are presented. Recommendations and improvements for future studies are also listed.

6.1 Summary

The re-analysis of wave run-up on monopiles in Chapter 3 focused on updating the existing run-up factor m, by re-analysing data with no band pass filter for previous small scale and large scale laboratory tests. It also validated the use of reflection analysis in order to obtain the wave heights and periods.

The results obtained showed the following:

- In the previous analysis, m is found to decrease with increasing wave steepness, whereas in the current analysis, m increases with wave steepness
- New m-factor values are reduced almost to half compared previous analysis due to bandpass filter off. Therefore, the expected values for wave run-up on monopile are lower than the obtained from previous studies.
- Small scale test results are found to be compatible with Level A results from large scale tests
- For increasing levels of run-up, m-factor is found to increase

The analysis of slamming coefficient C_s is based on data from an experiment conducted in GWK Hannover and compared with results from small scale tests conducted at AAU. Both measured and calculated run-up values by use of the equations obtained in Chapter 3 are used to determine the theoretical slamming force. Previous results are based on maximum pressures from small scale tests which do not distinguis between different run-up levels has therefore not been included, whereas they are included in this report. The effect of platform with different solidity is investigated and a grate multiplication factor is obtained.

- C_s has been found to be in the range of $0-1$ for slamming forces for Level B, while the factor is $0-10$ for slamming pressures for Level C, which is the same result found in small scale
- The grate multiplication factor is approximately the same as the solidity. The results indicated a factor of 0.2 for grates with 20% solidity and a factor of 0.35 for 40% solidity

The last part of the thesis dealt with the study on the effect of secondary structures on monopiles. The laboratory tests performed in Aalborg University facilities led to the following conclusions:

- For the current model, influence of secondary structure on wave forces is almost negligible for inertia dominated regular waves
- Since it is not possible to obtain a clear conclusion solely from the time series of irregular waves, probability distributions are used to fit the data and find which configuration of secondary structure registers higher wave forces for different sea states. As expected, forces are higher for the rough model and the presence of secondary structure increases the forces in most of the cases. Nevertheless, this increment is found to be very low with a maximum of 5.3% for smooth monopile with respect to the monopile with no secondary structure.
- Secondary structure at 45° is found to register higher forces compared to that at 90°. This may be due to the fact that at 45°, the secondary structure is almost aligned with the front face of the monopile and hence receives more slamming from the incoming wave
- Analytical calculations from existing theories are also performed to obtain the forces for the tandem (monopile and secondary structure). These results also show the influence of the secondary structure being low. The distance between both structures,$0.035m$, in the current model is such that it does not create a significant flow interaction between them
- Steady potential flow was used in this case to account for flow disturbance created by the monopile, but the use of oscillatory potential flow might provide more realistic results
- The forces calculated from analytical theory are found in better agreement with the design forces from experimental analysis when $C_M = 2$ is used

6.2 Future steps

In light of the present study, following steps are recommended for the continuation of this research.

- Since it is challenging to measure run-up for thin layer and spray run-up levels, namely Levels B and C, and the measurement methods adopted in the previous studies are rather sensitive to observation errors, more experiments for these higher run-up levels are recommended to validate the existing results
- More experiments with different solidities in order to establish a relation between solidity and grate multiplication factor
- Decreasing the platform height in experimental analysis when accounting for slamming forces in order to register more run-up data to establish a more accurate value for slamming coefficient Level A.
- In the present thesis, only wave forces from the laboratory tests were analysed to assess the influence of secondary structures. It would be interesting to see how moments in x and y direction change due to the presence of these structures.
- Further research on drag dominated regular waves in order to obtain drag and inertia coefficients, C_D and C_M, for different positions of secondary structure and to compare

the forces with the theoretical results. One of the ways to obtain C_D and C_M is to find the laboratory forces when velocity, $u = 0$ (only inertia) and acceleration, $a = 0$ (only drag) and equate with Morison equation. The coefficients can also be obtained by trial and error method. In this, trial values of C_D and C_M can be used to fit the force curve and the ones which match the best with the lab results can be chosen.

- There is scope for further modifications in the lab model as given below:
  - Secondary structure can be placed at a lesser distance from the monopile. Also, the diameter of the secondary structure can be increased. This would decrease the $\frac{d_m}{D_b}$ factor and make for an interesting study comparing with the theoretical prediction given in Figure 5.20
  - More number of secondary structure elements can be attached on the monopile to study the effect of interference of cylinders
  - The experiment could be conducted with secondary structure which does not extend down to the bottom of the monopile. This would represent better the case of boat landings.

Bibliography

Annand, **1953**. W. J. D. Annand. *The Resistance to Air Flow of Wire Gauzes.* 1953.

API, **2003**. American Petroleum Institute API. *API RECOMMENDED PRACTICE 2A-WSD (RP 2A-WSD) TWENTY-FIRST EDITION.* 2003.

ATI, **2014**. Industrial Automation ATI. *Multi-Axis Force/Torque Sensor.* 2014.

Battjes, **1974**. J.A. Battjes. *Surf similarity.* 1974.

Battjes and Groenedijk, **2000**. J.A. Battjes and H.W. Groenedijk. *Wave height distributions on shallow foreshores.* 2000.

Brorsen, **2007**. Michael Brorsen. *Non-linear Waves.* 2007.

Damsgaard et al., **2007**. Mathilde L. Damsgaard, Helge Gravesen and T. Lykke Andersen. *Design loads on platforms on offshore wind turbine foundations with respect to vertical wave run-up.* 2007.

Damsgaard et al., **2013**. Mathilde L. Damsgaard, Helge Gravesen and T. Lykke Andersen. *Design loads on platforms on offshore wind turbine foundations with respect to vertical wave run-up.* 2013.

De Vos et al., **2006**. Leen De Vos, P Frigaard and J De Rouck. *Wave run-up on cylindrical and cone shaped foundations for offshore wind turbines.* 2006.

DNV, **2014**. Det Norske Veritas. AS DNV. *DNV-RP-C205.Environmental Conditions and Environmental Loads.* 2014.

Galvin and Hallermeier, **1972**. C. J. Galvin and R. J. Hallermeier. *Wave run-up on vertical cylinders.* 1972.

GL, **2005**. Germanischer Lloyd WindEnergie GmbH GL. *Guideline for the Certification of Offshore Wind Turbines.* 2005.

Goda, **2010**. Y. Goda. *Random Seas and Design of Maritime Structures. 3rd Edition.* 2010.

Gravesen, **2006**. H Gravesen. *Run-up Assessment.* 2006.

Hallermeier, **1976**. R. J. Hallermeier. *Nonlinear flow of wave crests past a thin piles.* 1976.

Hallowel et al., **2015**. S. Hallowel, A. T. Myers and S. R. Arwade. *Variability of breaking wave characteristics and impact loads on offshore wind turbines supported by monopiles.* 2015.

Haney and Herbich, **1982**. J. P. Haney and J. B. Herbich. *Wave flow around thin piles and pile groups.* 1982.

Isaacson, **1978**. M. Isaacson. *Wave runup around large circular cylinder.* 1978.

Klopmann and Stive, **1989**. G. Klopmann and M.J.F. Stive. *Extreme waves and wave loading in shallow water.* 1989.

Kriebel, **1992**. D. L. Kriebel. *Nonlinear wave runup on large circular cylinders.* 1992.

Kriebel, **1993**. D. L. Kriebel. *Nonlinear runup of random waves on a large cylinder.* 1993.

Lin and Lin, **2005**. Lin W.J. Lin, C. and S.S. Lin. *low Characteristics around a Circular Cylinder near a Plane Boundary.* 2005.

Lykke Andersen and Brorsen, **2006a**. T. Lykke Andersen and M. Brorsen. *Horns Rev II, 2-D Model Tests. Impact Pressures on Horizontal and Cone Platforms.* 2006.

Lykke Andersen and Brorsen, **2006b**. T. Lykke Andersen and M. Brorsen. *Horns Rev II, 2-D Model Tests. Impact Pressures on Horizontal and Cone Platforms.* 2006.

Lykke Andersen and Brorsen, **2007**. T. Lykke Andersen and M. Brorsen. *Horns Rev II, 2-D Model Tests Impact Pressures on Horizontal and Cone Platforms from Irregular Waves.* 2007.

Lykke Andersen and Frigaard, **2006**. T Lykke Andersen and P Frigaard. *Horns Rev II, 2-D Model Tests. Wave Run-Up on Pile.* 2006.

Lykke Andersen and Frigaard, **2011**. T. Lykke Andersen and P. Frigaard. *Lecture Notes for the Course in Water Wave Mechanics. Aalborg:Department of Civil Engineering, Aalborg University. (DCE Lecture Notes; No. 24).* 2011.

Lykke Andersen et al., **2006**. T. Lykke Andersen, M. Rasmussen and P. Frigaard. *Detailed Investigations of Load Coefficients on Grates Influence of Air and Angle of Attack.* 2006.

Lykke Andersen et al., **2007**. T. Lykke Andersen, M. Rasmussen and P. Frigaard. *Load coefficients on grates used for wind turbine access platforms Model Test Investigations.* 2007.

Lykke Andersen et al., **2010**. T. Lykke Andersen, M. Rasmussen, P. Frigaard and L. Martinelli. *Loads on wind turbines access platforms with gratings.* 2010.

Lykke Andersen et al., **2011**. T. Lykke Andersen, P. Frigaard, M.L. Damsgaard and L. De Vos. *Wave run-up on slender piles in design conditions — Model tests and design rules for offshore wind.* 2011.

MacCamy and Fuchs, **1954**. R.C. MacCamy and R.A. Fuchs. *Wave forces on piles, a diffraction theory.* 1954.

Martin et al., **2001**. A.J. Martin, W.J. Easson and T Bruce. *Run-up on columns in steep, deep water regular waves .* 2001.

Mase et al., **2001**. H. Mase, K. Kosho and S Nagahashi. *Wave run-up of random waves on a small circular pier on sloping seabed.* 2001.

Mendoza and Hiroo Hirata, **2009**. Alcântara Pereira L.A. W.J. Mendoza, A. and M. Hiroo Hirata. *Simulation of Viscous Flow around a Circular Cylinder near a Moving Groundy.* 2009.

Moe, **2008**. G. Moe. *Linear wave theory.* 2008.

Morgan, **1962**. P. G. Morgan. *Flow through screens of low solidity.* 1962.

Niedzwecki and Huston, **1992**. J. M. Niedzwecki and J. R. Huston. *Wave interaction with tension leg platforms.* 1992.

Niedzwecki and Duggal, **1992**. J.M. Niedzwecki and S.D. Duggal. *Wave run-up and forces on cylinders in regular and random waves.* 1992.

NORSOK, **2007**. NORSOK. *NORSOK STANDARD Actions and action effects N-003.* 2007.

Price and Paidoussis, **2002**. Summer D. Smith J.G. Leong K. Price, S.J. and M.P. Paidoussis. *Flow Vizualization around a Circular Cylinder near to a Plane Wall.* 2002.

Ramirez et al., **2013**. J. Ramirez, P Frigaard, T. Lykke Andersen and L. de Vos. *Large scale model test investigation on wave run-up in irregular waves at slender piles.* 2013.

Richards and Robinson, **1999**. P. J. Richards and M. Robinson. *Wind Loads on Porous Structures.* 1999.

Roshko and Chattoorgoon, **1975**. Steinolfson A. Roshko, A. and V. Chattoorgoon. *Flow Forces on a Cylinder near a Wall or near Another Cylinder.* 1975.

Sarpakaya, **2010**. T. Sarpakaya. *Wave Forces on Offshore Structures.* Cambridge University Press, 2010.

Sarpakaya and Isaacson, **1982**. T. Sarpakaya and M. Isaacson. *Mechanics of wave forces on offshore structures.* Van Nostrand Reinhold Co, 1982.

Segeren, **2011**. M.L.A Segeren. *Influence of J-tubes on Wave Loads and Wall Thickness of the MOnopile Support Structure design.* 2011.

Skjelbreia and Hendrickson. L. Skjelbreia and J. Hendrickson. *Fifth Order Gravity Wave Theory.*

Sorensen, **1997**. R.M Sorensen. *Basic coastal engineering.* Springer, 1997.

Stive, **1986**. M.J.F. Stive. *Extreme shallow water conditions.* 1986.

Taneda, **1965**. S. Taneda. *Experimental Investigation of Vortex Streetsr.* 1965.

Yokoi and Hirao, **2013**. Y. Yokoi and K. Hirao. *The Interaction Vortex Flow Around Two Bluff Cylinders.* 2013.

Appendix: Problem Analysis A

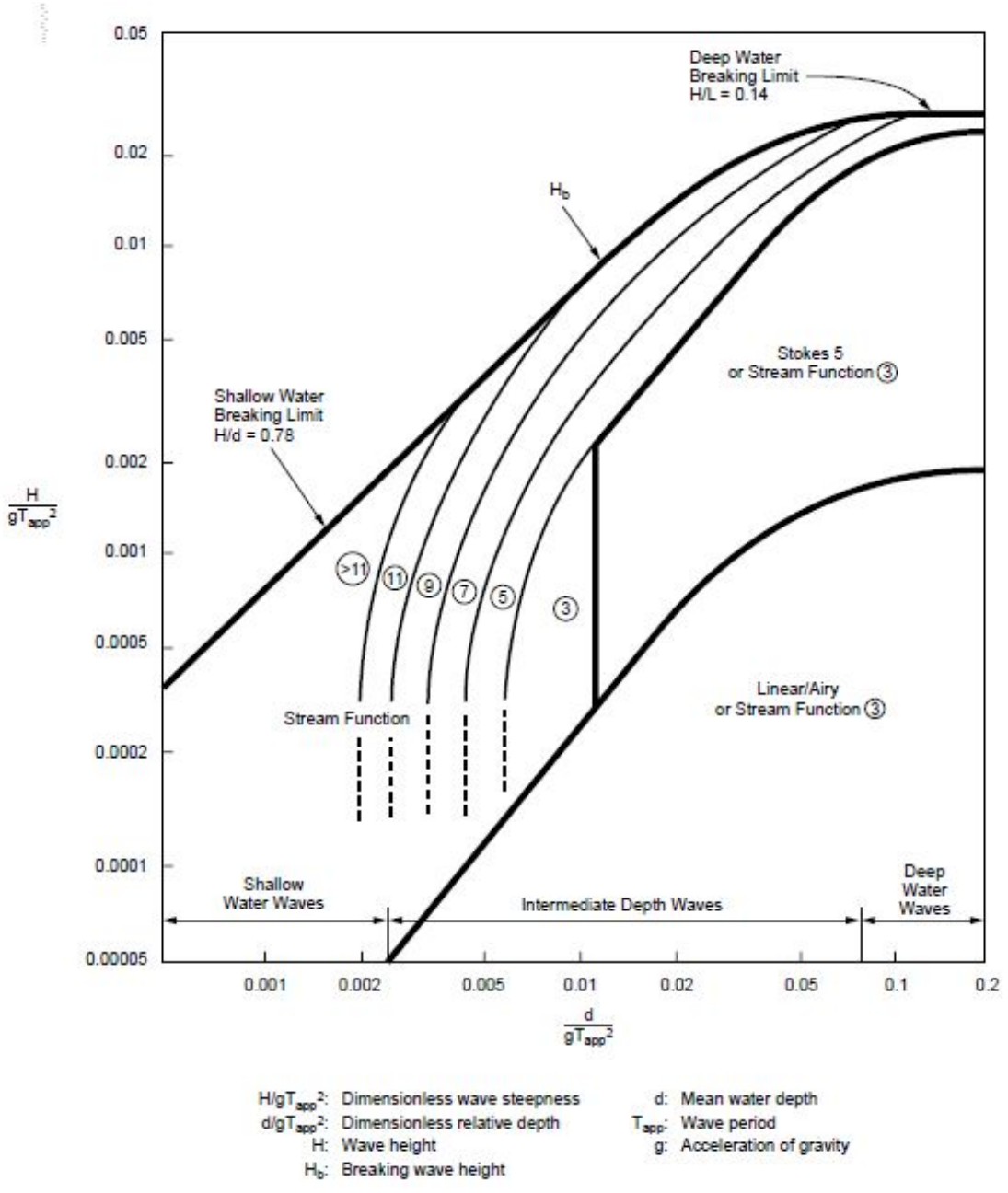

Figure A.1. Recommended wave theories for shallow, intermediate and deep water waves.[API, 2003]

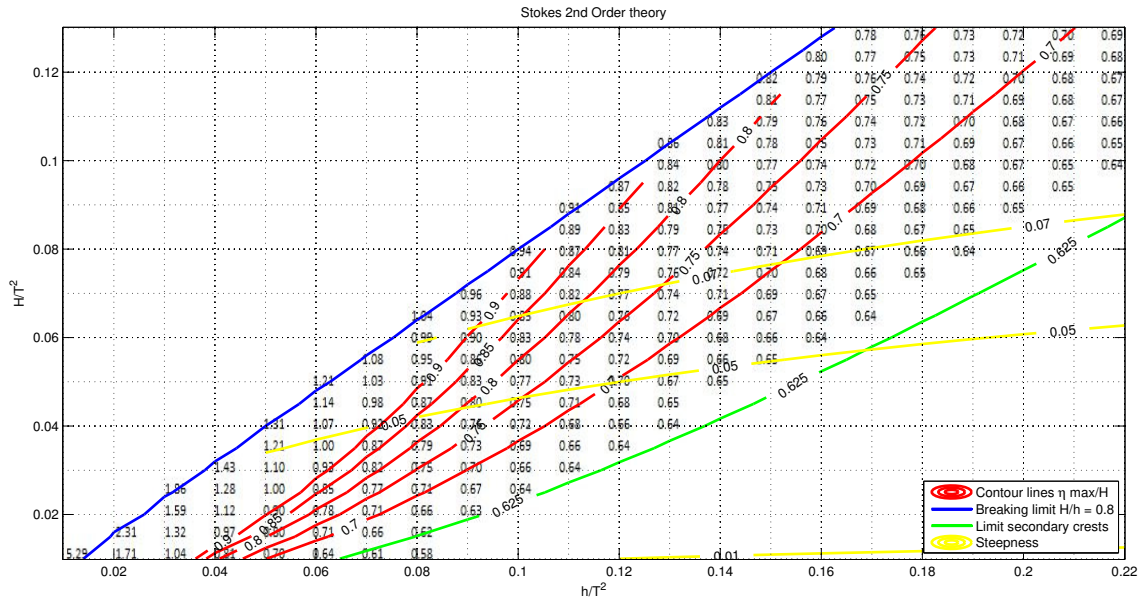

Figure A.2. Analysis of η_{max}/H for Stokes 2nd order theory.

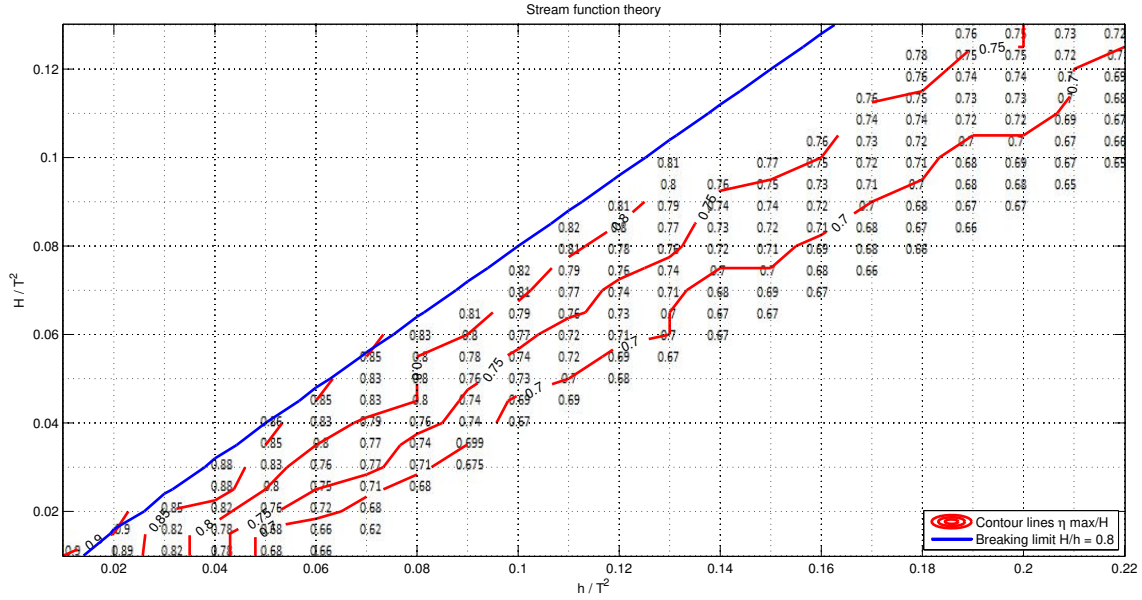

Figure A.3. Analysis of η_{max}/H for stream function theory.

Figure A.2 and Figure A.3 remark the difference between Stream Function Theory and Stokes Second Order Theory. More accurate and realistic results are obtained for Stream function since the breaking limit matches with the theory limits. On the other hand, Stokes Second Order Theory reches unrealistic values for η_{max}/H in the lower side of the chart. The limit for the secondary crests shows that even for some reasonable values of η_{max}/H, the theory is invalid since part of this surface elevation would be caused by these secondary crests or bumps. Therefore, if looking at the previous Figure A.1 and the comparison, it can be concluded that Stream Function Theory is the most appropiate for shallow waters.

Sarpkaya charts are used to obtain C_D and C_M values for waves within the range of

Reynolds number, KC and β showed in Figure A.4 and Figure A.5.

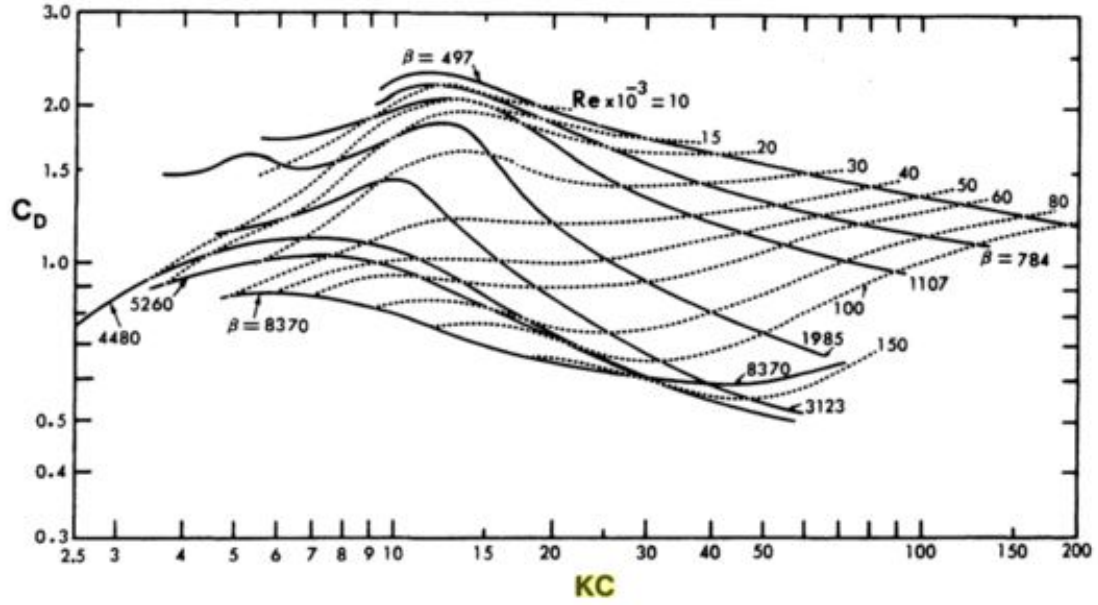

Figure A.4. C_D values dependent on R_e,KC and β.[Sarpakaya, 2010]

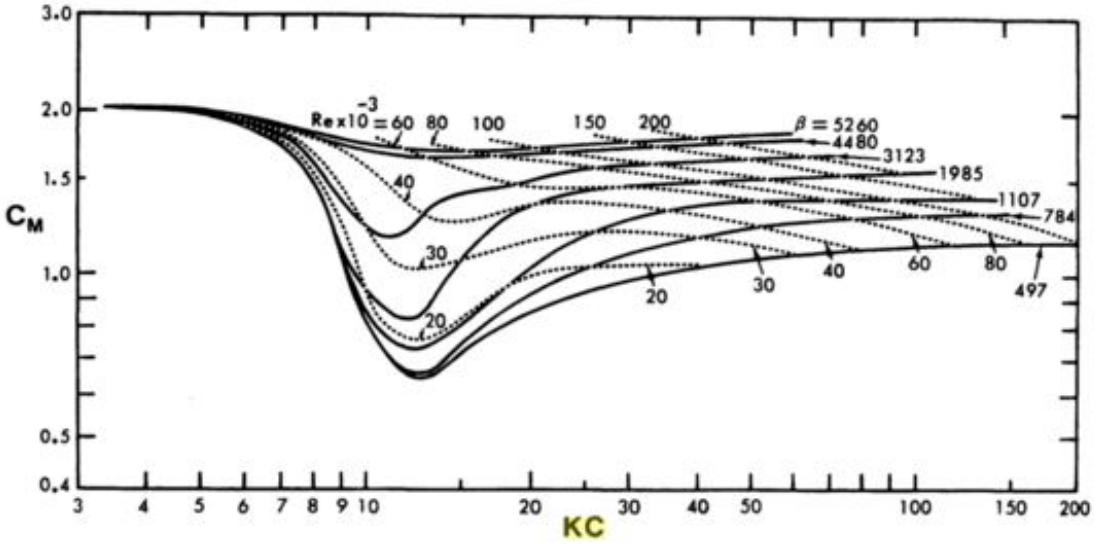

Figure A.5. C_M values dependent on R_e, KC and β.[Sarpakaya, 2010]

h/d	Nishino (2007) without end-plates	Nishino (2007) with end-plates	Roshko et al. (1975)	Moura (2007)	Bimbato (2008)
0.50	-	-	0.795	-	-
0.55	0.965	-	0.857	1.809	1.154
0.60	0.958	-	-	-	0.832
0.65	0.952	-	0.954	1.656	1.293
0.70	0.939	-	-	-	1.376
0.75	0.933	-	1.029	1.440	1.406
0.80	0.930	-	-	-	1.393
0.85	0.931	-	-	-	1.415
0.90	0.922	-	1.136	1.365	1.421
0.95	0.926	1.311	-	1.453	1.403
1.00	0.924	1.323	-	1.491	1.391
1.10	0.920	1.373	1.281	1.466	1.383
1.30	0.899	1.385	-	1.410	1.362
1.40	-	-	1.266	-	-
1.50	0.881	1.375	-	1.385	1.346
2.00	0.854	1.337	-	1.346	1.277
2.30	-	-	1.243	-	-
2.50	0.845	1.304	-	-	1.269
3.50	-	-	1.234	-	-

Figure A.6. Summary of results for drag coefficient on the flow around a circular cylinder near a plane boundary.[Mendoza and Hiroo Hirata, 2009]

Appendix: Wave forces on platforms B

B.1 Slamming forces

Results of re-analysis of slamming forces for large scale test performed in GWK are presented.

B.1.1 Analysis of slamming forces by use of max values

When the peak over threshold (POT) is performed, the maximum pressure and the maximum run-up regardless of location is used for the analysis. The first three figures below shows the results with the run-up level measured with high speed camera. The last three figures shows the results with the run-up level calculated by use of Equations 3.4, 3.5 and 3.6.

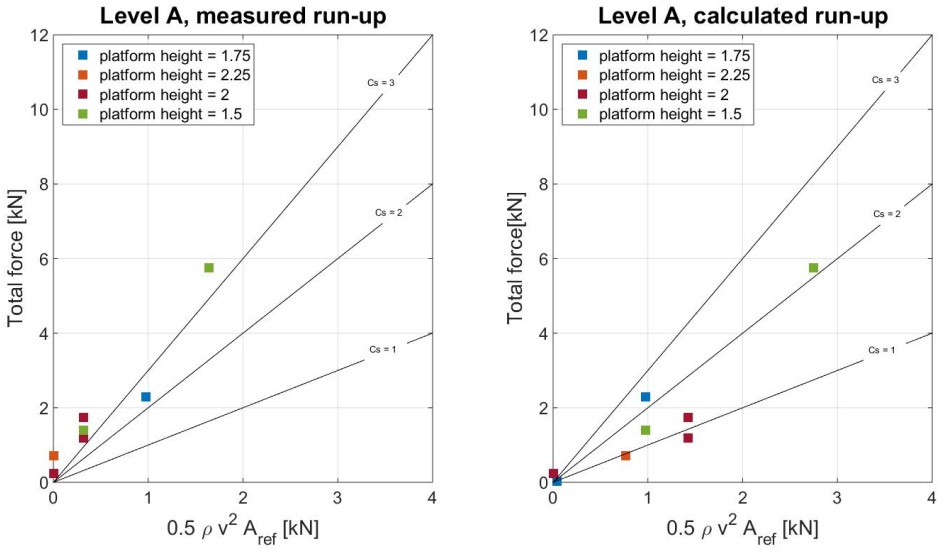

Figure B.1. Calculated and measured maximum forces for Level A.

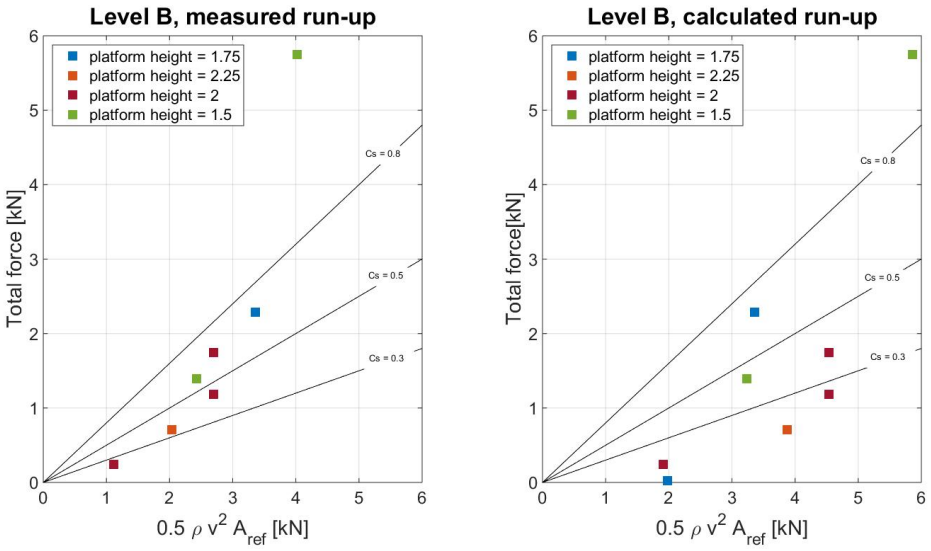

Figure B.2. Calculated and measured maximum forces for Level B.

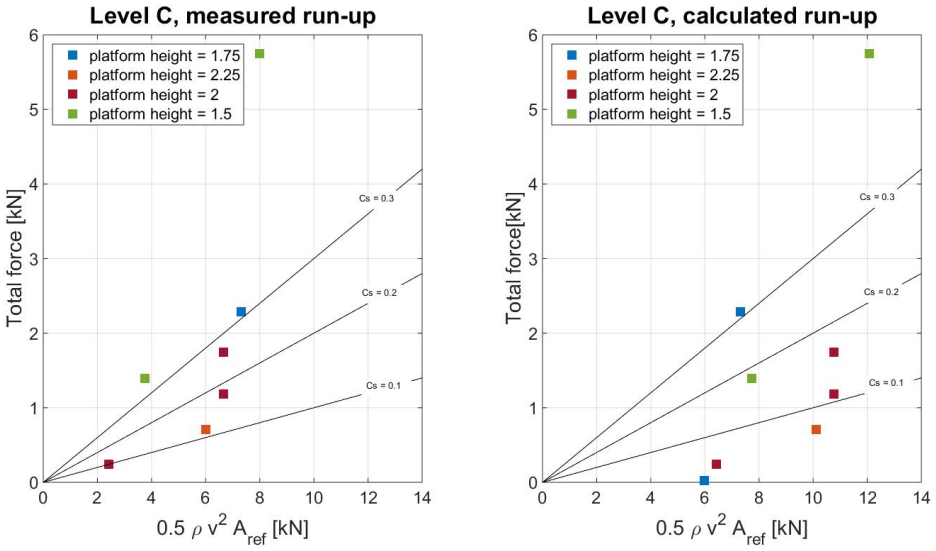

Figure B.3. Calculated and measured maximum forces for Level C.

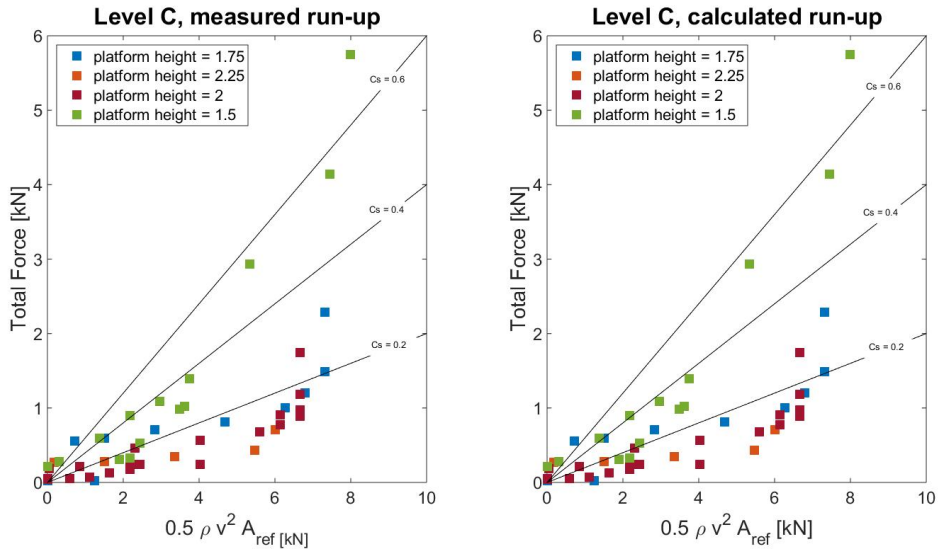

Figure B.4. Calculated and measured maximum forces for Level C

B.2 Slamming pressure

B.2.1 Re-analysis of slamming pressure by use of max values

When the peak over threshold (POT) is performed, the maximum pressure and the maximum run-up regardless of location is used for the analysis. The first three figures below showes the results with the run-up level measured with high speed camera. The last three figures shows the results with the run-up level calculted by use of Equations 3.4, 3.5 and 3.6.

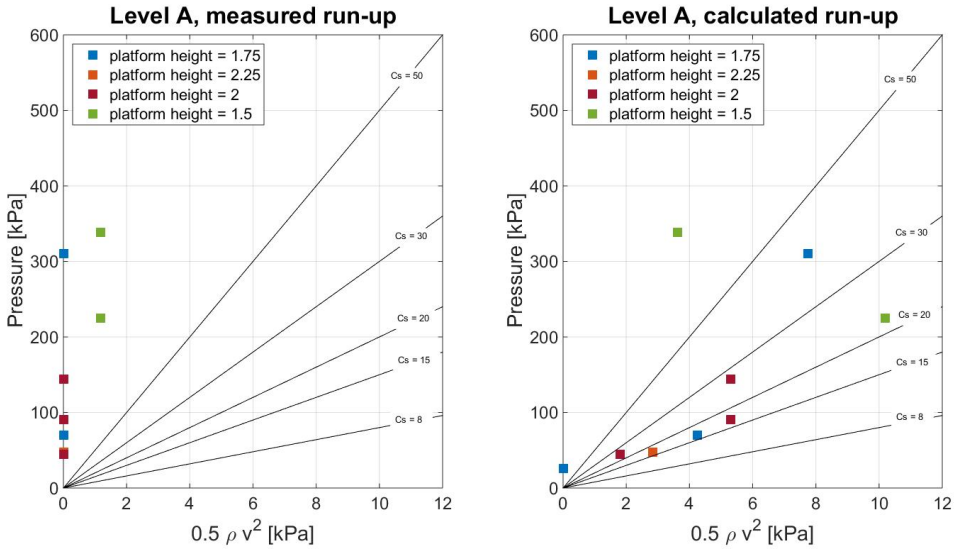

Figure B.5. Calculated and measured maximum forces for Level A

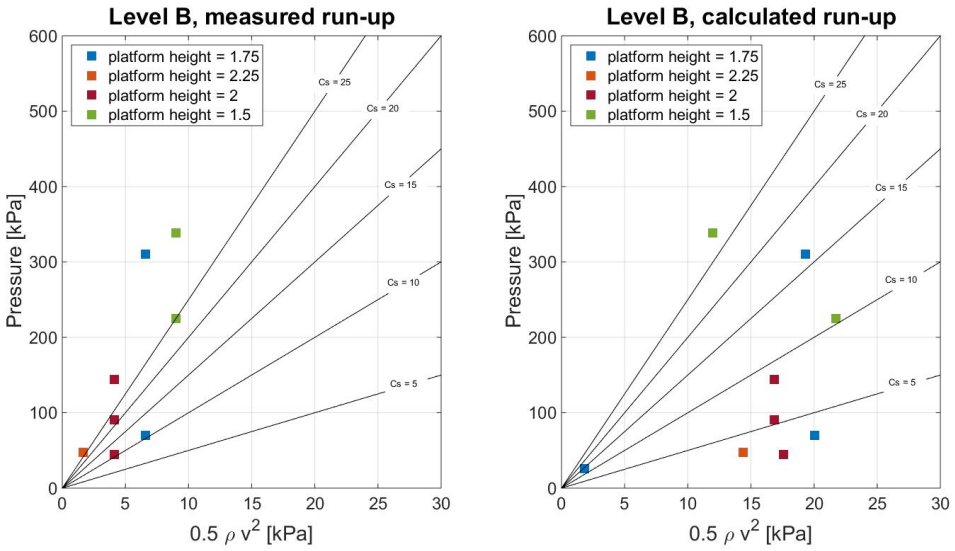

Figure B.6. Calculated and measured maximum forces for Level B

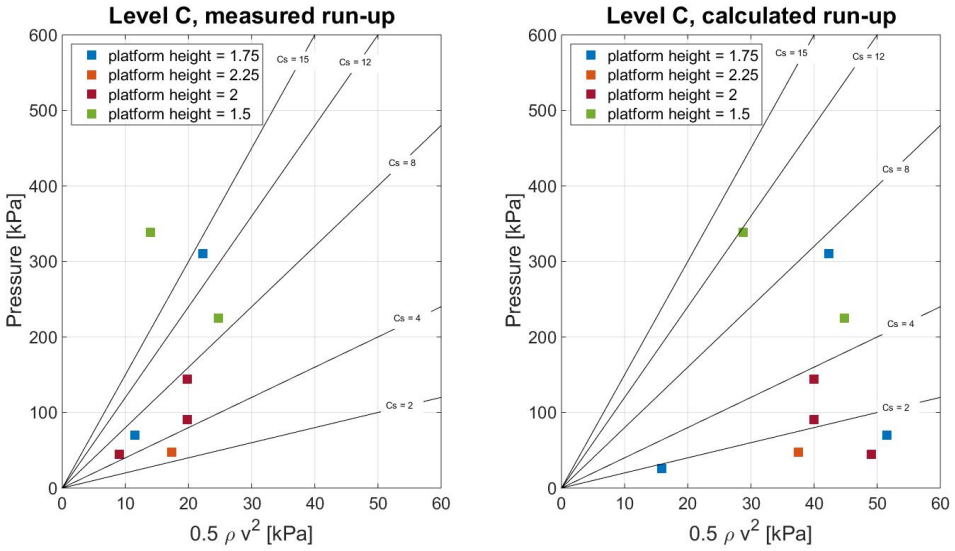

Figure B.7. Calculated and measured maximum forces for Level C

B.2.2 Re-analysis of slamming pressure by sorting the values

When the peak over threshold (POT) is performed, the pressure and the run-up is can be sorted regardless of time position. This means that the highest recorded pressure corresponds to the highest recorded run-up. The results are shown in this section. The last three figures shows the results with the run-up level calculted by use of Equations 3.4, 3.5 and 3.6.

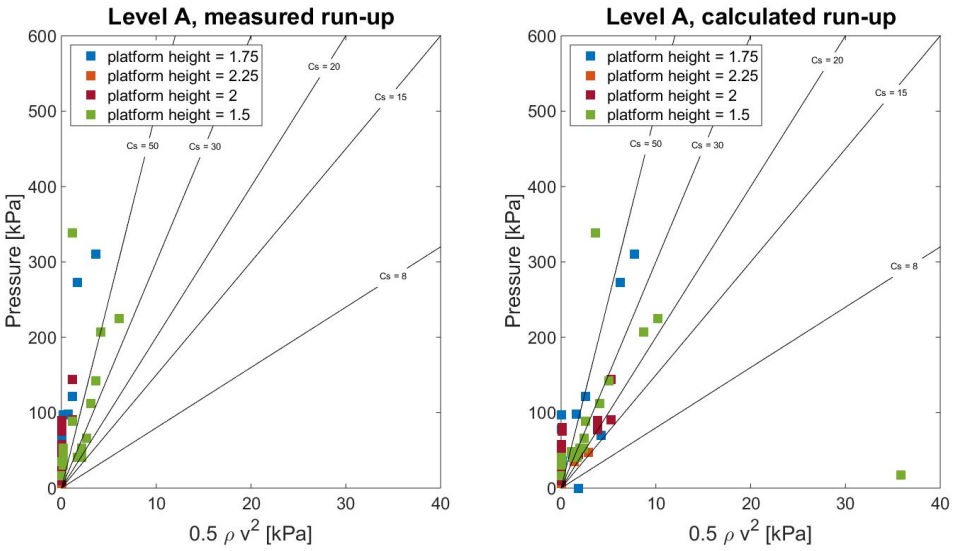

Figure B.8. Calculated and measured maximum forces for Level A

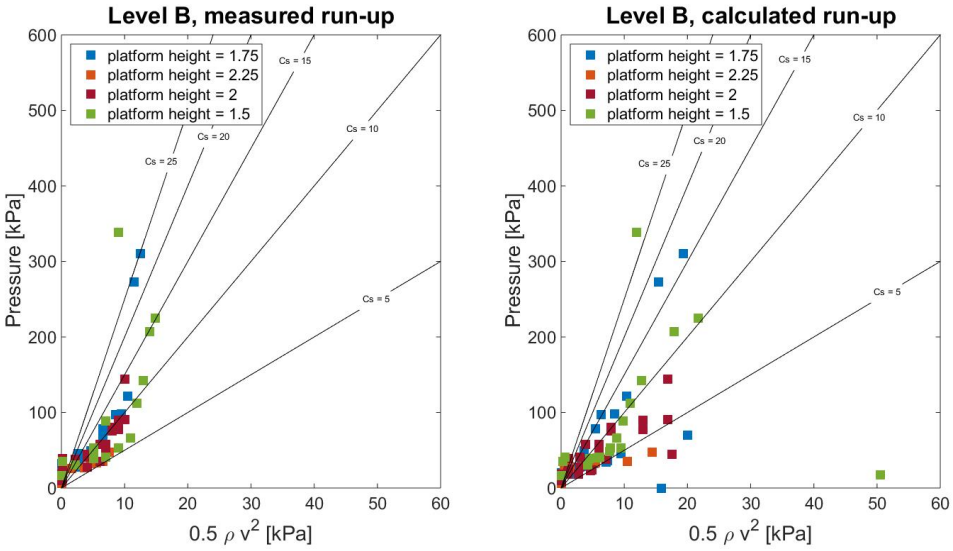

Figure B.9. Calculated and measured maximum forces for Level B

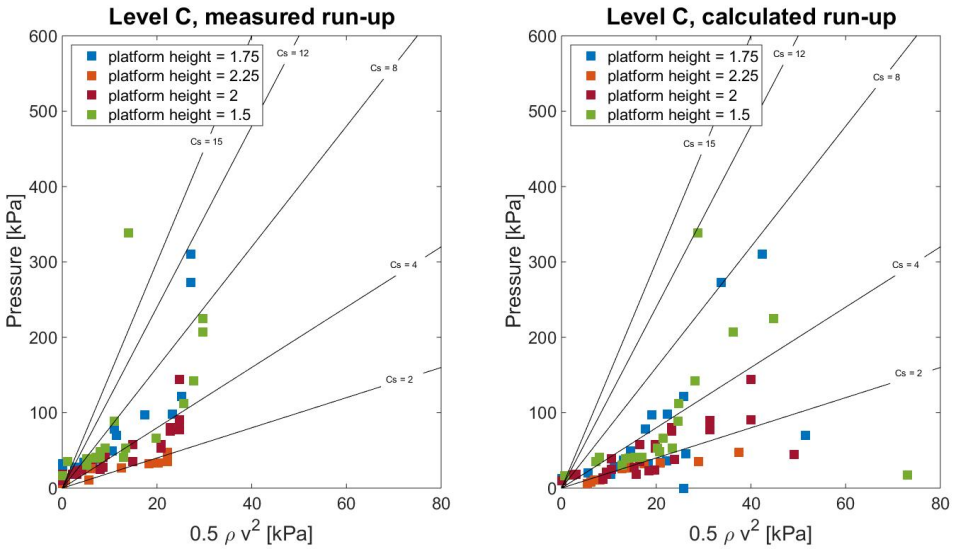

Figure B.10. Calculated and measured maximum forces for Level C

Appendix: Laboratory tests C

C.1 Eigen frequencies

The eigen frequencies for both rough and smooth models with and without secondary structure were found for the basin with water at $h = 0.45m$ and without water. The next table shows the results obtained for the mean value of three hits on each structure:

Structure	**Eigenfrequency [Hz]**	**Damping ratio**
Rough model with secondary structure	13.48	0.025
Rough with sec no water	28.92	0.010
Rough model	13.40	0.028
Smooth with secondary structure	14.85	0.052
Smooth with sec no water	25.13	0.016

Table C.1. Eigenfrequencies for different models

The eigenfrequency selected was 13.5 Hz and damping ratio of 0.025 for the filter wich will be used in all data. The cut off frequency was set to 25 Hz and the filter length to 1024. As expected, the presence of secondary structure alters slightly the eigenfrequency and water damps the structure.

C.2 Regular waves analysis

This section shows the time series of surface elevation, η and force, F_x for wave gauge, $WG3$ from the regular wave tests performed at the basin in AAU facilities.

Figures C.1-C.5 shows a part from the time series for regular waves A-F for a water depth, $h = 0.5m$.

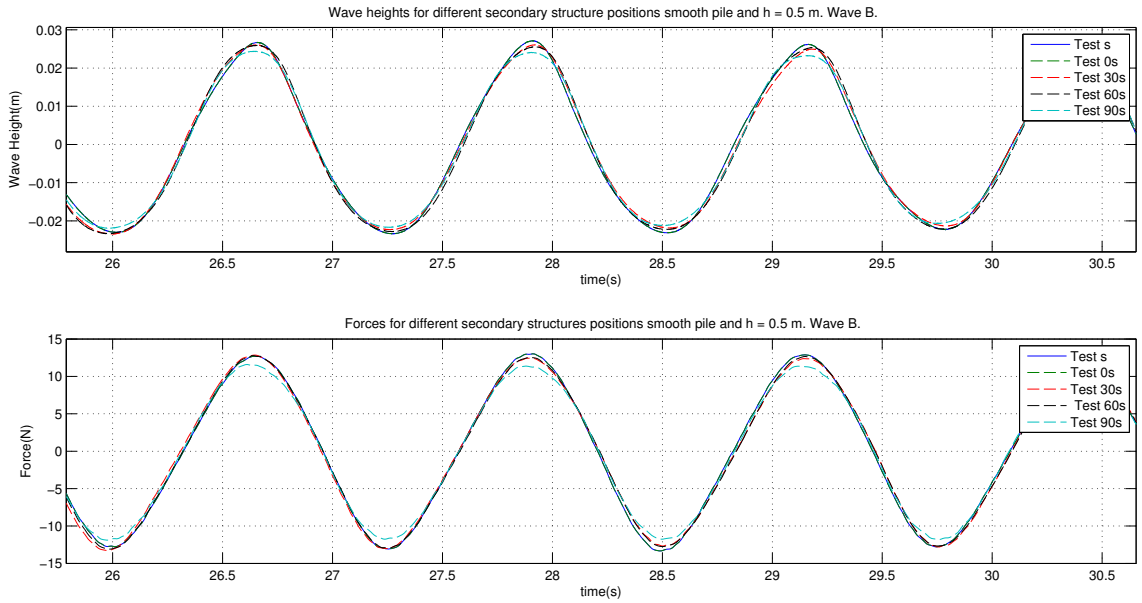

Figure C.1. Wave forces for smooth pile with and without secondary structure at different positions. Wave B.

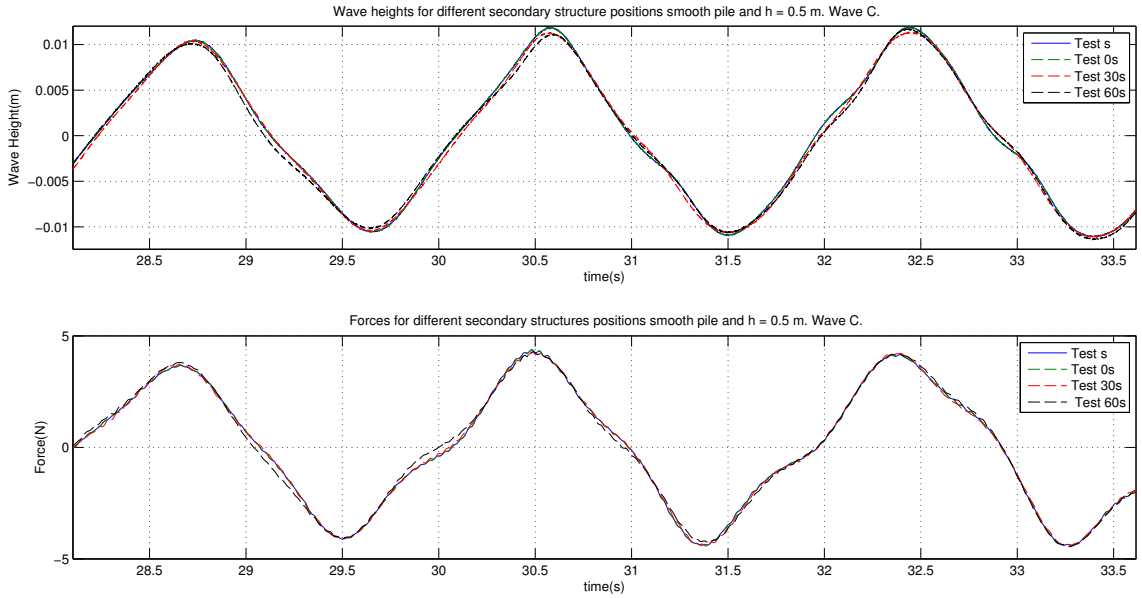

Figure C.2. Wave forces for smooth pile with and without secondary structure at different positions. Wave C.

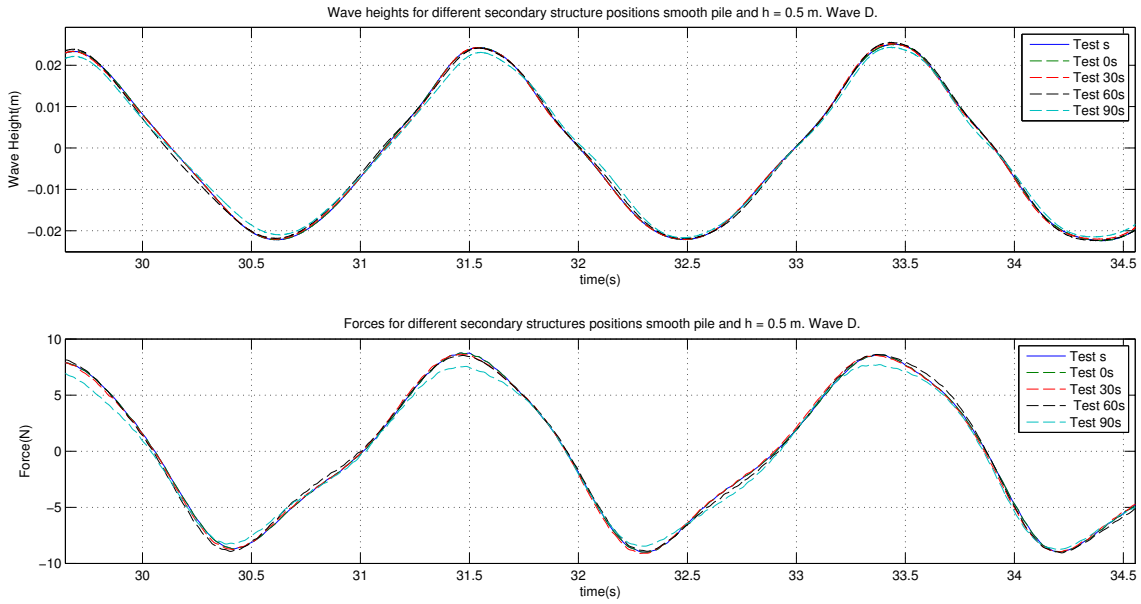

Figure C.3. Wave forces for smooth pile with and without secondary structure at different positions. Wave D.

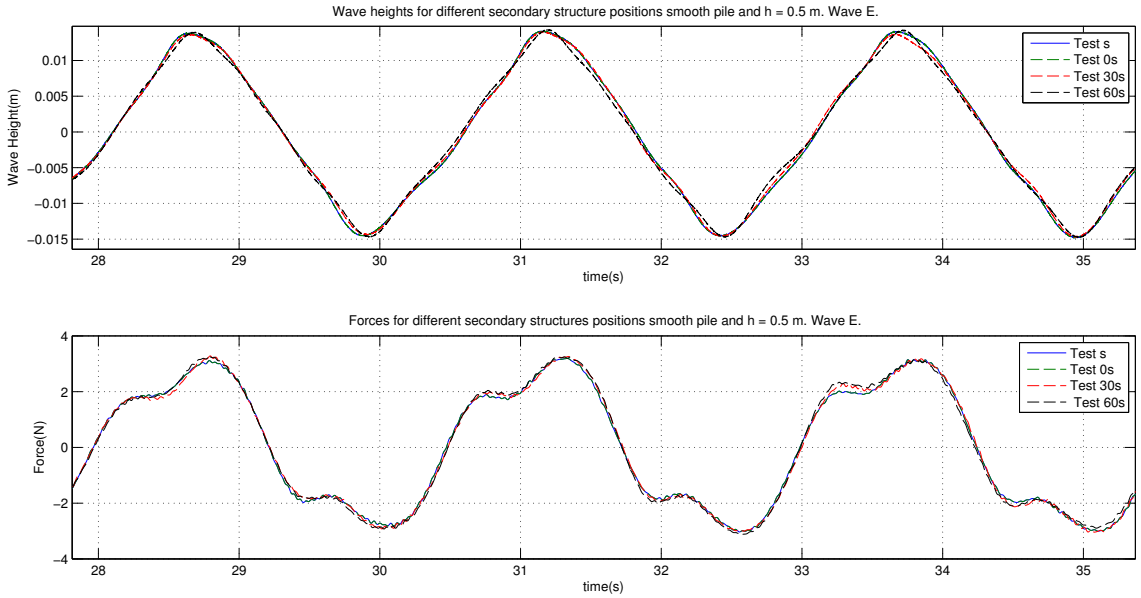

Figure C.4. Wave forces for smooth pile with and without secondary structure at different positions. Wave E.

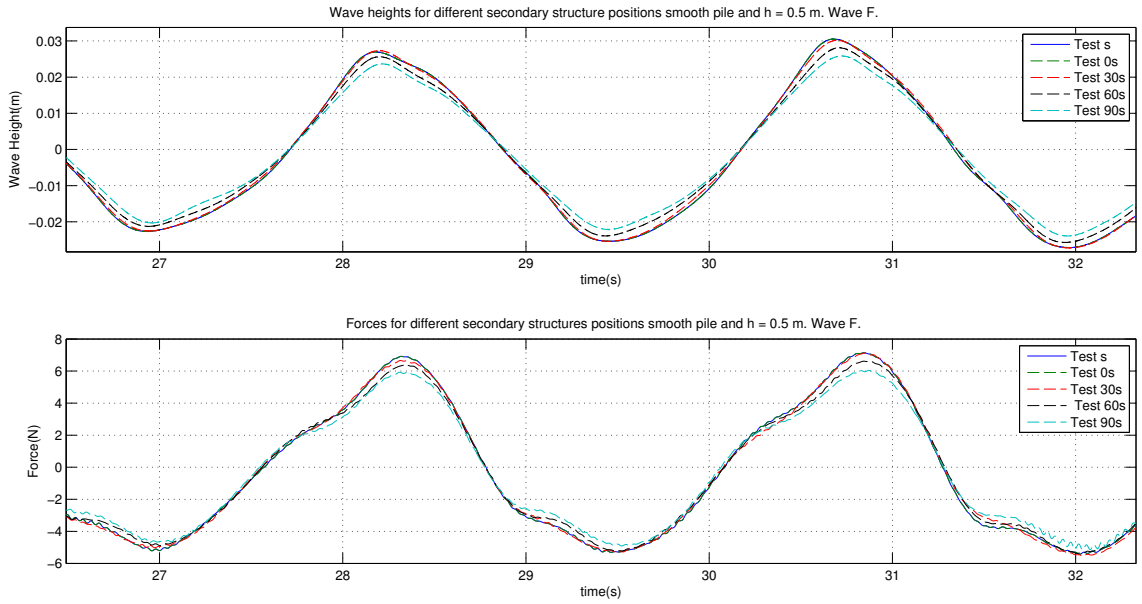

Figure C.5. Wave forces for smooth pile with and without secondary structure at different positions. Wave F.

C.3 Irregular wave analysis

Figure C.6 to Figure C.10 show the time series for F_x and η for waves from L to P.

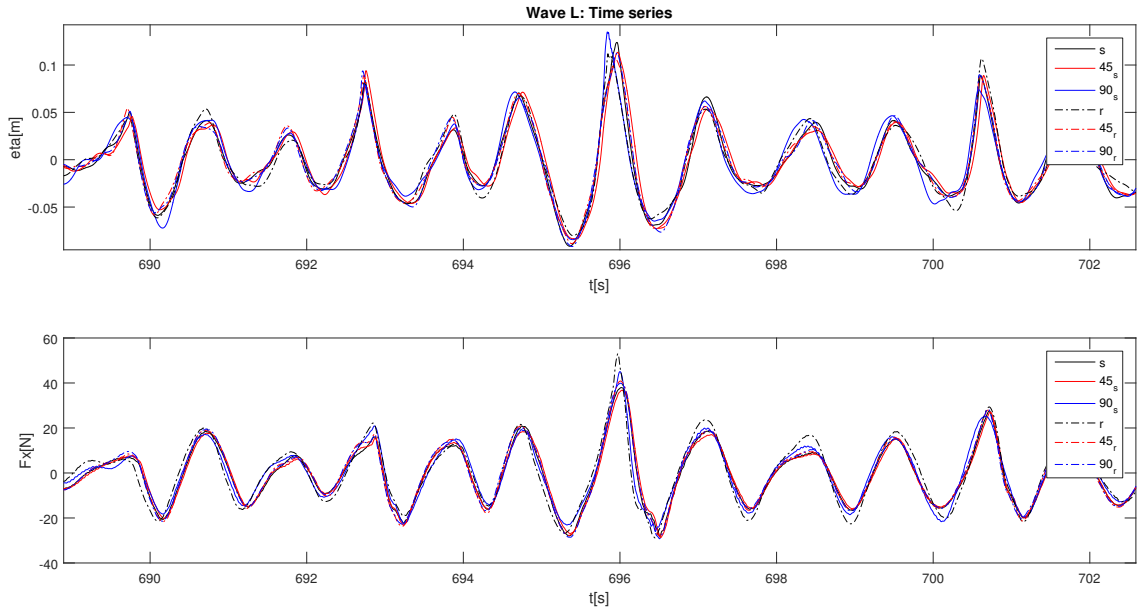

Figure C.6. Time series for wave L tests.

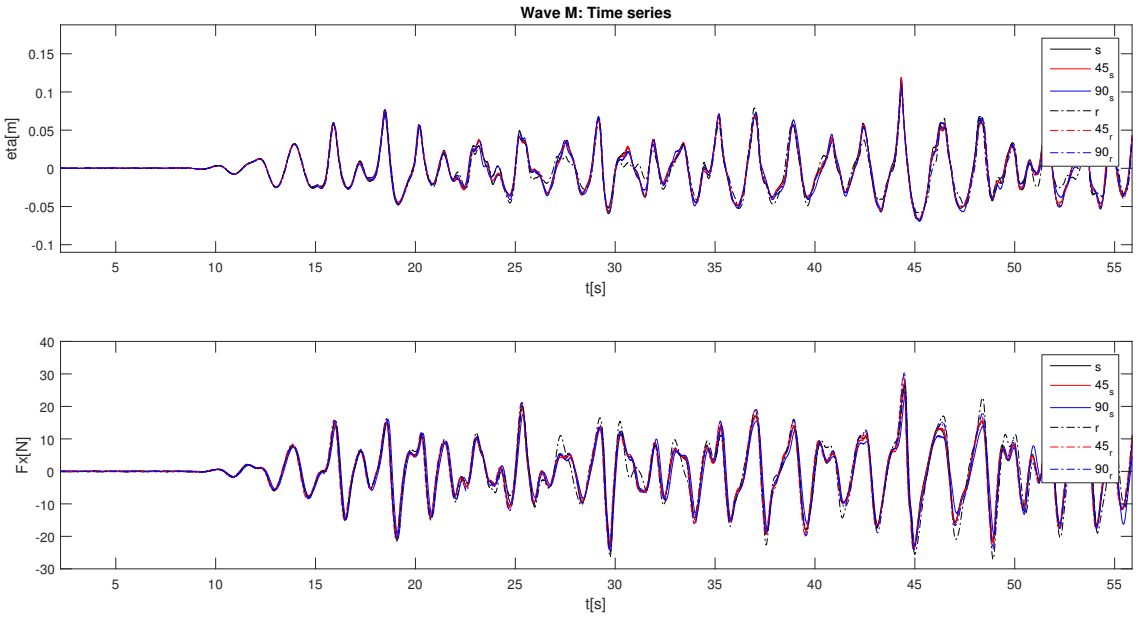

Figure C.7. Time series for wave M tests.

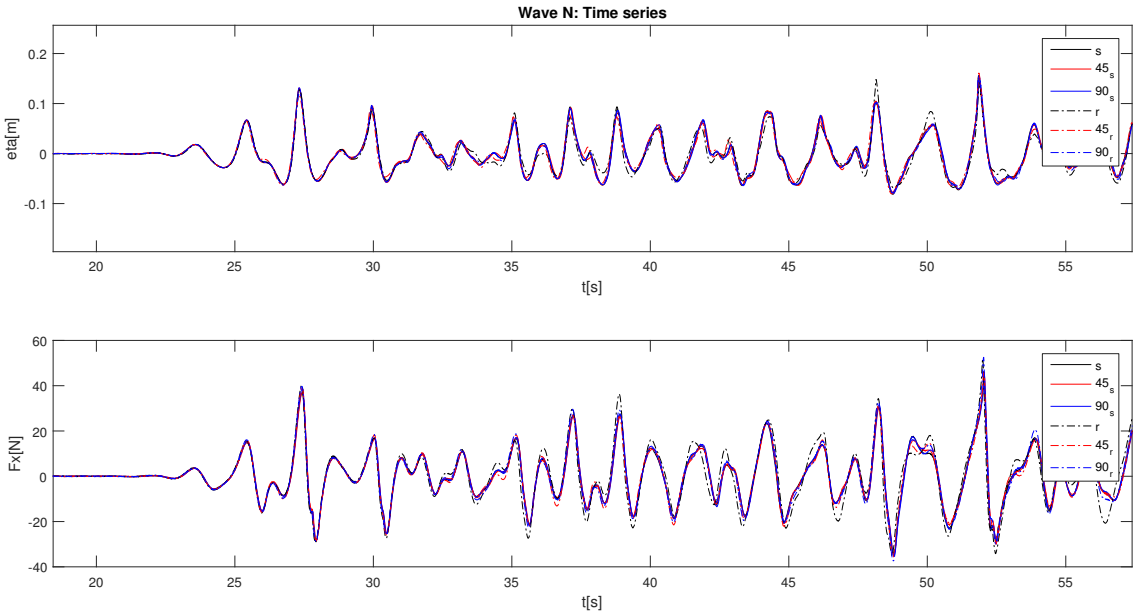

Figure C.8. Time series for wave N tests.

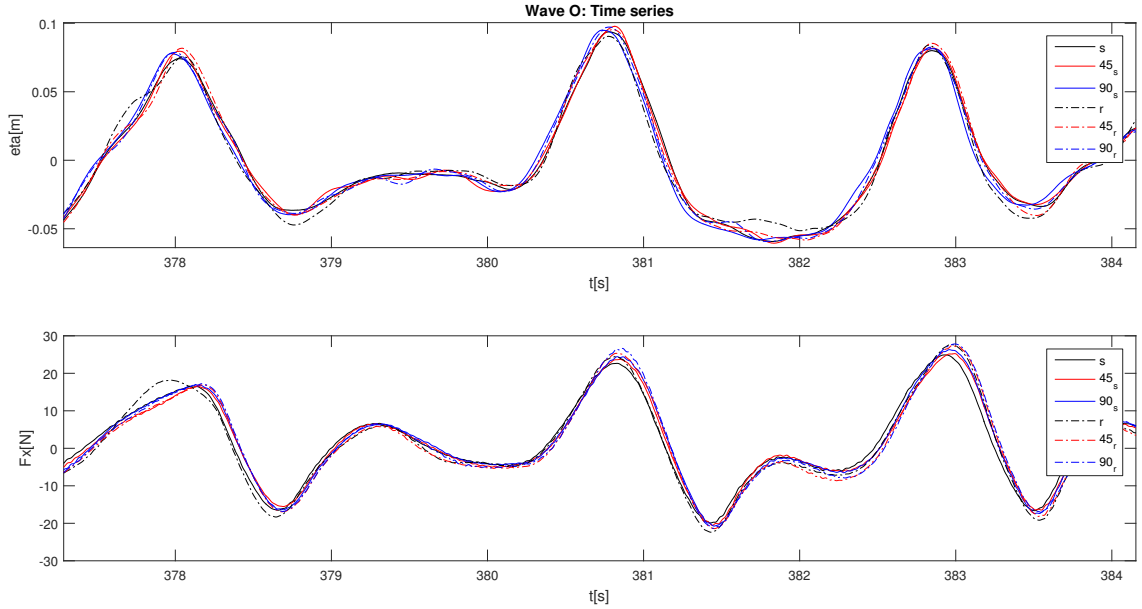

Figure C.9. Time series for wave O tests.

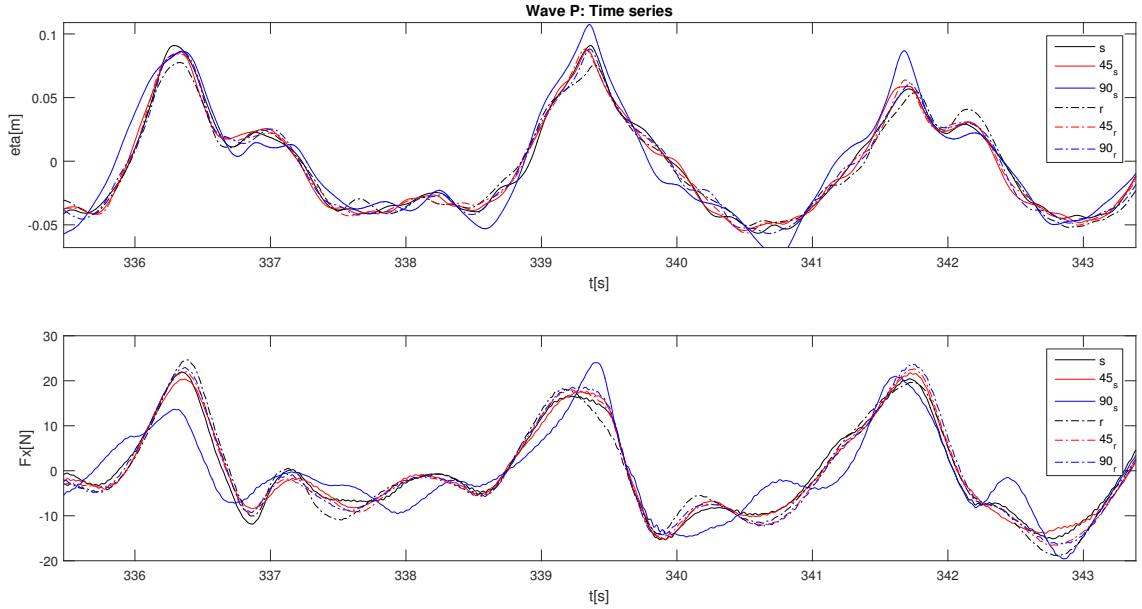

Figure C.10. Time series for wave P tests.

C.3.1 Weibull Distribution

The Weibull MLM fit for 100 peaks for F_x and H of waves L and N are shown in Figures C.11-C.18

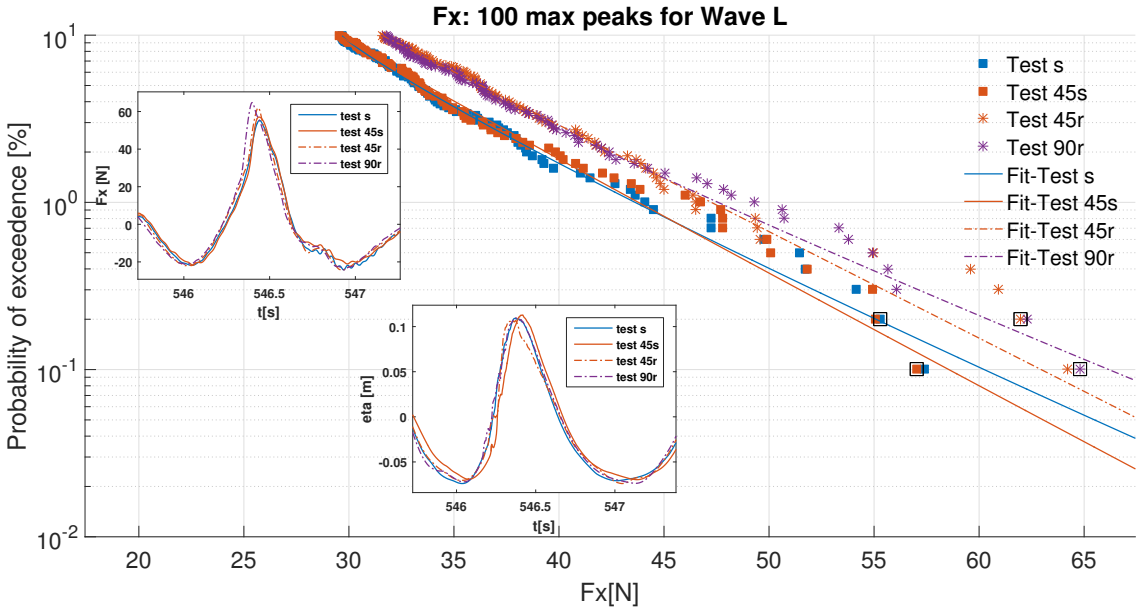

Figure C.11. Weibull fit for 100 F_x peaks for wave L tests. Peaks in boxes shown in inset.

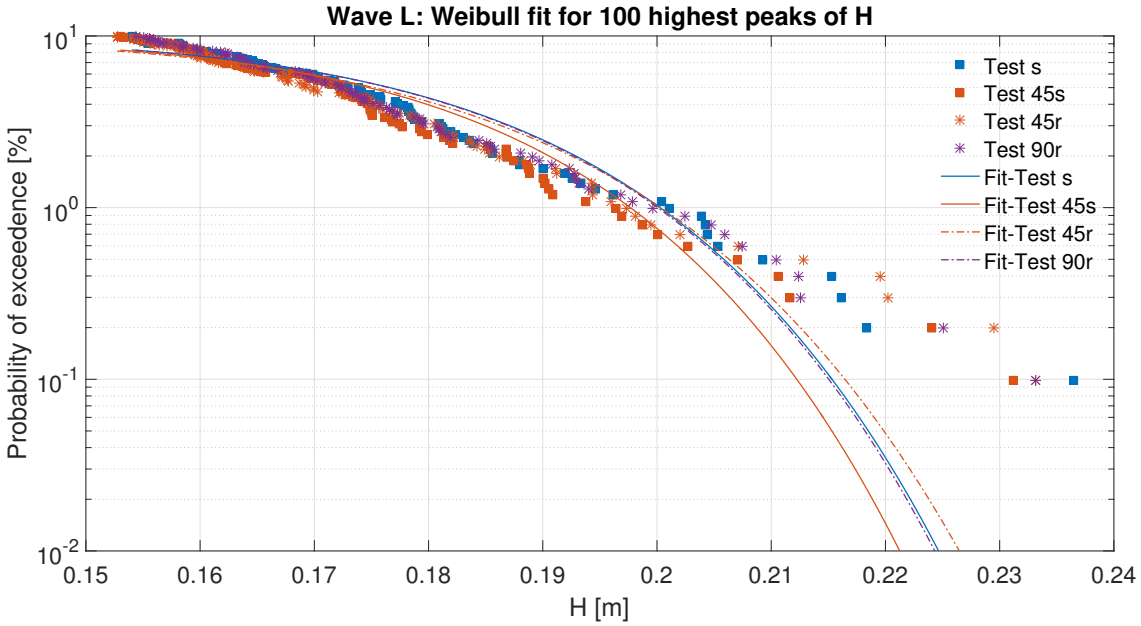

Figure C.12. Weibull fit for 100 H peaks for wave L tests.

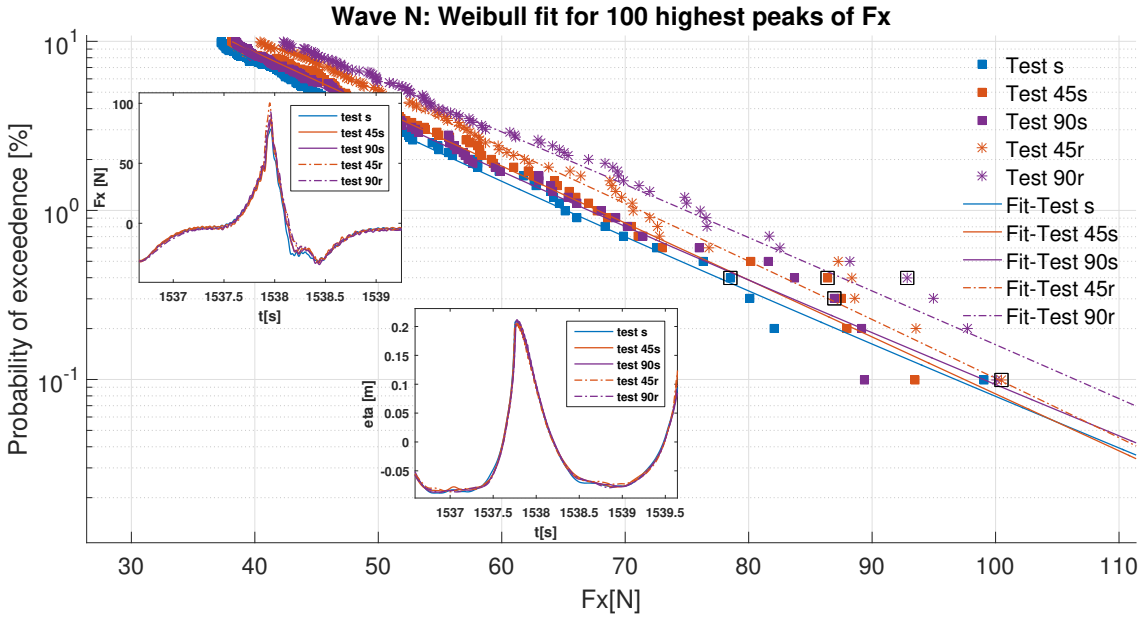

Figure C.13. Weibull fit for 100 F_x peaks for wave N tests. Peaks in boxes shown in inset.

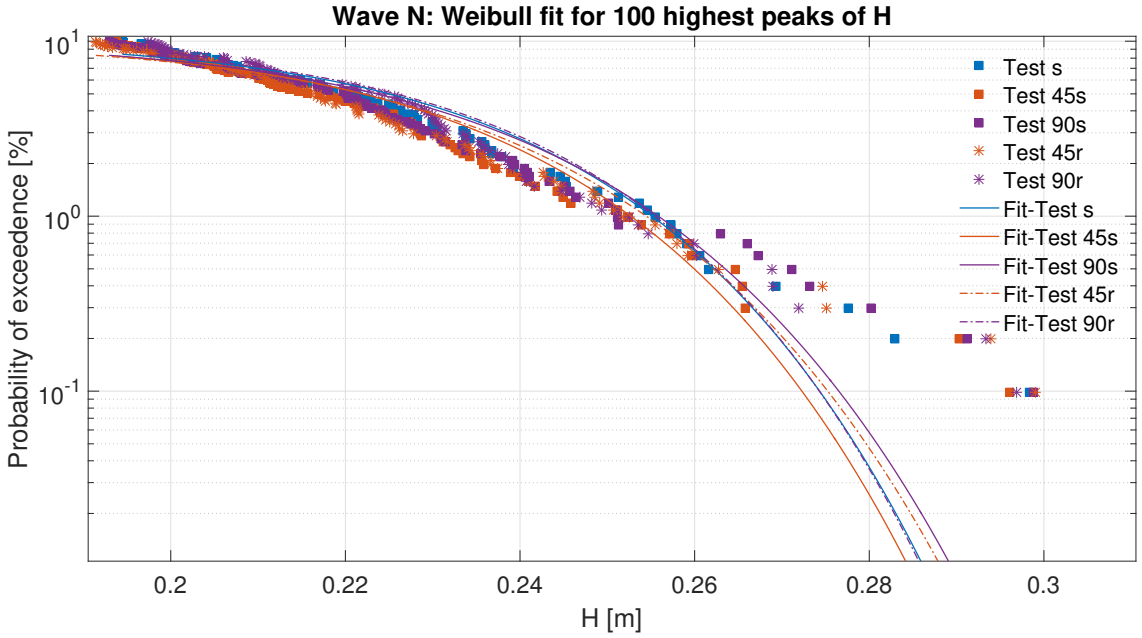

Figure C.14. Weibull fit for 100 H peaks for wave N tests.

C.3.2 For 20 peaks

The Weibull MLM fit for 20 highest peaks for F_x and H of waves L and N are shown in Figures C.15-C.20.

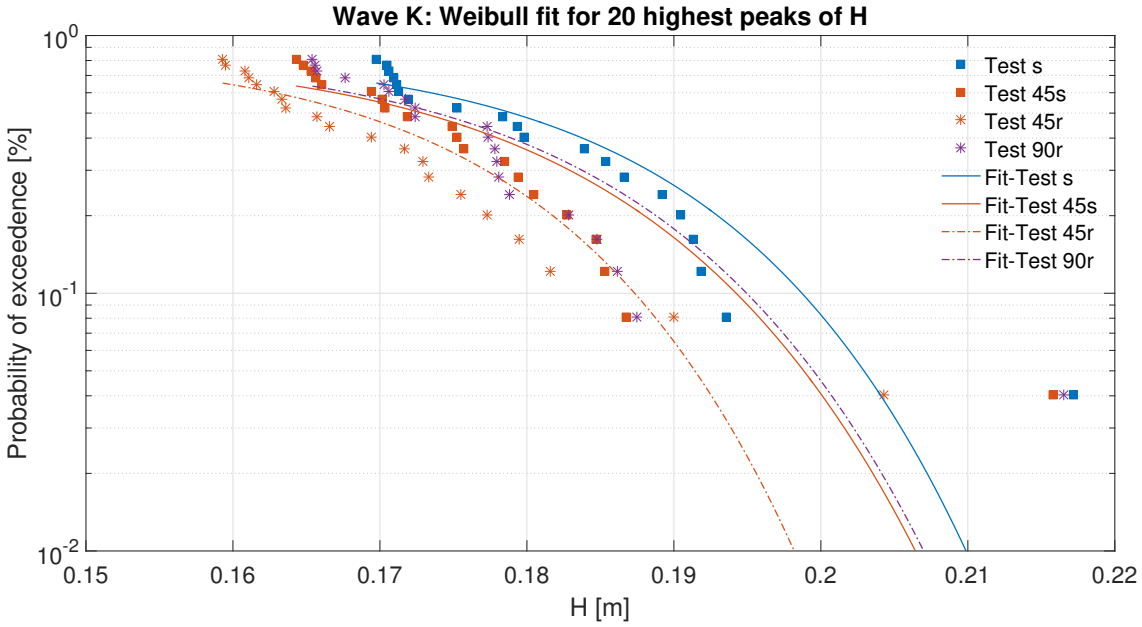

Figure C.15. Weibull fit for 20 H peaks for wave K tests.

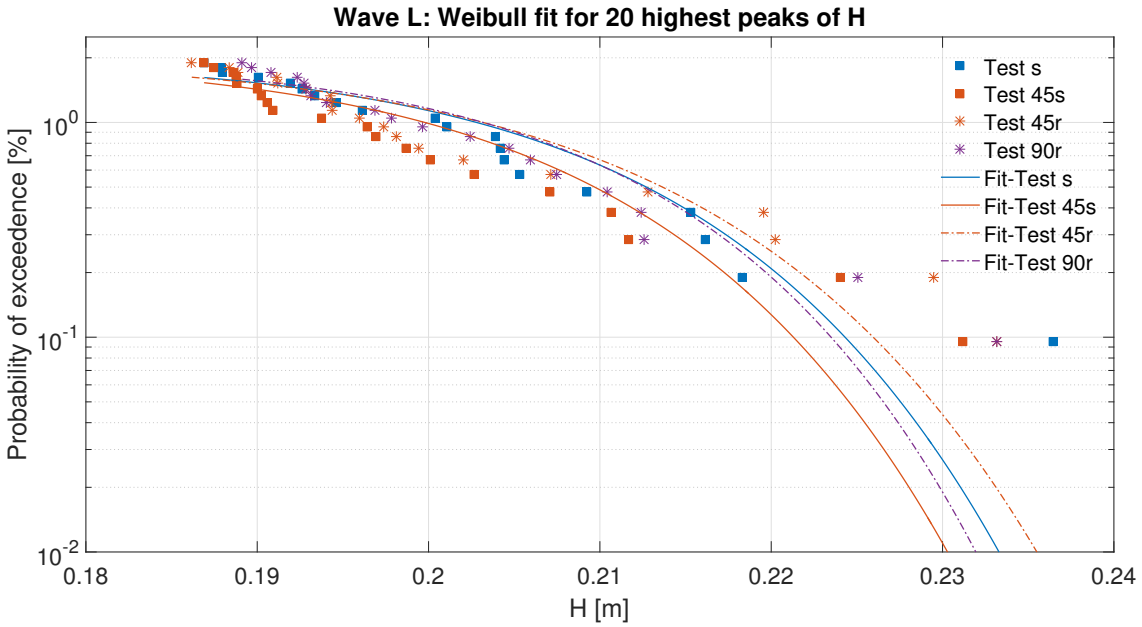

Figure C.16. Weibull fit for 20 H peaks for wave L tests.

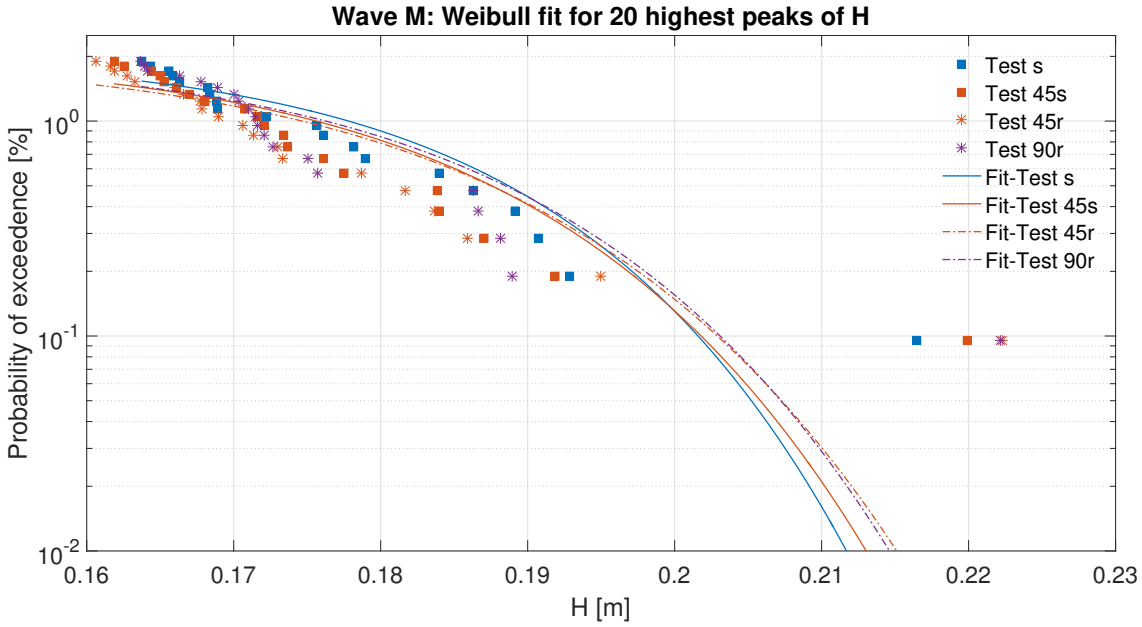

Figure C.17. Weibull fit for 20 H peaks for wave M tests.

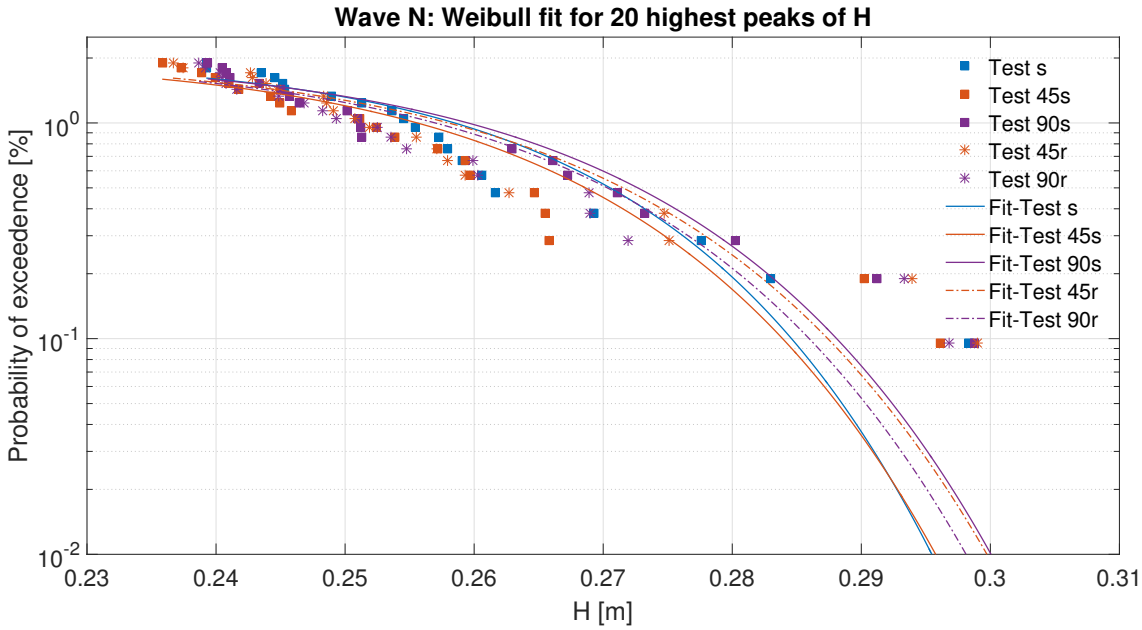

Figure C.18. Weibull fit for 20 H peaks for wave N tests.

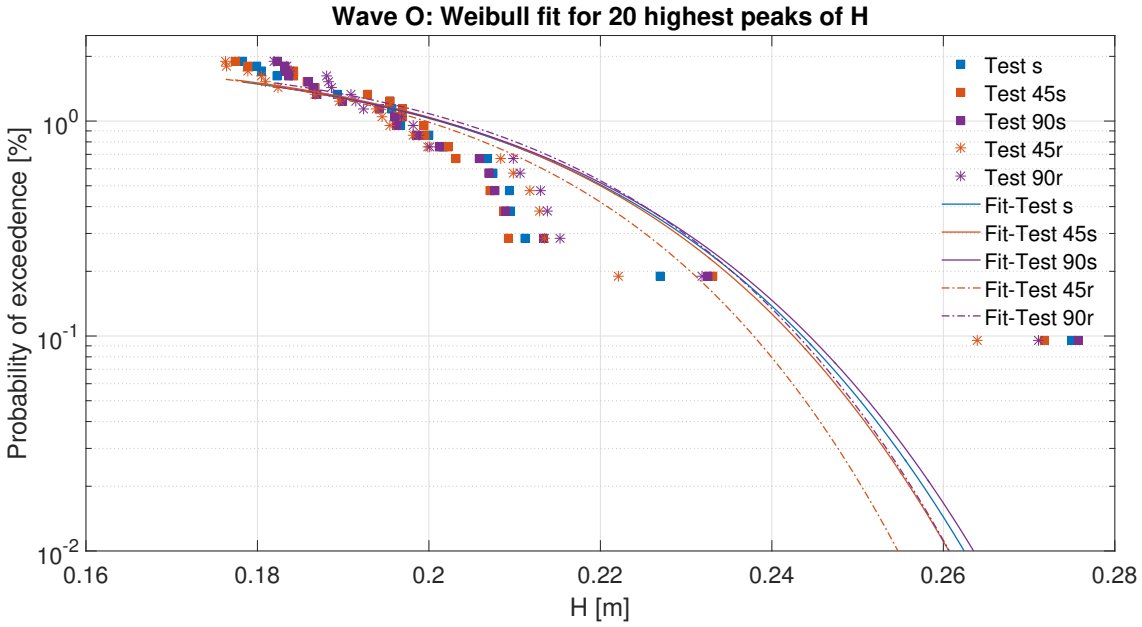

Figure C.19. Weibull fit for 20 H peaks for wave O tests.

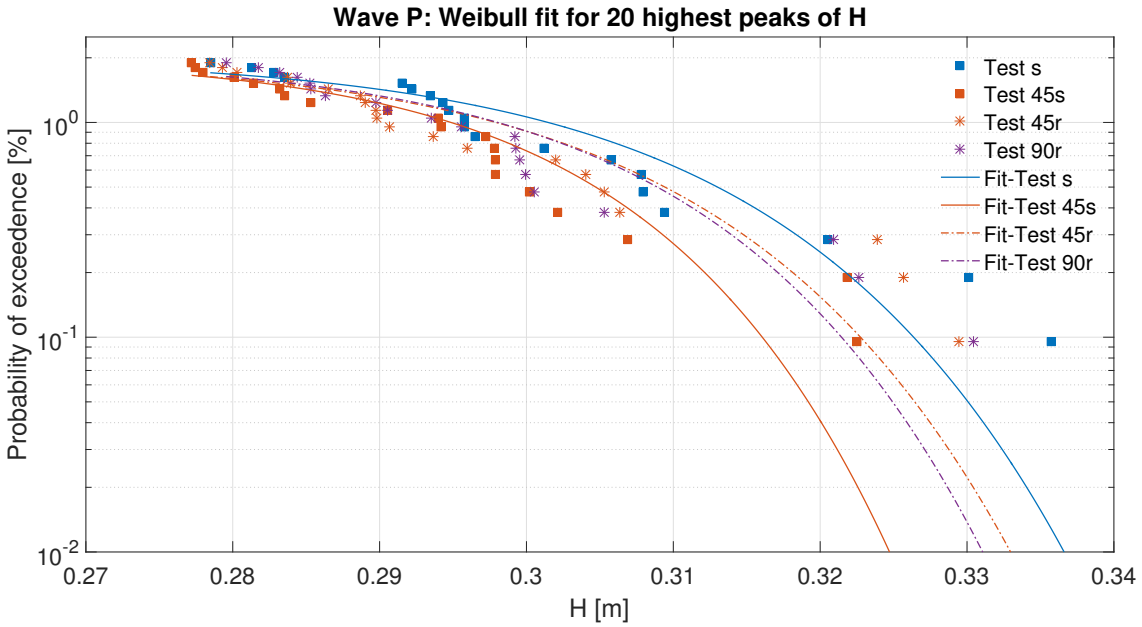

Figure C.20. Weibull fit for 20 H peaks for wave P tests.

The difference in design wave height, $H_{0.1\%}$ from 100 peaks and 20 peaks are given in Table C.2.

Wave	100 Peaks Avg. $H_{0.1\%}$ [m]	20 Peaks Avg. $H_{0.1\%}$ [m]	% Increase
K	0.189	0.194	2.4%
L	0.215	0.224	4.4%
M	0.191	0.201	5.1%
N	0.275	0.286	4.0%
O	0.224	0.242	7.9%
P	0.316	0.323	2.1%

Table C.2. Difference in design wave height from 100 peak and 20 peak Weibull distributions.

C.4 Validation of results

Figures C.21 and C.22 show the wave surface elevation measured by wave gauges $WG3$ and $WG7$. Both signals overlap validating the η measurements at the pile position.

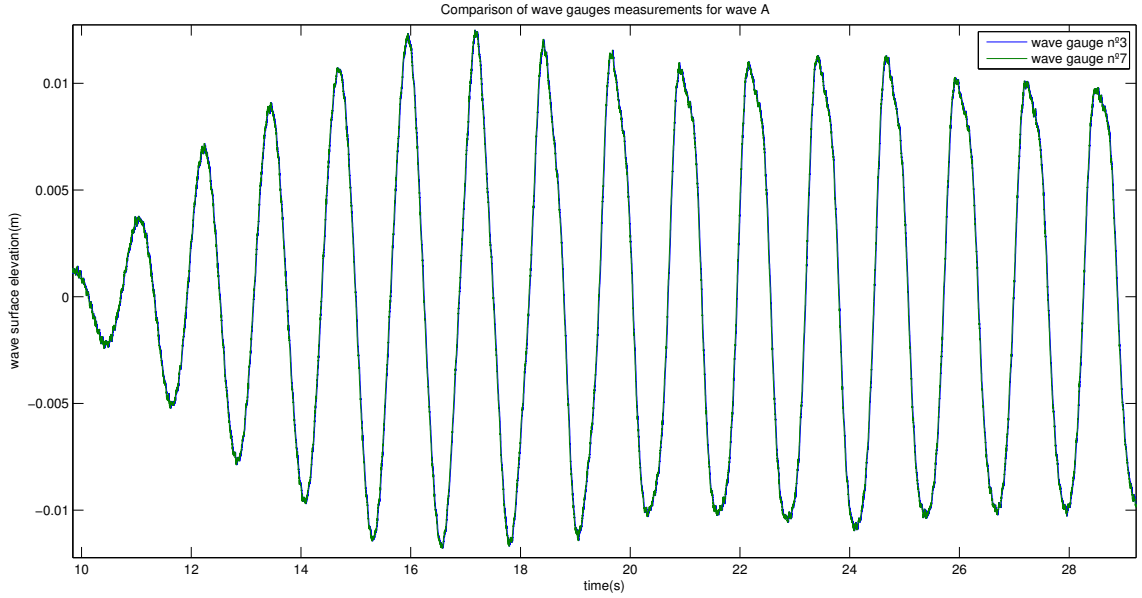

Figure C.21. Comparison of wave gauges measurements. regular tests

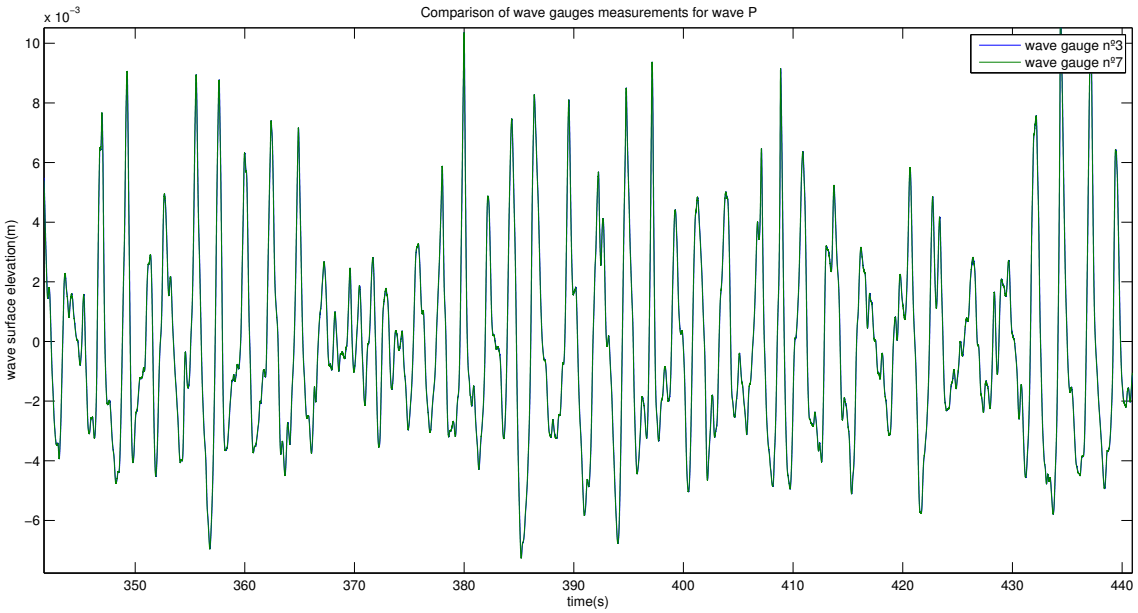

Figure C.22. Comparison of wave gauges measurements, irregular tests

In order to verify the correct force measurements, Morison force equation was used for waves A, F and J and compared to the laboratory tests results. The C_D and C_M coefficients were obtained with an approximation from Sarpkaya charts (See Appendix A), since values of Keulegan Carpenter number, KC (waves A and F), and β (waves A, F and $J4$) were out of the charts. The selected values were $C_D = 0.8$ and $C_M = 2$. Table C.3 shows Re, β and KC values for waves A, F and J.

Stream function was used to obtain the wave velocity at the same water depth at which the ADV measurements were taken and to calculate the wave surface elevation for the target waves and compare it with the data from wave gauge $WG13$. See Figures C.23-C.25

Wave	$U_{max}(m/s)$	Re	β	KC
A	0.073	11664	20236	0.57
F	0.134	21425	10078	2.12
J	0.749	119437	10078	11.85

Table C.3. Waves A, F and J values for Sarpkaya charts

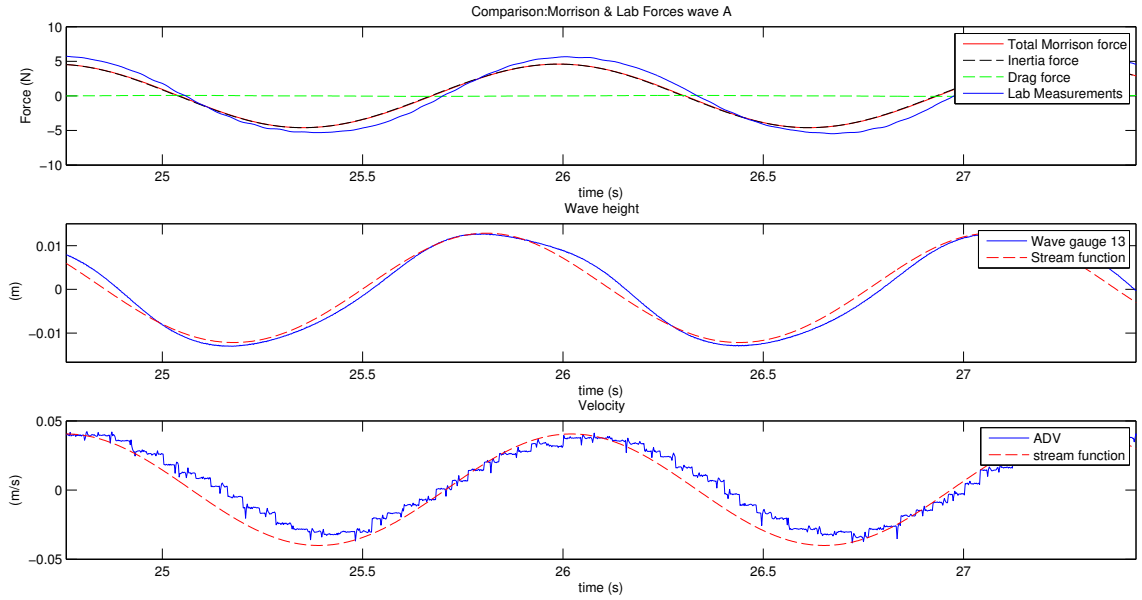

Figure C.23. Validation of measured wave forces,surface elevation and velocity for wave A

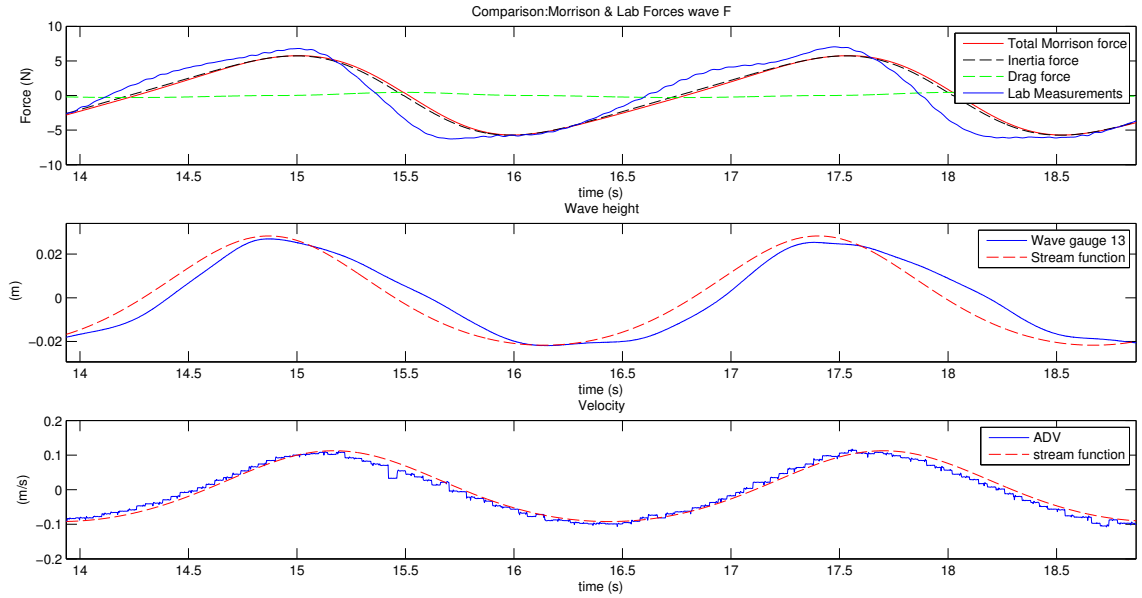

Figure C.24. Validation of measured wave forces,surface elevation and velocity for wave F

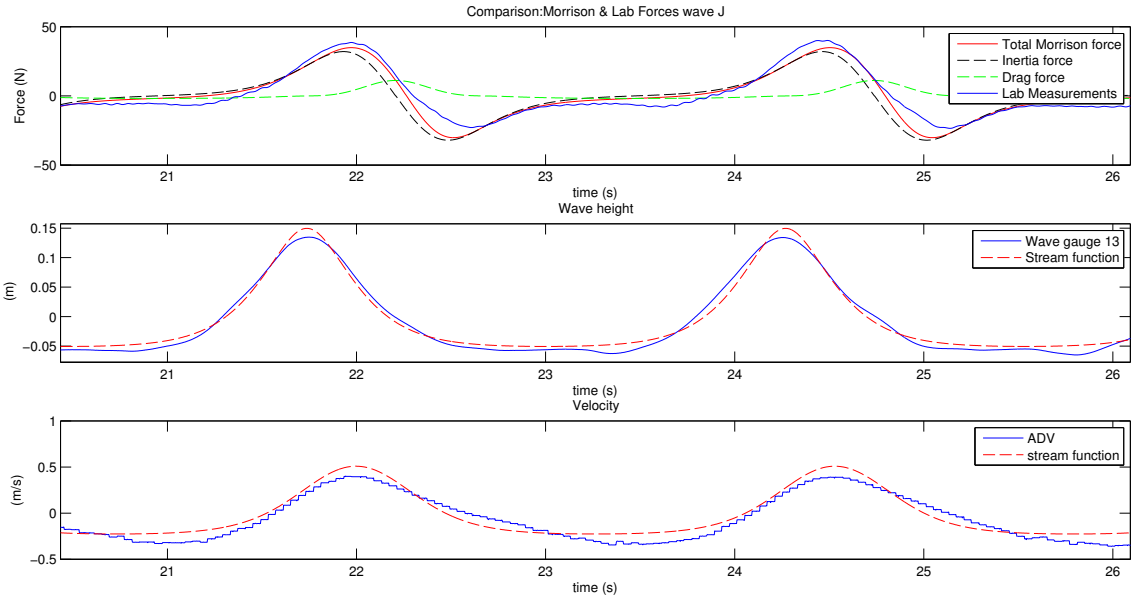

Figure C.25. Validation of measured wave forces,surface elevation and velocity for wave J

Appendix : Annex CD D

Run-up - *Calculations performed for run-up on monopiles*
Slamming on platforms - *Calculations performed for slamming forces and pressures on platforms*
Wave forces on monopile - *Analysis of laboratory test results at AAU and comparison with theories*